論文 / 著書情報
Article / Book Information

題目(和文)	ベリー曲率によるマグノンの熱ホール効果の理論
Title(English)	Theory of thermal Hall effect of magnons due to Berry curvature
著者(和文)	松本遼
Author(English)	Riyou Matsumoto
出典(和文)	学位:博士(理学), 学位授与機関:東京工業大学, 報告番号:甲第9353号, 授与年月日:2013年12月31日, 学位の種別:課程博士, 審査員:村上　修一,藤澤　利正,斎藤　晋,古賀　昌久,西田　祐介
Citation(English)	Degree:Doctor (Science), Conferring organization: Tokyo Institute of Technology, Report number:甲第9353号, Conferred date:2013/12/31, Degree Type:Course doctor, Examiner:,,,,
学位種別(和文)	博士論文
Type(English)	Doctoral Thesis

Theory of thermal Hall effect of magnons due to Berry curvature

Department of Physics, Tokyo Institute of Technology
Ryo Matsumoto
11D02050

October 18, 2013

abstract

In this thesis we construct a comprehensive theory of the thermal Hall effect of magnons, where a transversal thermal current of magnons appears by a longitudinal temperature gradient. The theory covers various magnons: not only the exchange magnons in ferromagnets but also those in antiferromagnets and the magnetostatic spin waves in magnetic films. The thesis consists of two parts. The first one is the linear response theory with a temperature gradient, and the other one is a semiclassical theory for dynamics of a magnon wavepacket. These investigations are of fundamental physical interest for understanding properties of the magnon transport phenomena, which gives a significant contribution to applications in electronic and magnonic devices.

By an approach in the linear response theory with a temperature gradient, we derive thermal transport coefficients and the thermal Hall conductivity of magnons. They are related to the Berry curvature in momentum space, which represents geometrical properties and is inherent in the magnon band structure. The theory presented here is applicable to generic spin waves, whose spin-wave Hamiltonians are written as the Bogoliubov-de Gennes Hamiltonian. In particular, as an example, we demonstrate an application to the magnetostatic spin waves in magnetic thin films. We analytically derive a thermal Hall conductivity of the magnetostatic spin wave, and clarify its dependences on a temperature and magnetic field.

The second approach is the semiclassical theory. By constructing the equation of motion for magnon wave packets, we verify that there are two unique orbital motions: a self rotation motion and a motion along an edge of the system (magnon edge current). The latter gives a good intuitive picture for understanding the thermal Hall effect of magnons: it occurs by breaking the balance of circulating thermal currents in equilibrium which are carried by the magnon edge current. Moreover, these orbital motions generate additional terms to the thermal transport coefficients from the Kubo formula. We confirm that the thermal conductivity from the semiclassical theory completely coincides with that from the linear response theory.

To clarify the details of orbital motions of magnons, we also calculate their angular momenta. They are represented by the Berry curvature in momentum space, that offers hints for researching the effect of the Berry phase in magnets. In particular, a self-rotating magnon wavepacket can be regarded as a circular spin current, which yields an electric polarization. The polarization in a gaussian-shaped magnon wave packet is roughly estimated, and its direction is found to be in the radial direction. In addition, we propose experimental methods to observe the magnon edge current.

Contents

Chapter 1

Introduction

A spin wave is a low energy excitation in magnetically ordered medium. Its concept was introduced by Bloch [1] in 1930. He first suggested that collective precessions of individual magnetizations can be represented as a propagating wave in magnets. Later, Holstein and Primakoff [2] and Dyson [3] introduced magnons, which is a quantum of spin waves. Magnons are to spin waves what lattice waves are to phonons. In addition, like phonons, magnons obey the Bose-Einstein statistics. Far below the Curie temperature, a magnetically ordered system is well described as a gas of magnons.

Experimental evidence for the existence of spin waves was indicated in the measurements of thermodynamic properties of magnets, for example, the temperature dependence of their saturation magnetization; the famous $T^{3/2}$ Bloch law indirectly implicated its existence. The direct observation was accomplished by Griffiths [4] in 1946, by using the ferromagnetic resonance (FMR). FMR is a uniform precession of magnetizations, which is a special case of spin waves with the wave vector being zero. Spin waves with a non-zero wave vector were observed by Fleury *et al.* [5], by using the Brillouin light scattering (BLS) technique [6, 7]. In this experiment, a spin wave mode appears as a peak in the spectrum, which is shifted by the spin wave frequency from the central peak in the spectrum of elastically scattered photons.

BLS is one of the important techniques in the field of magnetism to investigate magnetic excitations in various systems, such as bulk materials, thin films, and nanostructures. In particular, magnetic thin films are important for their variety of magnetic properties and practical applications to electromagnetic devices. They include not only single magnetic films but also multiple layered films, composed of ferromagnetic, antiferromagnetic, and nonmagnetic materials. Many theoretical and experimental study were devoted to understand its magnetic behaviors with all sorts of approaches such as neutron scattering [8], ferromagnetic resonance, magneto-optical Kerr effect (MOKE) [9–11].

Since the spin wave is a wave of course, it possesses characters inherent in waves, such as an acoustic wave or light wave. A number of theoretical and experimental study have been performed to confirm the properties: propa-

gation [12–15], reflection and refraction [16–20], radiation [21], interference and diffraction [22–25], scattering and tunnelling [26–32], and Doppler effect [33–35].

On the other hand, to measure properties of magnons as quasiparticles, kinetics of a magnon gas is of fascinating interest in magnetism. In particular, the Bose-Einstein condensation (BEC) of magnons, which is a macroscopic quantum phenomenon, was demonstrated in several magnetic systems [36–38]. Recently the BEC of magnons at room temperature is observed in yttrium-iron-garnet (YIG) [39], and has been continuously studied further [40, 41]. Besides the BEC of magnons, transport phenomena of magnons are also hot topics in condensed matter physics. Magnons can carry spins, which is called a spin current of magnons (or spin waves). It is reported that magnons in YIG propagates over centi-meter distance at room temperature [42]. This distance is far longer than that for spin currents by electrons in metals or doped semi-conductors. Thus the magnon is focused as a good candidate for a carrier of spins.

As an analogy of a photonic crystal, magnon band engineering is possible by constructing an artificial magnetic crystal, which is called "magnonic crystal" [43]. The research of magnonic crystals has been developed since the 1980s, when magnetic superlattices were studied. Numerous theoretical and experimental studies are devoted to clarify spin wave spectrum in superlattices consisting of multi layers of magnetic films [44–60]. They can be regarded as 1D magnonic crystals along the stacking direction, and it is shown that a band gap of the spin wave can exist in some magnetic superlattice [61–66]. In recent years, not only 1D but also 2D [61, 67, 68] and 3D [69, 70] magnonic crystals are studied extensively.

With these properties, magnons have cultivated a new field of nanotechnology, which is called "magnonics" nowadays [71–74]. This field aims to transmit, store and process information by using spin waves in a nanoscale. Research on the magnonics is challenging because of some peculiar characters of spin waves. For example, frequencies of spin waves are dispersive and sometimes anisotropic even in isotropic systems. Moreover, dominant interactions, e.g. the exchange interaction and dipolar interaction, have different length scales. Nevertheless, these various properties of spin waves in turn enable magnonic devices to operate novel and significant functions which cannot be seen in electronic or photonic devices. There are numerous advantages in magnonic devices, e.g., they are readily manipulated by magnetic fields or electric currents [75], including potential of non-volatile memory elements, and thus their integration will lead to reconfigurable devices at a sub-nanosecond time scale. In addition, magnonic devices harmonize in integration with electronics or optics devices since there is already developed technology which realizes a composition between magnetic nanostructure and other devices, such as magnetic random access memories or magneto-optical disks. Furthermore, in most practical situations, where frequencies of spin waves are in the range from gigahertz to terahertz, a wavelength of spin waves is shorter than that of electromagnetic waves. Thus magnonic devices have an advantage over other devices for miniaturization.

In order to realize magnonic devices, precise control of magnons is one of the essential subjects. Magnon Hall effect discussed in this thesis offers a new

approach to this subject. In particular, because of the experimental situations, the thermal Hall effect of magnons are studied both theoretically [76–78] and experimentally [79, 80]. Besides the magnon transport, the thermal Hall effect of magnons accompanies important properties of magnets, which is represented in terms of the Berry curvature in momentum space. These are inherent in materials with geometrical aspects, and exhibit unique properties in transport phenomena, similar to the quantum Hall effect in electron systems. Therefore, investigation of the thermal Hall effect of magnons also give us insight of nature which is hidden in magnetically ordered systems.

Though a basis for the thermal Hall effect of magnons has been constructed in the previous works [77, 79], some terms are missing in these works and it is applicable to only ferromagnets. Thus our motivation is to construct a comprehensive theory for the thermal Hall effect of magnons, and to verify influence of the geometrical properties on the magnon transport phenomena.

In this thesis, we discuss the thermal Hall effect of magnons. In chapter 2, we first address complementary topics which are necessary for the following discussions, and also state the background of the thermal Hall effect of magnons. In chapter 3, we present our basic theory, thermal Hall effect of magnons in ferromagnets, by using the linear response theory. In chapter 4, a generic theory for the thermal Hall effect of magnons is presented. The word "generic" means that we treat spin waves in antiferromagnets or magnetostatic spin waves, as well as those in ferromagnets. In chapter 5, we discuss the semiclassical theory of wavepackets of spin waves. An intuitive picture and a comparison between previous works and our theory is presented. Moreover, we mention orbital motions of magnon wavepackets, and also discuss experiments of the magnon Hall effect. In chapter 6 a conclusion of this thesis is stated.

Hereafter we focus on the clean limit of a magnon gas system; in other words, magnon-magnon interaction and magnon-phonon interactions are not taken into account. Though the words "magnon" and "spin wave" coexist in this context, the distinction is insignificant.

Chapter 2

Background

2.1 Spin wave

Historically, a discovery of the spin wave is closely related to the temperature dependence of the magnetization [1, 81, 82]. To understand the concept of spin waves, we start from a ferromagnet at zero temperature $T = 0$[K]. At $T = 0$, all magnetization are aligned to the same direction, and the total value of the magnetization is saturated to M_{S}. As the temperature increases, experimental results show that the magnetization decreases with $T^{3/2}$ law. Meanwhile the spin flip excitation leads to an exponential dependence on T [83], which is different from the experiments. The exponential dependence arise from an energy gap of spin flippings, whose magnitude is of the order of the exchange interaction, and the experimental results excludes presence of such a large energy gap.

In order to solve this problem, Bloch introduced the concept of spin waves as collective excitations of the magnetic moments. Spin waves consist of precessing spins around the direction of the magnetization in the ground state ($T = 0$), with a phase difference between the neighboring spins. Instead of one-spin flipping, all spins share the reversal by being slightly canted. The excitation of the spin waves is gapless, and thus the spin wave theory successfully gives an explanation of the $T^{3/2}$ law. Fig. 2.1 shows a schematic of a spin wave in ferromagnets. This figure visually indicates why this is called the spin "wave".

Generally speaking, there are two kinds of spin waves: an exchange spin wave and a dipolar spin wave (or magnetostatic spin wave). They are classified by dominant interactions, i.e., the exchange interaction and the dipolar interaction, respectively. If the tilting angle between the neighboring spins is large, in other words, if the wavelength of the spin wave is short, the exchange interaction is dominant. In contrast, when the angle is small, i.e., the wavelength is long, the dipolar interaction is dominant. Since the formalisms of deriving dispersion relations are quite different between these modes, we discuss them individually.

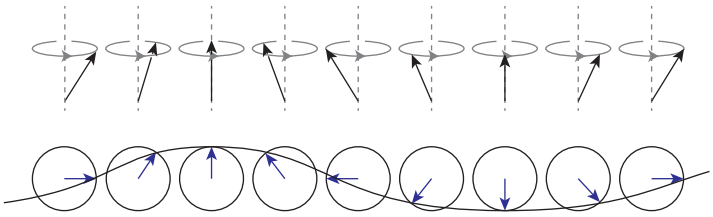

Figure 2.1: Schematic of a spin wave in ferromagnets. The upper panel shows the side view of spins. The lower panel shows the top view of spins. The blue arrows denote a dynamical component of spins.

2.1.1 Exchange spin wave

If the wavelength of the spin wave is in the range from about 1nm to 100nm, the exchange interaction is dominant and the dipolar interaction is negligible. For simplicity, we derive a dispersion relation of the exchange spin wave by using the Holstein-Primakoff approach. Let us consider a Heisenberg ferromagnet without any anisotropy,

$$H = -J_{ij} \sum_{\langle i,j \rangle} \boldsymbol{S}_i \cdot \boldsymbol{S}_j, \tag{2.1}$$

where J is an exchange coupling constant and $\langle i, j \rangle$ restricts the sum to nearest neighbor sites. The basic idea of the Holstein-Primakov transformation is to bosonize the spin Hamiltonian, by expressing the spin operators as follows:

$$S^z = S - \hat{n}, \tag{2.2}$$

$$S^- = \sqrt{2S} a^\dagger \left(1 - \frac{\hat{n}}{2S}\right)^{\frac{1}{2}}, \tag{2.3}$$

$$S^+ = \sqrt{2S} \left(1 - \frac{\hat{n}}{2S}\right)^{\frac{1}{2}} a. \tag{2.4}$$

Here S is the magnitude of the spin, $S^\pm = S^x \pm i S^y$, $\hat{n} = a^\dagger a$, and $a^\dagger, a$ denotes the creation and annihilation operators of a magnon, respectively. Magnons obey the bose statistics due to the commutation relation of spin operators. Actually, because they satisfy

$$[S^z, S^-] = \sqrt{2S}[S - \hat{n}, a^\dagger] \left(1 - \frac{\hat{n}}{2S}\right)^{\frac{1}{2}} = -[a, a^\dagger] S^-, \tag{2.5}$$

$$[S^z, S^+] = \sqrt{2S} \left(1 - \frac{\hat{n}}{2S}\right)^{\frac{1}{2}} [S - \hat{n}, a] = [a, a^\dagger] S^+, \tag{2.6}$$

$$\begin{aligned} [S^-, S^+] &= 2S \left\{ a^\dagger \left(1 - \frac{\hat{n}}{2S}\right) a - \left(1 - \frac{\hat{n}}{2S}\right)^{\frac{1}{2}} a a^\dagger \left(1 - \frac{\hat{n}}{2S}\right)^{\frac{1}{2}} \right\} \\ &= -2[a, a^\dagger] (S - \hat{n}) = -2[a, a^\dagger] S^z, \end{aligned} \tag{2.7}$$

and $[S^\alpha, S^\beta] = i\varepsilon_{\alpha\beta\gamma}S^\gamma$ with $\varepsilon_{\alpha\beta\gamma}$ being the Levi-Civita symbol, it is easily seen that a and $a^\dagger$ satisfy the bose commutation relation:

$$[a, a^\dagger] = 1. \tag{2.8}$$

When $S \gg 1$, Eqs. (2.2)-(2.4) can be linearized as follows:

$$S^z = S - \hat{n} \tag{2.9}$$

$$S^- = \sqrt{2S}a^\dagger \tag{2.10}$$

$$S^+ = \sqrt{2S}a. \tag{2.11}$$

With these representations, the spin Hamiltonian is rewritten as

$$H = \frac{1}{2}\sum_{\langle i,j\rangle} J_{ij}\left(S^2 - 2Sa_i^\dagger a_i + 2Sa_i^\dagger a_j\right). \tag{2.12}$$

Introducing the Fourier transformation,

$$a_{\boldsymbol{q}} = \frac{1}{\sqrt{N}}\sum_i e^{-i\boldsymbol{q}\cdot\boldsymbol{r}_i}a_i, \tag{2.13}$$

$$a_{\boldsymbol{q}}^\dagger = \frac{1}{\sqrt{N}}\sum_i e^{i\boldsymbol{q}\cdot\boldsymbol{r}_i}a_i^\dagger, \tag{2.14}$$

with N being the number of sites, one obtains the diagonalized Hamiltonian:

$$H = E_0 + \sum_{\boldsymbol{q}} \hbar\omega_{\boldsymbol{q}} a_{\boldsymbol{q}}^\dagger a_{\boldsymbol{q}}, \tag{2.15}$$

$$\omega_{\boldsymbol{q}} = S\left(J(\boldsymbol{q}) - J(\boldsymbol{0})\right)\hbar. \tag{2.16}$$

In the above equation $J(\boldsymbol{q})$ denotes the Fourier transformation of J_{ij}, $E_0 = NJ(\boldsymbol{0})S^2/2$ is an energy of the ground state, and $\omega_{\boldsymbol{q}}$ is the frequency of the spin wave with the wave vector $\boldsymbol{q}$. Equation (2.15) means that the excitation of a spin wave with its frequency $\omega_{\boldsymbol{q}}$ is equivalent to the excitation of one quasi-particle, namely the magnon, with its energy $\hbar\omega_{\boldsymbol{q}}$. Because we have neglected the anisotropic interaction, the dispersion relation does not depend on the direction of the magnetization. For small $|\boldsymbol{q}|$, the dispersion relation approaches to a quadratic form: $\omega \sim q^2$. A typical frequency of the exchange spin wave ranges from GHz to THz. At higher energies near the THz regime, the energy of exchange spin waves becomes comparable to the single spin flip excitation, which is called the Stoner excitation. Because these spin wave modes with high energy in the THz regime are heavily damped and thus their lifetime is quite short, they are not suitable for application to magnonic devices. Instead, for device applications there is a renewed interest in the low-energy spin wave, i.e., the dipolar spin wave which is introduced in the next subsection.

2.1.2 Dipolar spin wave

In this subsection, we address the dipolar spin wave, or equivalently, the magnetostatic spin wave. In magnetostatic spin waves, at a given wave number, the frequency of the spin wave is much lower than the that of the electromagnetic wave, and the wave length is long enough to neglect the exchange interaction. The dispersion relation of spin waves with both the exchange and dipolar interaction is given by the Herring-Kittel formula [84], which is valid only for isotropic and infinite ferromagnetic media. On the other hand, the experiments clearly show an anisotropic behavior for spin waves with small wave vectors, because the demagnetization field due to the dipolar interaction is sensitive to the shape of the magnet. Therefore, to understand magnetic excitations dominated by the dipolar interaction, numerous fundamental studies on the magnetostatic spin wave in finite systems have been made.

The spin wave in sphere-shaped magnets is studied by Walker [85]. There are various standing modes which are called Walker modes, and they are observed in experiments by White and Solt [86]. Later Röschmann and Dötsch [87] compiled a practical review, including the cases for spheroids as well as spheres.

The magnetostatic spin waves for ferromagnetic slabs and thin films were studied by Damon and Eshbach [88], and van de Vaart [89]. A detailed and nice review of the Damon-Eshbach (DE) theory was presented by Hurben and Patton [90, 91]. The DE theory has constructed a basis not only for studies of magnetic excitations in thin films and slabs of ferromagnetic materials but also for many device applications of microwave signal processing. There are three magnetostatic spin wave modes in thin films or slabs: the magnetostatic backward volume wave (MSBVW), the magnetostatic forward volume wave (MSFVW), and the magnetostatic surface wave (MSSW).

The MSBVW mode appears when the saturation magnetization and the wave vector are in-plane. This mode is reciprocal in-plane propagating mode at any angle between a magnetic field and a wave vector $\boldsymbol{k}$. "reciprocal" means that the wave can propagate both in $+\boldsymbol{k}$ and $-\boldsymbol{k}$ directions. The MSBVW mode has a negative dispersion: the spin wave frequency decreases as the wave number increases. In other words, it has a negative group velocity $\partial\omega/\partial k < 0$. If the wave vector is perpendicular to the static magnetization and the exchange interaction is neglected, all modes converge to a constant frequency, which is nothing but the FMR frequency. In modern scientific literature the MSBVW modes frequently refer only to the waves with the wave vector and static magnetization being parallel.

The MSFVW modes are similar to the MSBVW modes. The MSBVW modes appear in the situation where both the wave vector and static magnetization are in-plane. On the other hand, the MSFVW modes appear when the wave vector is in-plane but the static magnetization is perpendicular to the plane. In addition, the MSFVW modes have a positive dispersion in the sense that the frequency increases with the wave number, and they exhibit unique properties in their dynamics as we see in Chapter 5.

The MSSW modes are surface waves, which means their amplitude of the

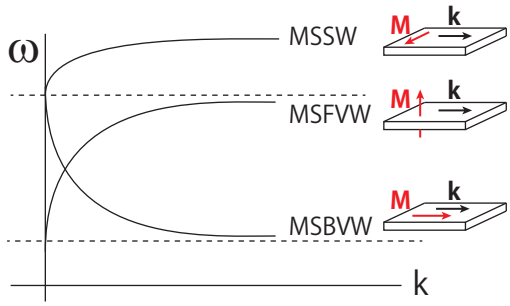

Figure 2.2: Typical dispersion relation of the magnetostatic spin waves and relative orientation between the magnetization $\boldsymbol{M}$ and wave vector $\boldsymbol{k}$.

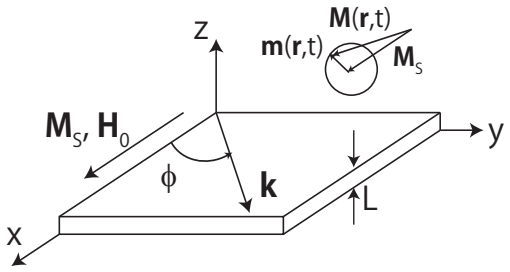

Figure 2.3: Coordinate system for calculation of the MSBVW mode ($\boldsymbol{k} = (k\cos\phi, k\sin\phi, 0)$).

dynamic magnetization is maximum at the surface of the film, and decays exponentially as a function of the distance from the surface into the bulk. The corresponding decay length is the same order as the wave length. This modes propagate nonreciprocally at angles which is larger than a critical angle, i.e., they exist only when the angle between the static magnetization and the wavevector is larger than a critical angle. "Nonreciprocal" means that it can propagate only in the either direction $+\boldsymbol{k}$ or $-\boldsymbol{k}$. In this point the MSSW modes resemble chirally moving electrons in the edge states of the quantum Hall systems. Figure 2.2 shows a typical dispersion of these three modes.

In the following we show a derivation of dispersion relations for the MSBVW mode by Damon-Eshbach approach as an example. All equations are written in SI unit and the coordinate system employed is shown in Fig. 2.3. The magnetic film lies in the xy plane and external magnetic field $\boldsymbol{H}_{\mathrm{ex}}$ is applied in the x direction so that the saturation magnetization $\boldsymbol{M}_{\mathrm{s}}$ and internal magnetic field $\boldsymbol{H}_0 = \boldsymbol{H}_{\mathrm{ex}} - \boldsymbol{M}_{\mathrm{s}}$ is parallel to the x direction. The dynamics of the

magnetization $\boldsymbol{M}$ is described by the Landau-Lifshitz equation:

$$\frac{d\boldsymbol{M}}{dt} = -\gamma \boldsymbol{M} \times \boldsymbol{H}, \tag{2.17}$$

where γ is a gyromagnetic ratio. $\boldsymbol{M}$ can be decomposed to the large saturation magnetization component and small dynamical components which rotate around $\boldsymbol{H}_0$: $\boldsymbol{M} = M_\mathrm{s}\boldsymbol{e}_x + m_y\boldsymbol{e}_y + m_z\boldsymbol{e}_z$. Similarly the magnetic field $\boldsymbol{H}$ is decomposed to the static and dynamical components: $\boldsymbol{H} = H_0\boldsymbol{e}_x + h_y\boldsymbol{e}_y + h_z\boldsymbol{e}_z$. Assuming solutions of the dynamical components $\boldsymbol{m} = \begin{pmatrix} m_y \\ m_z \end{pmatrix}$ and $\boldsymbol{h} = \begin{pmatrix} h_y \\ h_z \end{pmatrix}$ to be a plane wave with a frequency ω, one obtains the following equations from Eq. (2.17):

$$\begin{pmatrix} m_y \\ m_z \end{pmatrix} = \begin{pmatrix} \kappa & -i\nu \\ i\nu & \kappa \end{pmatrix} \begin{pmatrix} h_y \\ h_z \end{pmatrix}, \tag{2.18}$$

where

$$\kappa = \frac{\Omega_H}{\Omega_H^2 - \Omega^2}, \nu = \frac{\Omega}{\Omega_H^2 - \Omega^2}, \tag{2.19}$$

$$\Omega = \frac{\omega}{\gamma M_\mathrm{s}}, \Omega_H = \frac{H_0}{M_\mathrm{s}}. \tag{2.20}$$

By using the so-called "magnetostatic" approximation [90], the Maxwell equations are simply reduced to

$$\nabla \cdot \boldsymbol{b} = 0, \tag{2.21}$$

$$\nabla \times \boldsymbol{h} = 0, \tag{2.22}$$

where $\boldsymbol{b} = \mu_0 (\boldsymbol{h} + \boldsymbol{m})$ is a magnetic flux density and μ_0 is the magnetic permeability in vacuum. The condition Eq. (2.22) is automatically satisfied by expressing $\boldsymbol{h}$ as a gradient of a scalar magnetic potential ψ: $\boldsymbol{h} = \nabla\psi$. This magnetic potential is denoted as ψ^i for inside ($|z| < L/2$, where L is a thickness of the film) and ψ^e for outside ($|z| > L/2$) of the film, respectively,

$$\psi^\mathrm{i}(x, y, z) = X(x)Y(y)Z^\mathrm{i}(z), \tag{2.23}$$

$$\psi^\mathrm{e}(x, y, z) = X(x)Y(y)Z^\mathrm{e}(z). \tag{2.24}$$

These functions are constructed to give an in-plane propagating wave with a wave vector $\boldsymbol{k} = (k\cos\phi, k\sin\phi, 0)$,

$$X(x) = e^{i(k\cos\phi)x}, Y(y) = e^{i(k\sin\phi)y}. \tag{2.25}$$

$Z^\mathrm{i}(z)$ and $Z^\mathrm{e}(z)$ are determined by the symmetry of the film geometry so that they are harmonic solutions inside and exponentially decay outside:

$$Z^\mathrm{i}(z) = a\sin(k_z^\mathrm{i} z) + b\cos(k_z^\mathrm{i} z) \qquad (|z| < L/2), \tag{2.26}$$

$$Z^\mathrm{e}(z) = ce^{-k_z^\mathrm{e} z} \qquad (z > +L/2), \tag{2.27}$$

$$Z^\mathrm{e}(z) = de^{+k_z^\mathrm{e} z} \qquad (z < -L/2). \tag{2.28}$$

It is worth noting that k_z^{i} can be real or imaginary. A real value of k_z^{i} corresponds to a harmonic solution for $Z^{\mathrm{i}}(z)$, which is equivalent to the MSBVW mode. On the other hand, an imaginary value of k_z^{i} corresponds to a decaying exponential solution, which is equivalent to the MSSW mode. The condition $\nabla \cdot \boldsymbol{b} = \nabla \cdot (\boldsymbol{h} + \boldsymbol{m}) = 0$ leads to a differential equation for ψ^{i} and ψ^{e},

$$\left[\left(\frac{\partial^2}{\partial x^2}\right) + (1+\kappa)\left(\frac{\partial^2}{\partial y^2} + \frac{\partial^2}{\partial z^2}\right)\right]\psi^{\mathrm{i}}(x,y,z) = 0, \tag{2.29}$$

$$\left(\frac{\partial^2}{\partial x^2} + \frac{\partial^2}{\partial y^2} + \frac{\partial^2}{\partial z^2}\right)\psi^{\mathrm{e}}(x,y,z) = 0. \tag{2.30}$$

With Eqs. (2.23)-(2.30), one obtains

$$k_x^2 + (1+\kappa)\left(k_y^2 + \left(k_z^{\mathrm{i}}\right)^2\right) = 0, \tag{2.31}$$

$$k_x^2 + k_y^2 - \left(k_z^{\mathrm{e}}\right)^2 = 0. \tag{2.32}$$

The last step is to apply the usual boundary conditions for the continuity of the parallel components of $\boldsymbol{h}$ and the perpendicular component of $\boldsymbol{b}$. They yields the following relations:

$$a = \frac{c-d}{2}\frac{e^{-k_z^{\mathrm{e}}S/2}}{\sin\left(k_z^{\mathrm{i}}S/2\right)}, \tag{2.33}$$

$$b = \frac{c+d}{2}\frac{e^{-k_z^{\mathrm{e}}S/2}}{\cos\left(k_z^{\mathrm{i}}S/2\right)}. \tag{2.34}$$

It is useful to consider the ratio $(c-d)/(c+d)$,

$$\begin{aligned}\frac{c-d}{c+d} &= \frac{\nu k_y}{(1+\kappa)k_z^i \cot\left(k_z^{\mathrm{i}}S/2\right) + k_z^{\mathrm{e}}} \\ &= -\frac{(1+\kappa)k_z^{\mathrm{i}} \tan\left(k_z^{\mathrm{i}}S/2\right) - k_z^{\mathrm{e}}}{\nu k_y}.\end{aligned} \tag{2.35}$$

The second equality in Eq. (2.35) leads to

$$\left(k_z^{\mathrm{e}}\right)^2 - \left(k_z^{\mathrm{i}}\right)^2(1+\kappa)^2 - \nu^2 k^2 \sin^2\phi + 2k_z^{\mathrm{i}}k_z^{\mathrm{e}}(1+\kappa)\cot\left(k_z^{\mathrm{i}}S\right) = 0. \tag{2.36}$$

Here, the parameters k_z^{i} and k_z^{e} are related to k from (2.31) and (2.32),

$$k_z^{\mathrm{i}} = \pm k\sqrt{-\frac{1+\kappa\sin^2\phi}{1+\kappa}}, \tag{2.37}$$

$$k_z^{\mathrm{e}} = k. \tag{2.38}$$

Consequently, the dispersion relation is given by the following equations,

$$\begin{aligned}&(1+\kappa)^2\left(-\frac{1+\kappa\sin^2\phi}{1+\kappa}\right) + \nu^2\sin^2\phi - 1 \\ &-2(1+\kappa)\sqrt{-\frac{1+\kappa\sin^2\phi}{1+\kappa}}\cot\left(k_z^{\mathrm{i}}S\right) = 0.\end{aligned} \tag{2.39}$$

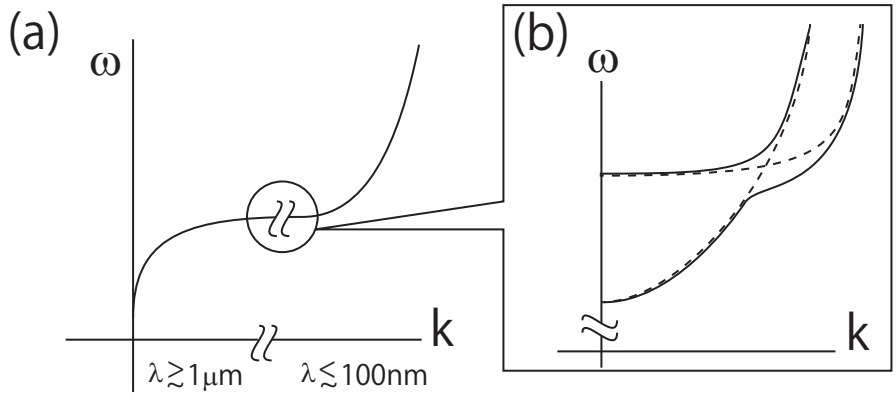

Figure 2.4: (a) Dispersion relation of a MSFVW mode and (b) a dipole hybridisation when exchange and dipolar interactions coexist. The horizontal axis is drawn with a logarithmic scale. The solid lines denote the dispersion curves with dipole hybridization.

Since $k_z^{\mathrm{i}} > 0$ for MSBVW mode, there is a restriction for the spin wave frequency Ω from Eq. (2.37). By using $\kappa = \frac{\Omega_H}{\Omega_H^2 - \Omega^2}$, the inside of the square root of Eq. (2.37) is rewritten as

$$-\frac{1+\kappa\sin^2\phi}{1+\kappa} = \frac{\Omega^2 - \Omega_H(\Omega_H + \sin^2\phi)}{\Omega_H(\Omega_H+1) - \Omega^2}. \tag{2.40}$$

Thus the value of Ω lies in the region

$$\sqrt{\Omega_H(\Omega_H + \sin^2\phi)} < \Omega < \sqrt{\Omega_H(\Omega_H+1)}. \tag{2.41}$$

If the propagating angle ϕ becomes larger, the width of the MSBVW band becomes smaller. If $\phi = \pi/2$ then all MSBVW bands are degenerated to $\Omega = \sqrt{\Omega_H(\Omega_H+1)}$, which is the FMR frequency.

2.1.3 Cross-over regime

Here we briefly mention roles of the dipolar and exchange interaction in constructing dispersion relations of spin waves. In the range of a long wave length, the dipolar interaction determines the slope of the spin wave dispersion curves. On the other hand, in the short wave length regime, the exchange interaction plays the same role and the dispersion relation follows the usual quadratic law ($\omega \propto k^2$). Figure. 2.4 (a) shows the schematic illustration of the dispersion relation of the MSFVW mode, as an example. There are a number of modes depending on the number of nodes in the direction perpendicular to the film. They are degenerate at $k = 0$ when the exchange interaction is ignored. When

the exchange interaction is taken into account, in the regime of intermediate wavenumber, there is a hybridisation of the spin wave dispersion, shown as Fig. 2.4 (b). The exchange interaction shifts up the dispersion branches [92]. The frequency shift increases as the index n become larger and the film becomes thinner. This shift removes the degeneracy of spin wave bands at $\boldsymbol{k} = 0$ and gives rise to crossings of dispersion curves (the broken line in Fig. 2.4 (b)). If these branches have similar symmetry [93], repulsion between dispersion branches occurs at these crossing points (the solid line in Fig. 2.4 (b)). Consequently, a "dipole gap" appears in the spin wave spectrum. However, in this thesis we consider the regime where either the exchange interaction or the dipole-dipole interaction exist. Thus the band crossing is not taken into account in the following context.

2.2 Experimental material for spin waves

In this section we review the material YIG ($Y_3Fe_5O_{12}$), which is a popular material in experiments of spin waves. In order to realize device applications of spin waves, one of the most important themes is to find a magnetic material which has a small damping parameter for spin wave propagation. The magnon lifetime in iron or in permalloy (Ni81Fe19), which is commonly used in experiments, is of the order of nanoseconds [94,95]. The corresponding mean free path of the spin wave is less than 10 [μm] [96, 97]. In this point of view, YIG is an excellent material for spin waves: it has low-damping parameter $\alpha \sim 10^{-4}$–10^{-5} and allows spin waves to propagate over centimeter distance. Therefore YIG is widely used both for microwave devices and for study of spin wave dynamics.

YIG has a complicated cubic crystal structure with its lattice constant is 12.376 [Å]. Each unit cell contains 80 atoms, where twenty magnetic Fe^{3+} ions are distributed over two antiferromagnetically coupled octahedral (8 ions) and tetrahedral (12 ions) sub-lattices. For device applications, a high-quality thin film of YIG is required. According to the recent studies, the best way for producing thin films is to grow by high-temperature liquid phase epitaxy on gallium gadolinium garnet (GGG) substrates [98–100]. Since the lattice constant of GGG (12.383 Å) is well matched to YIG, fabrication of high quality films is possible. It is known that the best matching is obtained by light doping of lanthanum or gallium into YIG [100]. Such high-quality thin films will present advantages for magnetostatic wave devices in the point of low cost, small size, and compatibility with planar circuit designs.

2.3 Geometric phase

In early stages of the development of quantum mechanics, it is known that physical quantities is derived as an expectation value of an observable operator with an eigen wave function. In the expectation value, a phase factor of the wavefunction cancels out. Thus the phase factor was believed not to play a

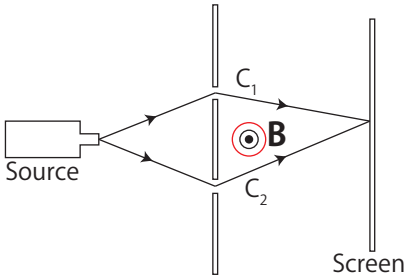

Figure 2.5: Schematic of the Aharonov-Bohm effect in a double-slit experiment. The magnetic field is confined by an infinitely long solenoid (a red circle in the figure).

significant role in physical phenomena. However, it is discovered by Pancharatnam in 1956 [101] and rediscovered by Berry in 1984 [102] that an additional phase factor appears in adiabatically evolving systems and is not negligible in quantum mechanics. It is called geometric phase.

As a good example for appearance of the geometric phase, let us first mention the Aharonov-Bohm (AB) effect [103] briefly. We consider a double-slit experiment of electron beams with a local magnetic field $\boldsymbol{B}$ (Fig. 2.5). Without the magnetic field, the electrons go through the double slits and form an interference pattern on the screen. If the magnetic field is nonzero but confined by an infinitely long solenoid and two electron paths C_1 and C_2 are far away from the solenoid, the field does not affect the electrons from a classical point of view. However, in quantum mechanics, the magnetic field appears as a vector potential $\boldsymbol{A}$ in the Schrödinger equation:

$$i\hbar\frac{\partial}{\partial t}\psi = \left[\frac{1}{2m}\left(\frac{\hbar}{i}\nabla + e\boldsymbol{A}\right)^2\right]\psi, \tag{2.42}$$

where m is a mass of the electron and $-e$ is the electron charge. Putting the solution of Eq. (2.42) with $\boldsymbol{A} = 0$ as $\psi_0(\boldsymbol{r})$, one derives $\psi(\boldsymbol{r})$ as

$$\psi(\boldsymbol{r}) = \psi_0(\boldsymbol{r})\exp\left(-i\frac{e}{\hbar}\int_{C_i}^{\boldsymbol{r}}\boldsymbol{A}\cdot d\boldsymbol{l}\right), \tag{2.43}$$

where $C_i (i = 1, 2)$ is a path of the line integration. Eq. (2.43) means that the electron through the path C_i acquires a phase $\phi_i = -\frac{e}{\hbar}\int_{C_i}\boldsymbol{A}\cdot d\boldsymbol{l}$. Therefore the phase difference between the two paths are obtained as

$$\Delta\phi = \phi_1 - \phi_2 = \frac{e}{\hbar}\oint_C \boldsymbol{A}\cdot d\boldsymbol{l} = \frac{e}{\hbar}\iint_S \boldsymbol{B}dS = \frac{e\Phi}{\hbar}. \tag{2.44}$$

S is a surface which is enclosed by the loop $C = C_2 - C_1$, Φ is a magnetic flux inside the solenoid, and we have used the Stokes theorem in Eq. (2.44).

Consequently, the interference pattern shifts due to this additional phase. It is worth noting that $\Delta\phi$ does not rely on details of the path: its value only depends on whether the loop C encloses the solenoid or not. This represents the geometric aspect of the geometric phase.

Now we return to the general geometric phase. Because this concept has been formulated by Berry, the geometric phase is commonly called the Berry phase. In the rest of this section we follow Berry's original paper [102] to derive the general formula of the Berry phase.

Let us consider a Hamiltonian which depends on variable parameters $\boldsymbol{R} = (X, Y, \dots)$. These parameters adiabatically change with time from $t = 0$ to $t = T$, and forms a closed path such that $\boldsymbol{R}(t = 0) = \boldsymbol{R}(t = T)$. At any moment there are eigenstates $|n(\boldsymbol{R})\rangle$ of the Hamiltonian $H(\boldsymbol{R}(t))$ for $\boldsymbol{R} = \boldsymbol{R}(t)$: $H(\boldsymbol{R})\,|n(\boldsymbol{R})\rangle = E_n(\boldsymbol{R})\,|n(\boldsymbol{R})\rangle$, with eigen energies $E_n(\boldsymbol{R})$. We assume that the eigenvalues have no degeneracies. As an initial condition, the state $|\psi(t)\rangle$ is assumed to be equal to the n-th eigenstate for $\boldsymbol{R}(t = 0)$. The adiabatic condition requires that the state stays the same n-th eigenstate during the time evolution. Within this condition, the wave function $|\psi(t)\rangle$ at t is written as

$$|\psi(t)\rangle = \exp\left(-\frac{i}{\hbar}\int_0^t dt' E_n(\boldsymbol{R}(t'))\right)\exp(i\gamma_n(t))\,|n(\boldsymbol{R}(t))\rangle\,. \tag{2.45}$$

The first exponential is a usual dynamical phase factor, and the second one $\exp(i\gamma_n(t))$ is the Berry phase. $\gamma_n(t)$ is determined by the fact that $|\psi(t)\rangle$ satisfies the Schrödinger equation, that leads to

$$\dot{\gamma}_n(t) = i\,\langle n(\boldsymbol{R}(t))|\,\nabla_{\boldsymbol{R}} n(\boldsymbol{R}(t))\rangle\cdot\dot{\boldsymbol{R}}(t). \tag{2.46}$$

Thus the total geometric phase change, namely the Berry phase, is

$$\gamma_n(C) = i\oint_C \langle n(\boldsymbol{R})|\,\nabla_{\boldsymbol{R}} n(\boldsymbol{R})\rangle\cdot d\boldsymbol{R}, \tag{2.47}$$

where C is a path in the parameter space from $t = 0$ to $t = T$. In Eq. (2.47), we define a quantity

$$\boldsymbol{\mathcal{A}}_n(\boldsymbol{R}) \equiv i\,\langle n(\boldsymbol{R})|\,\nabla_{\boldsymbol{R}} n(\boldsymbol{R})\rangle\,, \tag{2.48}$$

which is called the Berry connection. Compared with the AB effect, the Berry connection corresponds to the vector potential in the parameter space. In addition, if the parameter space $\boldsymbol{R}$ is three-dimensional, in analogy to the magnetic field $\boldsymbol{B} = \nabla\times\boldsymbol{A}$, we can also define a quantity,

$$\boldsymbol{\omega}_n(\boldsymbol{R}) \equiv \nabla\times\boldsymbol{\mathcal{A}}_n(\boldsymbol{R}), \tag{2.49}$$

which is called the Berry curvature. If we perform the gauge transformation,

$$|n(\boldsymbol{R})\rangle \to e^{i\chi(\boldsymbol{R})}\,|n(\boldsymbol{R})\rangle\,, \tag{2.50}$$

$\boldsymbol{\mathcal{A}}_n(\boldsymbol{R})$ transforms as

$$\boldsymbol{\mathcal{A}}_n(\boldsymbol{R}) \to \boldsymbol{\mathcal{A}}_n(\boldsymbol{R}) - \nabla_{\boldsymbol{R}}\chi(\boldsymbol{R}). \tag{2.51}$$

Therefore the Berry curvature is a gauge invariant. Like a magnetic field influencing on the dynamics of electrons as the Lorentz force, the Berry curvature also affects dynamics of a wavepacket in crystals, as we see in Ch. 5.

Chapter 3

Thermal Hall effect of exchange magnon in Ferro magnets

3.1 Introduction

For purpose of manipulating magnon propagation, Hall effect is one of the useful and fundamental phenomena. Recently the thermal Hall effect of magnons is studied both theoretically [76–78] and experimentally [79,80]. Fujimoto showed that a transversal magnon current is induced by a longitudinal gradient of a magnetic field in a noncoplanar spin structure [76]. Katsura *et al.* showed that the thermal Hall effect of magnons occurs even in a collinear ferromagnet with a particular lattice structure such as the Kagomé lattice, by using the linear response theory [77]. Later we studied dynamics of a wavepacket of magnons by using the semiclassical theory in analogy with electrons, and derived a correction term for the thermal Hall conductivity due to an orbital motion of magnons, which is missing in Ref. [77]. There it is clarified that the thermal Hall conductivity of magnons is expressed in terms of the Berry curvature in momentum space. We also derived the same result by using the linear response theory with the temperature gradient, which was developed by Smrčka and Středa in electron systems [104]. On the other hand, in experiments, Onose *et al.* succeeded in observing the thermal Hall effect of magnons in $Lu_2V_2O_7$, which is a ferromagnetic insulator with pyrochlore structure [79]. In addition, Ideue *et al.* observed the thermal Hall effect of magnons in various ferromagnetic insulators with the Dzyaloshinskii-Moriya (DM) interaction in pyrochlore and perovskite structure, and discussed the geometric and topological aspect of the magnon Hall effect which is caused by the Berry curvature due to the DM interaction [80].

In this section, the linear response theory to a temperature gradient and

the orbital motions of magnons are discussed. Besides the thermal transport coefficient from the Kubo formula in the previous works [77, 79], we find another contribution to the thermal transport coefficient. The total thermal Hall conductivity is expressed in terms of the Berry curvature in momentum space. Our results for the thermal Hall conductivity in $Lu_2V_2O_7$ roughly reproduces the experiment [79]. For simplicity we study exchange magnons in ferromagnets here, where the dipolar interaction is negligible. Later more complex systems, such as exchange magnons in antiferromagnets and magnetostatic spin waves, are studied in Ch. 4.

3.2 Linear response theory

Here we shortly discuss the linear response theory to external fields [104–110]. In the presence of the temperature gradient, it is convenient to introduce a fictitious gravitational potential $\psi(\boldsymbol{r})$, which exerts a force proportional to the energy of the particle [111]. This is because in order to obtain the thermal transport coefficients by the linear response theory, the temperature gradient should be taken into the Hamiltonian as an external field. However, it is not possible to directly incorporate the temperature gradient into the linear response theory, since the temperature gradient is not a dynamical force which exerts force to the particles, but a statistical force which affects the particles through the distribution function. Therefore, to avoid this difficulty, the fictitious potential ψ, giving a dynamical force, has been introduced. As we see below, the thermal transport coefficients from the temperature gradient are derived by calculating the coefficient from the gradient of the fictitious potential ψ. This is analogous to the fact that the calculation of the transport coefficients from the gradient of the chemical potential can be obtained by calculating the coefficients from the electric field.

In the following we first review the work by Smrčka and Středa [104,105] for the electron systems, in order to derive some identities which are useful to the calculation for the magnon systems.

3.2.1 Electron system

The relation of both the electric current and the energy current to the fields can be written as

$$\boldsymbol{J} = (L^F)_{11}\left[\boldsymbol{E} + \tfrac{T}{e}\nabla\left(\tfrac{\mu}{T}\right)\right] + (L^F)_{12}\left[T\nabla\left(\tfrac{1}{T}\right) - \tfrac{\nabla\psi}{c^2}\right], \tag{3.1}$$

$$\boldsymbol{J}_{\mathrm{E}} = (L^F)_{12}\left[\boldsymbol{E} + \tfrac{T}{e}\nabla\left(\tfrac{\mu}{T}\right)\right] + (L^F)_{22}\left[T\nabla\left(\tfrac{1}{T}\right) - \tfrac{\nabla\psi}{c^2}\right], \tag{3.2}$$

where the superscript "F" means a fermion, $\boldsymbol{E}$ is an electric field, $-e$ ($e > 0$) is the electron charge, μ is the chemical potential, T is the temperature, $(L^F)_{ij}$ is the transport coefficients ($i, j = 1, 2$), c is the speed of light and ψ is the gravitational field. The external electrostatic potential $\phi(\boldsymbol{r})$ and the

gravitational potential $\psi(\boldsymbol{r})$ are assumed to be linear in the coordinate $\boldsymbol{r}$,

$$\phi(\boldsymbol{r}) = -\boldsymbol{E}\cdot\boldsymbol{r}, \quad \psi(\boldsymbol{r}) = \boldsymbol{r}\cdot\nabla\psi. \tag{3.3}$$

In the presence of these fields, the Hamiltonian of the system is written as

$$H_{\rm T} = H + F \equiv \sum_j H_j, \tag{3.4}$$

where H is the unperturbed Hamiltonian, j is an index for particles, and F describes the interaction with the applied fields [104, 105],

$$F = \sum_j (-e)\boldsymbol{E}\cdot\boldsymbol{r}_j + \frac{1}{2}\left\{H_j, \frac{1}{c^2}\sum_j \boldsymbol{r}_j\cdot\nabla\psi(\boldsymbol{r})\right\}. \tag{3.5}$$

Here $\{\hat{A},\hat{B}\} = \hat{A}\hat{B}+\hat{B}\hat{A}$ represents the anticommutator. The electric current $\boldsymbol{j}(\boldsymbol{r})$ and energy current operator $\boldsymbol{j}_{\rm E}(\boldsymbol{r})$ are defined by the equations of continuity:

$$\frac{\partial n(\boldsymbol{r})}{\partial t} = \frac{1}{i\hbar}[n(\boldsymbol{r}), H_{\rm T}] = -\nabla\cdot\boldsymbol{j}(\boldsymbol{r}), \tag{3.6}$$

$$\frac{\partial h_{\rm T}(\boldsymbol{r})}{\partial t} = \frac{1}{i\hbar}[h_{\rm T}(\boldsymbol{r}), H_{\rm T}] = -\nabla\cdot\boldsymbol{j}_{\rm E}(\boldsymbol{r}). \tag{3.7}$$

$n(\boldsymbol{r}) = \sum_j e\delta(\boldsymbol{r}-\boldsymbol{r}_j)$ is a particle density and $h(\boldsymbol{r}) = \frac{1}{2}\sum_j\{H,\delta(\boldsymbol{r}-\boldsymbol{r}_j)\}$ is a hamiltonian density. From Eqs. (3.6) and (3.7), one obtains

$$\boldsymbol{j}(\boldsymbol{r}) = \boldsymbol{j}^{(0)}(\boldsymbol{r}) + \boldsymbol{j}^{(1)}(\boldsymbol{r}) = \boldsymbol{j}^{(0)}(\boldsymbol{r}) + \frac{1}{2}\left\{\boldsymbol{j}^{(0)}(\boldsymbol{r}), \frac{1}{c^2}\sum_j \boldsymbol{r}_j\cdot\nabla\psi(\boldsymbol{r})\right\}, \tag{3.8}$$

$$\begin{aligned}\boldsymbol{j}_{\rm E}(\boldsymbol{r}) &= \boldsymbol{j}_E^{(0)}(\boldsymbol{r}) + \boldsymbol{j}_{\rm E}^{(1)}(\boldsymbol{r}) \\ &= \boldsymbol{j}_{\rm E}^{(0)}(\boldsymbol{r}) + \frac{1}{2}\left\{\phi(\boldsymbol{r}_j), \boldsymbol{j}^{(0)}(\boldsymbol{r})\right\} \\ &\quad + \frac{1}{4c^2}\sum_j\left(\left\{\left\{H, \boldsymbol{r}_j\cdot\nabla\psi(\boldsymbol{r})\right\}, v_j\right\} + \left\{\left\{v_j, \boldsymbol{r}_j\cdot\nabla\psi(\boldsymbol{r})\right\}, H\right\}\right),\end{aligned} \tag{3.9}$$

where $\boldsymbol{r}_j$ denotes the position of the jth electron, $\boldsymbol{j}^{(0)}(\boldsymbol{r}) = -\frac{e}{2}\sum_j\{\boldsymbol{v}_j,\delta(\boldsymbol{r}-\boldsymbol{r}_j)\}$ with $\boldsymbol{v}_j$ being the velocity operator of the jth electron, $\boldsymbol{j}_{\rm E}^{(0)}(\boldsymbol{r}) = -\frac{1}{2e}\left\{H,\boldsymbol{j}^{(0)}(\boldsymbol{r})\right\}$. We note that $\boldsymbol{r}_j$ is a quantum mechanical operator, while $\boldsymbol{r}$ is a c-number. As seen below, these additional terms $\boldsymbol{j}^{(1)}(\boldsymbol{r})$ and $\boldsymbol{j}_{\rm E}^{(1)}(\boldsymbol{r})$ produce correction terms for the thermal transport coefficients. The measurable current densities are obtained by taking the quantum-mechanical and thermodynamic averages of these current operators, i.e.,

$$\begin{aligned}\boldsymbol{J} &= {\rm Tr}[g(H)\boldsymbol{j}(\boldsymbol{r})] \\ &= {\rm Tr}[f_0(H)\boldsymbol{j}^{(0)}(\boldsymbol{r})] + {\rm Tr}[f_0(H)\boldsymbol{j}^{(1)}(\boldsymbol{r})] + {\rm Tr}[f_1(H)\boldsymbol{j}^{(0)}(\boldsymbol{r})],\end{aligned} \tag{3.10}$$

$$\begin{aligned}\boldsymbol{J}_{\rm E} &= {\rm Tr}[g(H)\boldsymbol{j}_{\rm E}(\boldsymbol{r})] \\ &= {\rm Tr}[f_0(H)\boldsymbol{j}_{\rm E}^{(0)}(\boldsymbol{r})] + {\rm Tr}[f_0(H)\boldsymbol{j}_{\rm E}^{(1)}(\boldsymbol{r})] + {\rm Tr}[f_1(H)\boldsymbol{j}_{\rm E}^{(0)}(\boldsymbol{r})],\end{aligned} \tag{3.11}$$

where $g(H)$ is the density matrix $g(H) = f_0(H) + f_1(H)$, $f_0(H)$ is the Fermi distribution function $f_0(H) = f(H)$, $f(\eta) = (e^{(\eta-\mu)/k_{\rm B}T} + 1)^{-1}$ and $f_1(H)$ is the deviation from the equilibrium due to the fields. Thus the thermal transport coefficients $(L^F)^{\alpha\beta}_{ij}$, which are expressed as $(L^F)^{\alpha\beta}_{ij} = (S^F)^{\alpha\beta}_{ij} + (M^F)^{\alpha\beta}_{ij}$ $(\alpha, \beta = x, y, z)$, can be obtained from the equation (3.10) and (3.11):

$$(S^F)^{\alpha\beta}_{ij} = \frac{i\hbar}{V}\int f(\eta){\rm Tr}\left(j_i^\alpha \frac{dG^+}{d\eta} j_j^\beta \delta(\eta - H) - j_i^\alpha \delta(\eta - H) j_j^\beta \frac{dG^-}{d\eta}\right) d\eta, \tag{3.12}$$

$$(M^F)^{\alpha\beta}_{11} = 0, \quad (M^F)^{\alpha\beta}_{12} = -\frac{e}{2V}\int f(\eta){\rm Tr}[\delta(\eta - H)(r^\alpha v^\beta - r^\beta v^\alpha)]d\eta, \tag{3.13}$$

$$\begin{aligned}(M^F)^{\alpha\beta}_{22} &= \frac{1}{V}\int \eta f(\eta){\rm Tr}\delta(\eta - H)(r^\alpha v^\beta - r^\beta v^\alpha)d\eta \\ &\quad + \frac{i\hbar}{4V}\int f(\eta){\rm Tr}\delta(\eta - H)[v^\alpha, v^\beta]d\eta.\end{aligned} \tag{3.14}$$

Here H is the unperturbed Hamiltonian of the system, V is a volume of the system, $f(\eta) = (e^{(\eta-\mu)/k_{\rm B}T} + 1)^{-1}$ is the Fermi distribution function, $G^\pm$ is the Green's function $G^\pm(\eta) = (\eta - H \pm i\epsilon)^{-1}$ which is introduced in equation (3.12) via $\delta(\eta - H) = -(G^+ - G^-)/2\pi i$, $\boldsymbol{j}_1 = -e\boldsymbol{v}$, $\boldsymbol{j}_2 = \frac{1}{2}(H\boldsymbol{v} + \boldsymbol{v}H)$, and v is the velocity. $(S^F)^{\alpha\beta}_{ij}$ represent results from the usual Kubo formula since the equation (3.12) is indeed the Kubo formula itself; $(M^F)^{\alpha\beta}_{ij}$ represent the correction terms.

From these results derived by Smrčka and Středa, some useful equations are derived which are applicable for generic systems including magnon systems. First, $(S^F)^{\alpha\beta}_{ij}$ is expressed in terms of Berry phase by taking the trace. For example, $(S^F)^{\alpha\beta}_{12}$ is written as follows:

$$\begin{aligned}(S^F)^{\alpha\beta}_{12} &= -\frac{i\hbar e}{2V}\int f(\eta) \\ &\times {\rm Tr}\left(v^\alpha \frac{dG^+}{d\eta}\left(v^\beta H + Hv^\beta\right)\delta(\eta - H) - v^\alpha \delta(\eta - H)\left(v^\beta H + Hv^\beta\right)\frac{dG^-}{d\eta}\right)d\eta \\ &= -\frac{i\hbar e}{2V}\int f(\eta) \\ &\times \sum_{\lambda,\nu}\left(-\langle u_\lambda|v^\alpha|u_\nu\rangle \frac{1}{(\eta - \varepsilon_\nu)^2}\left(\langle u_\nu|v^\beta|u_\lambda\rangle\varepsilon_\lambda + \varepsilon_\nu\langle u_\nu|v^\beta|u_\lambda\rangle\right)\delta(\eta - \varepsilon_\lambda)\right. \\ &\qquad \left. + \langle u_\lambda|v^\alpha|u_\nu\rangle\delta(\eta - \varepsilon_\nu)\left(\langle u_\nu|v^\beta|u_\lambda\rangle\varepsilon_\lambda + \varepsilon_\nu\langle u_\nu|v^\beta|u_\lambda\rangle\right)\frac{1}{(\eta - \varepsilon_\lambda)^2}\right)d\eta \\ &= -\frac{e}{\hbar V}{\rm Im}\sum_\lambda\left(f(\varepsilon_\lambda)\left\langle\frac{\partial u_\lambda}{\partial k_\alpha}\right|(H + \varepsilon_\lambda)\left|\frac{\partial u_\lambda}{\partial k_\beta}\right\rangle\right).\end{aligned} \tag{3.15}$$

Here we have used the relation $\langle u_\lambda|v^\alpha|u_\nu\rangle = \langle u_\lambda|\frac{1}{\hbar}\frac{\partial H}{\partial k_\alpha}|u_\nu\rangle = \frac{(\varepsilon_\lambda - \varepsilon_\nu)}{\hbar}\left\langle\frac{\partial u_\lambda}{\partial k_\alpha}\right|u_\nu\rangle$, the indices λ, ν denote both the band index n and wave number $\boldsymbol{k}$, and u is the

periodic part of the Bloch wave function. Second, at zero temperature, $(L^F)_{12}^{\alpha\beta}$ and $(S^F)_{12}^{\alpha\beta}$ is written as

$$(L^F)_{12}^{\alpha\beta} = \frac{\mu}{-e}(L^F)_{11}^{\alpha\beta} = -\frac{2e\mu}{\hbar V}\sum_{\lambda}\Theta(\mu-\varepsilon_\lambda)\mathrm{Im}\left\langle\frac{\partial u_\lambda}{\partial k_\alpha}\middle|\frac{\partial u_\lambda}{\partial k_\beta}\right\rangle, \tag{3.16}$$

$$(S^F)_{12}^{\alpha\beta} = -\frac{2e}{\hbar V}\mathrm{Im}\sum_{\lambda}\Theta(\mu-\varepsilon_\lambda)\left\langle\frac{\partial u_\lambda}{\partial k_\alpha}\middle|\left(\frac{H+\varepsilon_\lambda}{2}\right)\middle|\frac{\partial u_\lambda}{\partial k_\beta}\right\rangle. \tag{3.17}$$

It is to be noted that the Fermi distribution function $f(\eta)$ becomes the step function $\Theta(\mu-\eta)$ at zero temperature. Using the relation $(L^F)_{12}^{\alpha\beta} = (S^F)_{12}^{\alpha\beta} + (M^F)_{12}^{\alpha\beta}$ and equation (3.13) in the zero temperature limit, one obtains the following relation:

$$\begin{aligned}
&\mathrm{Tr}[\delta(\mu-H)(r^\alpha v^\beta - r^\beta v^\alpha)] \\
&= \frac{d}{d\mu}\int_{-\infty}^{\mu}\mathrm{Tr}[\delta(\eta-H)(r^\alpha v^\beta - r^\beta v^\alpha)]d\eta = \frac{2V}{-e}\frac{d}{d\mu}\,(M^F)_{12}^{\alpha\beta}\Big|_{T\to 0} \\
&= -\frac{2}{\hbar}\frac{d}{d\mu}\sum_{\lambda}\Theta(\mu-\varepsilon_\lambda)\mathrm{Im}\left\langle\frac{\partial u_\lambda}{\partial k_\alpha}\middle|\,(H+\varepsilon_\lambda-2\mu)\,\middle|\frac{\partial u_\lambda}{\partial k_\beta}\right\rangle.
\end{aligned} \tag{3.18}$$

This equation is useful for the later calculation in the next section. It is worth noting that the l.h.s. of equation (3.18) corresponds to the orbital angular momentum. Hence by following the theories in [106–110], one can also derive equation (3.18) directly. It turns out that equation (3.18) holds whichever the particle is a boson or a fermion. Therefore this equation (3.18) is applicable to the magnon system as well.

3.2.2 Magnon system

Now we consider the magnon systems. Since the magnon has no charge, it is impossible to use the electric field $\boldsymbol{E}$ as an external field to drive magnons. Instead, the gradient of the confining potential $-\nabla U(r)$ for magnons is adopted here. The confining potential for magnons are discussed in appendix A. In a similar way as in Refs. [104, 105], the perturbation Hamiltonian is written as $H' = \sum_j U(\boldsymbol{r}_j) + \frac{1}{2}\left\{H, \frac{1}{c^2}\sum_j \boldsymbol{r}_j\cdot\nabla\psi(\boldsymbol{r})\right\}$, where $\mathrm{r_j}$ is the position of the jth magnon, and H is the unperturbed Hamiltonian. In equilibrium, the magnon current density and energy current density are written as

$$\boldsymbol{j}^{(0)}(\boldsymbol{r}) = \frac{1}{2}\sum_j\left\{\boldsymbol{v}_j, \delta(\boldsymbol{r}-\boldsymbol{r}_j)\right\}, \tag{3.19}$$

$$\boldsymbol{j}_E^{(0)}(\boldsymbol{r}) = \frac{1}{2}\left\{H, \boldsymbol{j}^{(0)}(\boldsymbol{r})\right\}, \tag{3.20}$$

where $\boldsymbol{v}_j$ is the velocity operator of the jth magnon. In the presence of the external fields H', they acquire additional terms,

$$\boldsymbol{j}(\boldsymbol{r}) = \boldsymbol{j}^{(0)}(\boldsymbol{r}) + \frac{1}{2}\left\{\boldsymbol{j}^{(0)}(\boldsymbol{r}), \frac{1}{c^2}\sum_j \boldsymbol{r}_j \cdot \nabla\psi(\boldsymbol{r})\right\}, \tag{3.21}$$

$$\begin{aligned}\boldsymbol{j}_E(\boldsymbol{r}) = \boldsymbol{j}_E^{(0)}(\boldsymbol{r}) &+ \frac{1}{2}\sum_j \left\{U(\boldsymbol{r}_j), \boldsymbol{j}^{(0)}(\boldsymbol{r})\right\} \\ &+ \frac{1}{4c^2}\sum_j \left(\left\{\left\{H, \boldsymbol{r}_j \cdot \nabla\psi(\boldsymbol{r})\right\}, \boldsymbol{j}^{(0)}(\boldsymbol{r})\right\}\right. \\ &+ \left.\left\{\left\{\boldsymbol{j}^{(0)}(\boldsymbol{r}), \boldsymbol{r}_j \cdot \nabla\psi(\boldsymbol{r})\right\}, H\right\}\right),\end{aligned} \tag{3.22}$$

where c is the speed of light. In this section the thermal transport coefficients $(L)_{ij}^{\alpha\beta}$ are defined as:

$$\boldsymbol{J} = (L)_{11}\left[-\nabla U - T\nabla\left(\frac{\mu}{T}\right)\right] + (L)_{12}\left[T\nabla\left(\frac{1}{T}\right) - \frac{\nabla\psi}{c^2}\right], \tag{3.23}$$

$$\boldsymbol{J}_E = (L)_{12}\left[-\nabla U - T\nabla\left(\frac{\mu}{T}\right)\right] + (L)_{22}\left[T\nabla\left(\frac{1}{T}\right) - \frac{\nabla\psi}{c^2}\right], \tag{3.24}$$

where $\alpha, \beta = x, y$, $i, j = 1, 2$. Corresponding to the additional terms to $\boldsymbol{j}(\boldsymbol{r})$ and $\boldsymbol{j}_E(\boldsymbol{r})$, the thermal transport coefficients consist of two parts: $(L)_{ij}^{\alpha\beta} = (S)_{ij}^{\alpha\beta} + (M)_{ij}^{\alpha\beta}$. A deviation of the distribution function from the equilibrium state generates $(S)_{ij}^{\alpha\beta}$, which is calculated by the Kubo formula; a deviation of the current operator due to external fields from the equilibrium state generates $(M)_{ij}^{\alpha\beta}$. In the clean limit they are expressed as

$$(S^B)_{ij}^{\alpha\beta} = \frac{i\hbar}{V}\int \rho(\eta)\mathrm{Tr}\left(j_i^\alpha \frac{dG^+}{d\eta} j_j^\beta \delta(\eta - H) - j_i^\alpha \delta(\eta - H) j_j^\beta \frac{dG^-}{d\eta}\right) d\eta, \tag{3.25}$$

$$(M^B)_{11}^{\alpha\beta} = 0, \quad (M^B)_{12}^{\alpha\beta} = \frac{1}{2V}\int \rho(\eta)\mathrm{Tr}[\delta(\eta - H)(r^\alpha v^\beta - r^\beta v^\alpha)]d\eta, \tag{3.26}$$

$$\begin{aligned}(M^B)_{22}^{\alpha\beta} = &\frac{1}{V}\int \eta\rho(\eta)\mathrm{Tr}\delta(\eta - H)(r^\alpha v^\beta - r^\beta v^\alpha)d\eta \\ &+ \frac{i\hbar}{4V}\int \rho(\eta)\mathrm{Tr}\delta(\eta - H)[v^\alpha, v^\beta]d\eta.\end{aligned} \tag{3.27}$$

Here $G^\pm$ is the Green's function $G^\pm(\eta) = (\eta - H \pm i\epsilon)^{-1}$ with ϵ being the positive infinitesimal, $\rho(\eta)$ is the Bose distribution function $\rho(\eta) = \left(e^{\beta(\eta-\mu)} - 1\right)^{-1}$, $\boldsymbol{j}_1 = \boldsymbol{v}$, $\boldsymbol{j}_2 = \frac{1}{2}(H\boldsymbol{v} + \boldsymbol{v}H)$, $\boldsymbol{v}$ is the velocity of magnons, and the label of the superscript "B" means a boson. Like Eq. (3.15), $(S^B)_{ij}^{\alpha\beta}$ is similarly expressed by the Bloch wave function. The calculation of correction terms $(M^B)_{12}^{\alpha\beta}$ and $(M^B)_{22}^{\alpha\beta}$ in terms of Berry phase is technical, because the expectation value of

the position operator $r^{\alpha,\beta}$ is not well-defined in the Bloch representation. To calculate these terms, we apply equation (3.18) to equation (3.26) and (3.27). For example, $(M^B)^{\alpha\beta}_{12}$ is calculated as the following:

$$
\begin{aligned}
&(M^B)^{\alpha\beta}_{12} \\
&= \frac{1}{2V}\int_{-\infty}^{\infty}\rho(\eta)\left(-\frac{2}{\hbar}\frac{d}{d\eta}\sum_{\lambda}\Theta(\eta-\varepsilon_\lambda)\mathrm{Im}\left\langle\frac{\partial u_\lambda}{\partial k_\alpha}\right|(H+\varepsilon_\lambda-2\eta)\left|\frac{\partial u_\lambda}{\partial k_\beta}\right\rangle\right)d\eta \\
&= \frac{1}{\hbar V}\int_{-\infty}^{\infty}\frac{d\rho(\eta)}{d\eta}\sum_{\lambda}\left(\Theta(\eta-\varepsilon_\lambda)\mathrm{Im}\left\langle\frac{\partial u_\lambda}{\partial k_\alpha}\right|(H+\varepsilon_\lambda-2\eta)\left|\frac{\partial u_\lambda}{\partial k_\beta}\right\rangle\right)d\eta \\
&= \frac{1}{\hbar V}\sum_{\lambda}\int_{\varepsilon_\lambda}^{\infty}\frac{d\rho(\eta)}{d\eta} \\
&\quad\times\left(\mathrm{Im}\left\langle\frac{\partial u_\lambda}{\partial k_\alpha}\right|(H+\varepsilon_\lambda-2\mu)\left|\frac{\partial u_\lambda}{\partial k_\beta}\right\rangle-2(\eta-\mu)\mathrm{Im}\left\langle\frac{\partial u_\lambda}{\partial k_\alpha}\left|\frac{\partial u_\lambda}{\partial k_\beta}\right\rangle\right)d\eta\right. \\
&= \frac{1}{\hbar V}\mathrm{Im}\sum_{\lambda}\left(-c_0(\rho(\varepsilon_\lambda))\left\langle\frac{\partial u_\lambda}{\partial k_\alpha}\right|(H+\varepsilon_\lambda-2\mu)\left|\frac{\partial u_\lambda}{\partial k_\beta}\right\rangle\right. \\
&\qquad\left.+2c_1(\rho(\varepsilon_\lambda))k_\mathrm{B}T\left\langle\frac{\partial u_\lambda}{\partial k_\alpha}\left|\frac{\partial u_\lambda}{\partial k_\beta}\right\rangle\right), \qquad (3.28)
\end{aligned}
$$

where u_n is the periodic part of the Bloch wave function with the band index n and $c_q(\rho) = \int_{\varepsilon_{n\boldsymbol{k}}}^{\infty} d\varepsilon(\beta\varepsilon)^q\left(-\frac{d\rho}{d\varepsilon}\right)\Big|_{\mu=0} = \int_0^\rho\left(\log(1+t^{-1})\right)^q dt$. For example, $c_0(\rho) = \rho$, $c_1(\rho) = (1+\rho)\log(1+\rho) - \rho\log\rho$, $c_2(\rho) = (1+\rho)\left(\log\frac{1+\rho}{\rho}\right)^2 - (\log\rho)^2 - 2\mathrm{Li}_2(-\rho)$, and $\mathrm{Li}_2(z)$ is the polylogarithm function. Similarly the equations (3.25)- (3.27) are rewritten to convenient expressions,

$$(S^B)^{\alpha\beta}_{ij} = \frac{2}{\hbar V}\mathrm{Im}\sum_{n,\boldsymbol{k}}\rho_n\left\langle\frac{\partial u_n}{\partial k_\alpha}\right|\left(\frac{H+\varepsilon_{n\boldsymbol{k}}}{2}\right)^q\left|\frac{\partial u_n}{\partial k_\beta}\right\rangle, \qquad (3.29)$$

$$(M^B)^{\alpha\beta}_{11} = 0, \qquad (3.30)$$

$$(M^B)^{\alpha\beta}_{12} = -(S^B)^{\alpha\beta}_{12} + \frac{2}{\hbar V}\mathrm{Im}\sum_{n,\boldsymbol{k}}\left[(\mu\rho_n + k_\mathrm{B}Tc_1(\rho_n))\left\langle\frac{\partial u_n}{\partial k_\alpha}\left|\frac{\partial u_n}{\partial k_\beta}\right\rangle\right], \qquad (3.31)$$

$$
\begin{aligned}
&(M^B)^{\alpha\beta}_{22} = -(S^B)^{\alpha\beta}_{22} \\
&+\frac{2}{\hbar V}\mathrm{Im}\sum_{n,\boldsymbol{k}}\left[\left(\mu^2\rho_n + 2\mu k_\mathrm{B}Tc_1(\rho_n) + (k_\mathrm{B}T)^2c_2(\rho_n)\right)\left\langle\frac{\partial u_n}{\partial k_\alpha}\left|\frac{\partial u_n}{\partial k_\beta}\right\rangle\right], \qquad (3.32)
\end{aligned}
$$

where $\rho_n = \rho(\varepsilon_{n,\boldsymbol{k}})$. Therefore, the thermal transport coefficients $L^B(= S^B + M^B)$ for the magnon system can be written in terms of the wave function of

magnons:

$$(L^B)^{\alpha\beta}_{11} = -\frac{1}{\hbar V}\sum_{n,\boldsymbol{k}} \rho_n \Omega^z_n(\boldsymbol{k}), \tag{3.33}$$

$$(L^B)^{\alpha\beta}_{12} = -\frac{1}{\hbar V}\sum_{n,\boldsymbol{k}} \left(\mu\rho_n + k_{\mathrm{B}}Tc_1(\rho_n)\right)\Omega^z_n(\boldsymbol{k}), \tag{3.34}$$

$$(L^B)^{\alpha\beta}_{22} = -\frac{1}{\hbar V}\sum_{n,\boldsymbol{k}} \left(\mu^2\rho_n + 2\mu k_{\mathrm{B}}Tc_1(\rho_n) + (k_{\mathrm{B}}T)^2 c_2(\rho_n)\right)\Omega^z_n(\boldsymbol{k}), \tag{3.35}$$

where $\Omega^z_n(\boldsymbol{k})$ is the Berry curvature in momentum space:

$$\Omega^z_n(\boldsymbol{k}) = i\left[\left\langle \frac{\partial u_n}{\partial \boldsymbol{k}}\right| \times \left|\frac{\partial u_n}{\partial \boldsymbol{k}}\right\rangle\right]_z. \tag{3.36}$$

Consequently, the thermal Hall conductivity $\kappa^{xy} = \left(L^B\right)^{xy}_{22}/T$ is derived as

$$\kappa^{xy} = -\frac{k_{\mathrm{B}}^2 T}{\hbar V}\sum_{n,\boldsymbol{k}} c_2(\rho_n)\Omega_{n,z}(\boldsymbol{k}) \tag{3.37}$$

While this result contains two contributions from $(S^B)^{\alpha\beta}_{22}$ and $(M^B)^{\alpha\beta}_{22}$, the result in Refs. [77, 79], shown as $\bar{\kappa}^{xy} = \frac{2}{\hbar VT}\sum_{n,\boldsymbol{k}} \rho_n \mathrm{Im}\left\langle \frac{\partial u_n}{\partial k_x}\right| \left(\frac{H+\varepsilon_{n\boldsymbol{k}}}{2}\right)^2 \left|\frac{\partial u_n}{\partial k_y}\right\rangle$, contains only the contribution from $(S^B)^{\alpha\beta}_{22}$. Therefore the difference between the previous works and ours arises from the correction terms $(M^B)^{\alpha\beta}_{ij}$.

The coherence length of the magnons is important for transport. For the validity of the linear response theory developed above, it is implicitly assumed that the coherence length of the magnons is sufficiently short compared with the system size. By this assumption, when we apply temperature difference between the two opposite sides of the system, we can define a local temperature, and the temperature gradient becomes uniform. The linear response theory is then justified. Otherwise, when the coherence length is as long as the system size, the magnon transport is described in the similar way as the Landauer formula, and the above linear response theory no longer applies.

3.3 Application

In this section we apply our results to the ferromagnetic Mott-insulator $Lu_2V_2O_7$ with a pyrochlore structure, for which the thermal Hall effect has been measured and analyzed in Ref. [79]. Following Ref. [79], we briefly review the magnetic properties of this material. The magnetization comes from spin-1/2 V^{4+} ions, which are composed of corner-sharing tetrahedra and form the pyrochlore structure. The vanadium sublattice is shown in Fig. 3.1 (a), which can be seen as a stacking of alternating Kagomé and triangular lattices along [111] direction. In the pyrochlore structure, besides the exchange interaction, there is a non-zero

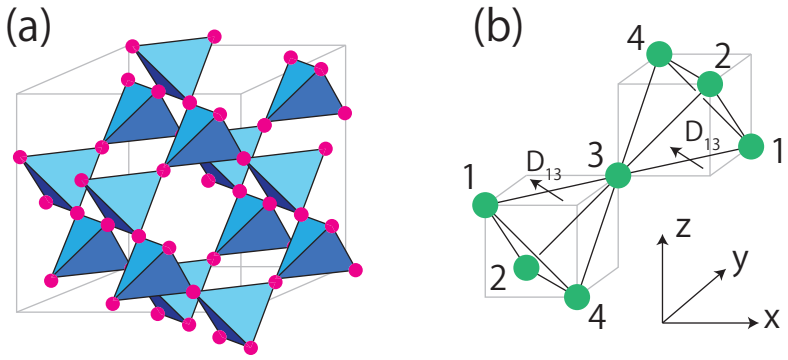

Figure 3.1: (a) The vanadium sublattice of $Lu_2V_2O_7$. (b) Direction of the DM vectors.

DM interaction [112,113] because of the spin-orbit coupling, which is determined by the Moriya's role [113] for crystal symmetries. The DM interaction affects the spin-wave dispersion, and the effective spin-wave Hamiltonian is written as

$$H_{\text{eff}} = \sum_{\langle i,j \rangle} -J\boldsymbol{S}_i \cdot \boldsymbol{S}_j + \boldsymbol{D}_{ij} \cdot (\boldsymbol{S}_i \times \boldsymbol{S}_j) - g\mu_{\text{B}}\boldsymbol{H} \cdot \sum_i \boldsymbol{S}_i, \tag{3.38}$$

where $\langle i,j \rangle$ denotes the nearest-neighbor pairs, J is the exchange interaction, $\boldsymbol{D}$ is the DM vector, g is the g-factor, μ_{B} is Bohr magneton, and $\boldsymbol{H}$ is the magnetic field in the z direction. The temperature is assumed to be much lower than the Curie temperature $T_C = 70$[K], for existence of well-defined Bloch waves of magnons. Despite of the presence of the DM interaction, the ground state is a collinear ferromagnet, because in the ferromagnetic ground state the total DM vectors for a single site is zero and thus DM interaction does not affect on the ground state. As a matter of fact, with a replacement of $\boldsymbol{S}_i \to \langle \boldsymbol{S} \rangle + \delta\boldsymbol{S}_i$, where $\langle \boldsymbol{S} \rangle$ is a mean field and $\delta\boldsymbol{S}_i$ is a small fluctuation, a deviation of the DM interaction term for a single tetrahedron is written up to the first order in $\delta\boldsymbol{S}$ as

$$\delta H_{\text{DM}} = \sum_{i=1}^{4} \sum_{j \neq i} \boldsymbol{D}_{ij} \cdot (\delta\boldsymbol{S}_i \times \langle \boldsymbol{S} \rangle)\,. \tag{3.39}$$

On the other hand, the DM vectors are distributed as follows:

$$\begin{aligned} &\boldsymbol{D}_{13} = \frac{D}{\sqrt{2}}(-1,1,0), \boldsymbol{D}_{24} = \frac{D}{\sqrt{2}}(-1,-1,0), \boldsymbol{D}_{43} = \frac{D}{\sqrt{2}}(0,-1,1), \\ &\boldsymbol{D}_{12} = \frac{D}{\sqrt{2}}(0,-1,-1), \boldsymbol{D}_{14} = \frac{D}{\sqrt{2}}(1,0,1), \boldsymbol{D}_{23} = \frac{D}{\sqrt{2}}(1,0,-1), \end{aligned} \tag{3.40}$$

and $\boldsymbol{D}_{ij} = -\boldsymbol{D}_{ji}$. $i,j = 1,2,3,4$ denote the sites and the coordinate is shown in Fig. 3.1 (b). If δH_{DM} in Eq. (3.39) is finite, the ferromagnetic ground state

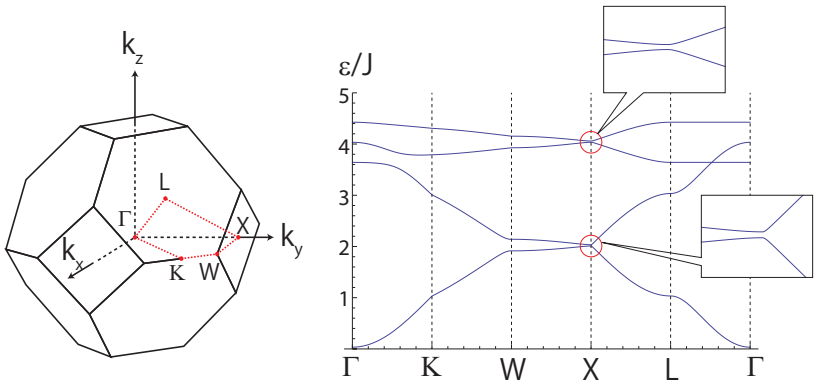

Figure 3.2: The Brillouin zone (left panel) and the band structure (right panel) of $Lu_2V_2O_7$ for $D/J = 0.32$ [79].

is unstable. However, it is easily seen that $\sum_{j\neq i} \boldsymbol{D}_{ij} = 0$ for any i. Therefore $\delta H_{\rm DM} = 0$ and the ferromagnetic state is stable against the DM interaction.

There are four magnon bands, which are shown in Fig. 3.2. The lowest band is well separated from the other higher bands, with the separation much larger than k_BT. Actually, the differences of the energies between the lowest band and other bands near $k = 0$ are written as $\varepsilon_2 - \varepsilon_1 \simeq 4JS\sqrt{1+f(\boldsymbol{k})} \simeq 8JS$ and $\varepsilon_3 - \varepsilon_1 = \varepsilon_4 - \varepsilon_1 \simeq 4JS + 2JS\sqrt{1+f(\boldsymbol{k})} \simeq 8JS$, where $f(\boldsymbol{k}) = \cos(2k_xA)\cos(2k_yA) + \cos(2k_yA)\cos(2k_zA) + \cos(2k_zA)\cos(2k_xA)$ with A being a quarter of the lattice constant and $8JS \simeq 13.6$[meV]. Therefore, the contribution from the lowest band is dominant, whose Berry curvature is $\Omega_{1,z} \simeq -\frac{A^4}{8\sqrt{2}}\frac{D}{J}\frac{H_z}{H}(k_x^2+k_y^2+2k_z^2)$ as calculated in Ref. [79]. The thermal Hall conductivity κ^{xy} is calculated by assuming that the contribution of the lowest band dominates. Figure 3.3 shows the result of the thermal Hall conductivity which is calculated from $(S)_{ij}^{\alpha\beta} + (M)_{ij}^{\alpha\beta}$ (solid curve) and $(S)_{ij}^{\alpha\beta}$ (broken curve). They correspond to our results and the previous results in Ref. [79], respectively. Our result (solid curve in Fig. 3.3) roughly agrees with the experimental data in Ref. [79].

3.4 Conclusion

In conclusion, thermal transport coefficients are derived in terms of the Bloch wave function by the linear response theory. Corresponding thermal Hall conductivity is described by the Berry curvature in momentum space. We conclude that the thermal Hall effect of the magnon in the clean limit is purely due to the magnon band structure.

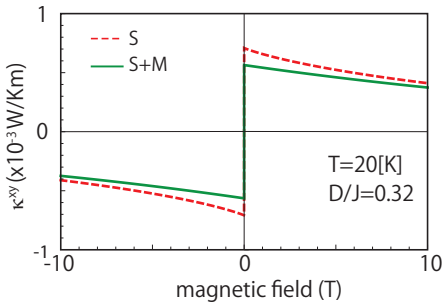

Figure 3.3: Dependence of the thermal Hall conductivity on a magnetic field. The red (broken) curve denotes the result which is calculated solely from $(S)_{ij}^{\alpha\beta}$ calculated in the previous work in Ref. [79]; the green (solid) curve denotes our result which is calculated from $(S)_{ij}^{\alpha\beta} + (M)_{ij}^{\alpha\beta}$.

Chapter 4

Thermal Hall effect of Magnetostatic Spin Wave

4.1 Introduction

In the previous chapter, we clarified that the thermal Hall effect via magnons is described by the Berry curvature in the momentum space. Non-zero Berry curvature for spin-wave bands usually results from interactions with 'spin-orbit-locking' i.e., fixed relative angle between the spin and the wave vector. This transfers a complex-valued character in spin wavefunctions into wavefunctions in the orbital space, leading to a finite Berry curvature in the momentum space. In magnetic insulators, either the short-ranged DM interaction [77, 79, 80] or a long-ranged dipole-dipole interaction [78,114,115] plays such a role. Apart from some exceptions [77, 79], these spin-orbit-locking-type interactions break global spin-rotation symmetry completely. Therefore associated spin-wave Hamiltonians usually do not conserve the total number of magnon; a continuity equation for magnon density and current no longer holds true. From a mathematical point of view, such spin waves are described by the so-called Bogoliubov-de Gennes Hamiltonian. Its off-diagonal terms break the conservation of the magnon number, that prevents us from utilizing the previous theories.

In the present section, we develop a comprehensive theory for magnon Hall effect in magnets in which a magnon number is not necessarily conserved. Following the theory of thermal Hall effect in superconductors [116–118], we begin with a continuity equation for energy density of magnons, to introduce a thermal current associated with magnon transport. Using the linear response theory developed by Smrčka and Středa, [104] we derive the thermal transport coefficient. It is shown that the thermal Hall conductivity is directly related to the Berry curvature [114, 115] in momentum space (Secs. 4.2, 4.3). Our theory is widely applicable to various types of magnets, including dipolar ferromagnets with magnetostatic spin waves and antiferromagnets with the DM interaction. Armed with this theory, we next calculate magnetic-field and temperature de-

pendence of the thermal Hall conductivity in ferromagnetic thin films (sec. 4.5). We clarify that the thermal Hall conductivity via the magnetostatic forward volume wave [71, 74, 119, 120] is mostly independent of the temperature as long as the temperature is much higher than the energy scale for the external magnetic field. Throughout this section, we assume that magnons do not interact with each other.

4.2 Bogoliubov Hamiltonian

We consider spin-wave Hamiltonians with a form of generic Bogoliubov-de Gennes (BdG) Hamiltonian. It is given in a quadratic form of the magnon field operators (creation/annihilation operators) and includes particle-particle pairing of magnon fields;

$$\mathcal{H} \equiv \frac{1}{2}\int d\boldsymbol{r}\Psi^{\dagger}(\boldsymbol{r})\hat{H}_0\Psi(\boldsymbol{r}), \tag{4.1}$$

where $\hat{H}_0$ is an arbitrary $2N\times 2N$ Hermite matrix, $\Psi^{\dagger}(\boldsymbol{r}) = (\beta_1^{\dagger}\dots\beta_N^{\dagger}\beta_1\dots\beta_N)$, $\beta_i^{\dagger}(\boldsymbol{r})$ and $\beta_i(\boldsymbol{r})(1\le i\le N)$ are bosonic (magnon) creation and annihilation operators, $[\beta_i(\boldsymbol{r}),\beta_j^{\dagger}(\boldsymbol{r'})] = \delta_{\boldsymbol{r}\boldsymbol{r}'}\delta_{ij}$, and N is a number of spin-wave bands (or a number of bosons within a unit cell for lattice models). Because of particle-particle pairing terms, $\beta_i^{\dagger}\beta_j^{\dagger}$ or $\beta_i\beta_j$, the total number of magnons is not conserved. Under the Fourier transformation:

$$\beta_i(\boldsymbol{r}) = \frac{1}{\sqrt{N_\Lambda}}\sum_{\boldsymbol{k}} e^{i\boldsymbol{k}\cdot\boldsymbol{r}}\beta_{i,\boldsymbol{k}}, \tag{4.2}$$

$$\beta_i^{\dagger}(\boldsymbol{r}) = \frac{1}{\sqrt{N_\Lambda}}\sum_{\boldsymbol{k}} e^{-i\boldsymbol{k}\cdot\boldsymbol{r}}\beta_{i,\boldsymbol{k}}^{\dagger}, \tag{4.3}$$

the Hamiltonian is written as

$$\mathcal{H} = \frac{1}{2}\sum_{\boldsymbol{k}}\left(\boldsymbol{\beta}_{\boldsymbol{k}}^{\dagger}\boldsymbol{\beta}_{-\boldsymbol{k}}\right)H_{\boldsymbol{k}}\begin{pmatrix}\boldsymbol{\beta}_{\boldsymbol{k}}\\ \boldsymbol{\beta}_{-\boldsymbol{k}}^{\dagger}\end{pmatrix}, \tag{4.4}$$

where $\boldsymbol{\beta}_{\boldsymbol{k}}^{\dagger} = (\beta_{1,\boldsymbol{k}}^{\dagger},\dots,\beta_{N,\boldsymbol{k}}^{\dagger})$. N_Λ is the number of the unit cells in the magnet. Though a lattice model is adopted for simplicity, it is straightforward to apply our theory to a continuous model. We call the diagonal block of $(H_{\boldsymbol{k}})_{ij}$ as particle space $(1\le i,j\le N)$ and hole space $(N<i,j\le 2N)$. The off-diagonal block represents the particle-particle pairing $(1\le i\le N, N<j\le 2N)$ and hole-hole pairing $(N<i\le 2N,\ 1\le j\le N)$. The BdG Hamiltonian is diagonalized by a para-unitary matrix $T_{\boldsymbol{k}}$ [121] :

$$\begin{aligned}\mathcal{H} &= \frac{1}{2}\sum_{\boldsymbol{k}}\left(\boldsymbol{\gamma}_{\boldsymbol{k}}^{\dagger}\boldsymbol{\gamma}_{-\boldsymbol{k}}\right)\mathcal{E}_{\boldsymbol{k}}\begin{pmatrix}\boldsymbol{\gamma}_{\boldsymbol{k}}\\ \boldsymbol{\gamma}_{-\boldsymbol{k}}^{\dagger}\end{pmatrix}\\ &= \sum_{\boldsymbol{k}}\sum_{n=1}^{N}\varepsilon_{n\boldsymbol{k}}\left(\gamma_{n\boldsymbol{k}}^{\dagger}\gamma_{n\boldsymbol{k}}+\frac{1}{2}\right),\end{aligned} \tag{4.5}$$

where $\boldsymbol{\gamma}_{\boldsymbol{k}}^{\dagger} = (\gamma_{1,\boldsymbol{k}}^{\dagger}, \ldots, \gamma_{N,\boldsymbol{k}}^{\dagger})$ and

$$\begin{pmatrix} \boldsymbol{\gamma}_{\boldsymbol{k}} \\ \boldsymbol{\gamma}_{-\boldsymbol{k}}^{\dagger} \end{pmatrix} = T_{\boldsymbol{k}}^{-1} \begin{pmatrix} \boldsymbol{\beta}_{\boldsymbol{k}} \\ \boldsymbol{\beta}_{-\boldsymbol{k}}^{\dagger} \end{pmatrix}, \tag{4.6}$$

$$\mathcal{E}_{\boldsymbol{k}} = T_{\boldsymbol{k}}^{\dagger} H_{\boldsymbol{k}} T_{\boldsymbol{k}} = \begin{pmatrix} E_{\boldsymbol{k}} & \\ & E_{-\boldsymbol{k}} \end{pmatrix}, \tag{4.7}$$

$$E_{\boldsymbol{k}} = \begin{pmatrix} \varepsilon_{1\boldsymbol{k}} & & \\ & \ddots & \\ & & \varepsilon_{N\boldsymbol{k}} \end{pmatrix}. \tag{4.8}$$

Equation (4.7) means that the eigen values doubly appear both in the particle space and in the hole space. By imposing that $\boldsymbol{\gamma}_{\boldsymbol{k}}$ observes the boson commutation relations, $T_{\boldsymbol{k}}$ must satisfy the para-unitary conditions,

$$T_{\boldsymbol{k}}^{\dagger} \sigma_3 T_{\boldsymbol{k}} = \sigma_3, \tag{4.9}$$

$$T_{\boldsymbol{k}} \sigma_3 T_{\boldsymbol{k}}^{\dagger} = \sigma_3. \tag{4.10}$$

4.3 Thermal Transport Coefficient

When a temperature gradient is applied, the Hamiltonian acquires another term,

$$H_{\mathrm{T}} = \mathcal{H} + F, \tag{4.11}$$

which represents a perturbing field from the temperature gradient

$$F \equiv \frac{1}{4} \int d\boldsymbol{r} \Psi^{\dagger}(\boldsymbol{r}) \left(\hat{H}_0 \chi + \chi \hat{H}_0 \right) \Psi(\boldsymbol{r}). \tag{4.12}$$

Here χ is the pseudo gravitational potential, which have appeared in Ch. 3. The thermal transport coefficient $L_{\mu\nu}$ is defined as

$$\left\langle J_{\mu}^{\mathrm{Q}} \right\rangle = L_{\mu\nu} \left(T \nabla_{\nu} \frac{1}{T} - \nabla_{\nu} \chi \right). \tag{4.13}$$

$\left\langle J_{\mu}^{\mathrm{Q}} \right\rangle$ is a macroscopic thermal current [104] where J_{μ}^{Q} is defined as $J_{\mu}^{\mathrm{Q}} \equiv \int d\boldsymbol{r} j_{\mu}^{\mathrm{Q}}(\boldsymbol{r})$ with $j_{\mu}^{\mathrm{Q}}(\boldsymbol{r})$ being a thermal current operator, and $\langle \ldots \rangle$ denotes a thermal and quantum mechanical average.

To calculate the thermal Hall conductivity, let us first calculate the thermal current (operator) when the pseudo gravitational field $\nabla\chi$ is applied. Since χ is small, the total Hamiltonian is rewritten as

$$H_{\mathrm{T}} = \frac{1}{2} \int d\boldsymbol{r} \left(1 + \frac{\chi}{2} \right) \Psi^{\dagger}(\boldsymbol{r}) \hat{H}_0 \left(1 + \frac{\chi}{2} \right) \Psi(\boldsymbol{r}). \tag{4.14}$$

From the conservation of the energy density, the continuity equation is

$$\dot{h}_{\mathrm{T}} + \nabla \cdot \boldsymbol{j}^{\mathrm{Q}}(\boldsymbol{r}) = 0, \tag{4.15}$$

where $h_{\mathrm{T}} = \frac{1}{2}\left(1+\frac{\chi}{2}\right)\Psi^{\dagger}(\boldsymbol{r})\hat{H}_0\left(1+\frac{\chi}{2}\right)\Psi(\boldsymbol{r})$ is an energy density. From Eq. (4.15), the thermal current operator up to the linear order in the external field $\nabla\chi$ is derived as the following (see appendix B for details):

$$j_{\mu}^{\mathrm{Q}}(\boldsymbol{r}) = j_{0,\mu}^{\mathrm{Q}}(\boldsymbol{r}) + j_{1,\mu}^{\mathrm{Q}}(\boldsymbol{r}), \tag{4.16}$$

where

$$j_{0,\mu}^{\mathrm{Q}}(\boldsymbol{r}) = \frac{1}{4}\Psi^{\dagger}(\boldsymbol{r})\left(V_{\mu}\sigma_3\hat{H}_0 + \hat{H}_0\sigma_3V_{\mu}\right)\Psi(\boldsymbol{r}), \tag{4.17}$$

$$\begin{aligned} j_{1,\mu}^{\mathrm{Q}}(\boldsymbol{r}) = &-\frac{i}{8}\nabla_{\nu}\chi\Psi^{\dagger}(\boldsymbol{r})(V_{\mu}\sigma_3V_{\nu} - V_{\nu}\sigma_3V_{\mu})\Psi(\boldsymbol{r}) \\ &+\frac{1}{8}\nabla_{\nu}\chi\Big(\Psi^{\dagger}(\boldsymbol{r})(x_{\nu}V_{\mu}\sigma_3 + 3V_{\mu}\sigma_3x_{\nu})\hat{H}_0\Psi(\boldsymbol{r}) \\ &+\Psi^{\dagger}(\boldsymbol{r})\hat{H}_0(3x_{\nu}\sigma_3V_{\mu} + \sigma_3V_{\mu}x_{\nu})\Psi(\boldsymbol{r})\Big), \end{aligned} \tag{4.18}$$

$V_{\mu} = \frac{1}{i\hbar}[x_{\mu}, \hat{H}_0]$ is a velocity operator, and $\sigma_3 = \begin{pmatrix} 1_{N\times N} & 0 \\ 0 & -1_{N\times N} \end{pmatrix}$. Here $j_{0,\mu}^{\mathrm{Q}}(\boldsymbol{r})$ is independent of $\nabla\chi$, and $j_{1,\mu}^{\mathrm{Q}}(\boldsymbol{r})$ is linear in $\nabla\chi$. The thermal transport coefficient $L_{\mu\nu}$ is derived by calculating a thermal and quantum-mechanical average of the thermal current operator:

$$\left\langle J_{\mu}^{\mathrm{Q}}\right\rangle = \left\langle J_{0,\mu}^{\mathrm{Q}}\right\rangle + \left\langle J_{1,\mu}^{\mathrm{Q}}\right\rangle \equiv -\left(S_{\mu\nu} + M_{\mu\nu}\right)\nabla_{\nu}\chi, \tag{4.19}$$

where $J_{0,\mu}^{\mathrm{Q}}$ and $J_{1,\mu}^{\mathrm{Q}}$ are Fourier transformations of Eqs. (4.17) and (4.18). The first term $S_{\mu\nu}$ represents the usual Kubo-Greenwood contribution to $L_{\mu\nu}$ and the second term $M_{\mu\nu}$ is related to orbital motions of magnons [78]. In a system with broken time-reversal symmetry, there is a circulation of heat current, leading to an additional contribution to the thermal transport coefficient which is called an energy magnetization term [117, 122, 123]. The total thermal transport coefficient is the sum of these two contributions: $L_{\mu\nu} = S_{\mu\nu} + M_{\mu\nu}$. In the following, we derive an expression for the thermal transport coefficients $S_{\mu\nu}$ and $M_{\mu\nu}$ in terms of the spin wave dispersion $\varepsilon_{n,\boldsymbol{k}}$ and the para-unitary matrix $T_{\boldsymbol{k}}$.

The Kubo-Greenwood contribution reads [124, 125]:

$$S_{\mu\nu} = -\frac{\delta\left\langle J_{0\mu}^{\mathrm{Q}}\right\rangle}{\delta\partial_{\nu}\chi} = -\lim_{\Omega\to 0}\frac{P_{\mu\nu}^{R}(\Omega) - P_{\mu\nu}^{R}(0)}{i\Omega}, \tag{4.20}$$

where $P_{\mu\nu}^{R}(\Omega)$ is a retarded current-current correlation function. Now that $\dot{F} = \frac{i}{\hbar}[\mathcal{H}, F] = J_{0,\mu}^{Q}\nabla_{\mu}\chi$, it is given as an analytical connection of the Matsubara correlation function:

$$P_{\mu\nu}^{R}(\Omega) = P_{\mu\nu}(i\Omega \to \Omega + i0), \tag{4.21}$$

with

$$P_{\mu\nu}(i\Omega) = -\int_0^\beta d\tau e^{i\Omega\tau} \left\langle T_\tau J^{\rm Q}_{0,\mu}(\tau) J^{\rm Q}_{0,\nu}(0) \right\rangle . \tag{4.22}$$

Here $J^{\rm Q}_{0,\mu}(\tau)$ is an interaction representation of the thermal current operator, $J^{\rm Q}_{0,\mu}(\tau) = e^{\tau\mathcal{H}} J^{\rm Q}_{0,\mu} e^{-\tau\mathcal{H}}$. Eq. (4.22) is calculated as follows:

$$\begin{aligned}
&P_{\mu\nu}(i\Omega) \\
&= -\frac{1}{16}\int_0^\beta d\tau e^{i\Omega\tau} \sum_{\boldsymbol{k},\boldsymbol{k}'} \\
&\times \left\langle T_\tau \left(\Psi^\dagger_{\boldsymbol{k}}(\tau'+\tau) X_{\boldsymbol{k},\mu} \Psi_{\boldsymbol{k}}(\tau'+\tau) \Psi^\dagger_{\boldsymbol{k}'}(\tau') X_{\boldsymbol{k}',\nu} \Psi_{\boldsymbol{k}'}(\tau') \right) \right\rangle \\
&= -\frac{1}{16}\int_0^\beta d\tau e^{i\Omega\tau} \sum_{\boldsymbol{k},\boldsymbol{k}'} \left(X_{\boldsymbol{k},\mu}\right)_{\alpha,\beta} \left(X_{\boldsymbol{k}',\nu}\right)_{\gamma,\delta} \\
&\times \Big[\left\langle T_\tau \Psi^\dagger_{\alpha,\boldsymbol{k}}(\tau'+\tau) \Psi_{\delta,\boldsymbol{k}'}(\tau') \right\rangle \left\langle T_\tau \Psi_{\beta,\boldsymbol{k}}(\tau'+\tau) \Psi^\dagger_{\gamma,\boldsymbol{k}'}(\tau') \right\rangle \\
&+ \left\langle T_\tau \Psi^\dagger_{\alpha,\boldsymbol{k}}(\tau'+\tau) \Psi^\dagger_{\gamma,\boldsymbol{k}'}(\tau') \right\rangle \left\langle T_\tau \Psi_{\beta,\boldsymbol{k}}(\tau'+\tau) \Psi_{\delta,\boldsymbol{k}'}(\tau') \right\rangle \\
&+ \left\langle T_\tau \Psi^\dagger_{\alpha,\boldsymbol{k}}(\tau'+\tau) \Psi_{\beta,\boldsymbol{k}}(\tau'+\tau) \right\rangle \left\langle T_\tau \Psi^\dagger_{\gamma,\boldsymbol{k}'}(\tau') \Psi_{\delta,\boldsymbol{k}'}(\tau') \right\rangle \Big] ,
\end{aligned} \tag{4.23}$$

where $\Omega = 2\pi n/\beta$, $n \in Z$, T_τ is a time ordering operator and $X_{\boldsymbol{k},\mu} \equiv V_{\boldsymbol{k},\mu}\sigma_3 H_{\boldsymbol{k}} + H_{\boldsymbol{k}}\sigma_3 V_{\boldsymbol{k},\mu}$ with $H_{\boldsymbol{k}} \equiv \sum_{\boldsymbol{\delta}} H_{\boldsymbol{\delta}} e^{i\boldsymbol{k}\cdot\boldsymbol{\delta}}$ and $V_{\boldsymbol{k},\mu} \equiv \frac{1}{\hbar}\frac{\partial H_{\boldsymbol{k}}}{\partial k_\mu}$. The last term in the right hand side of Eq. (4.23) does not contribute since it cancels out via integration over τ. The remaining contraction, such as $\left\langle T_\tau \Psi^\dagger_{\alpha,\boldsymbol{k}}(\tau'+\tau)\Psi_{\delta,\boldsymbol{k}'}(\tau') \right\rangle$, is expressed in terms of $T_{\boldsymbol{k}}$,

$$\begin{aligned}
&\left\langle T_\tau \Psi^\dagger_{\alpha,\boldsymbol{k}}(\tau'+\tau)\Psi_{\delta,\boldsymbol{k}'}(\tau') \right\rangle \\
&= \sum_{n=1}^{N} \Big[\left(T^\dagger_{\boldsymbol{k}}\right)_{n,\alpha} \left(T_{\boldsymbol{k}}\right)_{\delta,n} e^{\tau\varepsilon_{n\boldsymbol{k}}} \rho\left(\varepsilon_{n\boldsymbol{k}}\right) \\
&- \left(T^\dagger_{\boldsymbol{k}}\right)_{n+N,\alpha} \left(T_{\boldsymbol{k}}\right)_{\delta,n+N} e^{-\tau\varepsilon_{n,-\boldsymbol{k}}} \rho\left(-\varepsilon_{n,-\boldsymbol{k}}\right) \Big] .
\end{aligned} \tag{4.24}$$

Here we have used relations

$$\begin{aligned}
\left\langle \gamma^\dagger_{n,\boldsymbol{k}} \gamma_{m,\boldsymbol{k}} \right\rangle &= \delta_{n,m} \rho\left(\varepsilon_{n\boldsymbol{k}}\right) , \\
\left\langle \gamma_{n,\boldsymbol{k}} \gamma^\dagger_{m,\boldsymbol{k}} \right\rangle &= -\delta_{n,m} \rho\left(-\varepsilon_{n\boldsymbol{k}}\right) .
\end{aligned} \tag{4.25}$$

By integrating over τ in Eq. (4.23), the Kubo contribution to the thermal trans-

port coefficient is derived as

$$
\begin{aligned}
S_{\mu\nu} &= -\frac{i}{8}\sum_{n,m=1}^{N}\sum_{\boldsymbol{k}} \\
&\times \Bigg[\frac{\rho(\varepsilon_{n\boldsymbol{k}})-\rho(\varepsilon_{m\boldsymbol{k}})}{(\varepsilon_{n\boldsymbol{k}}-\varepsilon_{m\boldsymbol{k}})^2}(\varepsilon_{n\boldsymbol{k}}+\varepsilon_{m\boldsymbol{k}})^2\left(T_{\boldsymbol{k}}^{\dagger}V_{\boldsymbol{k},\mu}T_{\boldsymbol{k}}\right)_{nm}\left(T_{\boldsymbol{k}}^{\dagger}V_{\boldsymbol{k},\nu}T_{\boldsymbol{k}}\right)_{mn} \\
&- \frac{\rho(\varepsilon_{n\boldsymbol{k}})-\rho(-\varepsilon_{m,-\boldsymbol{k}})}{(\varepsilon_{n\boldsymbol{k}}+\varepsilon_{m,-\boldsymbol{k}})^2}(\varepsilon_{n\boldsymbol{k}}-\varepsilon_{m,-\boldsymbol{k}})^2\left(T_{\boldsymbol{k}}^{\dagger}V_{\boldsymbol{k},\mu}T_{\boldsymbol{k}}\right)_{n,m+N}\left(T_{\boldsymbol{k}}^{\dagger}V_{\boldsymbol{k},\nu}T_{\boldsymbol{k}}\right)_{m+N,n} \\
&- \frac{\rho(-\varepsilon_{n,-\boldsymbol{k}})-\rho(\varepsilon_{m\boldsymbol{k}})}{(\varepsilon_{n,-\boldsymbol{k}}+\varepsilon_{m\boldsymbol{k}})^2}(\varepsilon_{n,-\boldsymbol{k}}-\varepsilon_{m\boldsymbol{k}})^2\left(T_{\boldsymbol{k}}^{\dagger}V_{\boldsymbol{k},\mu}T_{\boldsymbol{k}}\right)_{n+N,m}\left(T_{\boldsymbol{k}}^{\dagger}V_{\boldsymbol{k},\nu}T_{\boldsymbol{k}}\right)_{m,n+N} \\
&+ \frac{\rho(-\varepsilon_{n,-\boldsymbol{k}})-\rho(-\varepsilon_{m,-\boldsymbol{k}})}{(\varepsilon_{n,-\boldsymbol{k}}-\varepsilon_{m,-\boldsymbol{k}})^2}(\varepsilon_{n,-\boldsymbol{k}}+\varepsilon_{m,-\boldsymbol{k}})^2 \\
&\quad\times\left(T_{\boldsymbol{k}}^{\dagger}V_{\boldsymbol{k},\mu}T_{\boldsymbol{k}}\right)_{n+N,m+N}\left(T_{\boldsymbol{k}}^{\dagger}V_{\boldsymbol{k},\nu}T_{\boldsymbol{k}}\right)_{m+N,n+N}\Bigg]. \qquad (4.26)
\end{aligned}
$$

$\rho(\varepsilon)$ is the Bose distribution function $\rho(\varepsilon)=1/(\exp(\varepsilon/k_{\mathrm{B}}T)-1)$ and k_{B} is the Boltzmann constant. The chemical potential is zero here, because the magnon number is not conserved.

On the other hand, $M_{\mu\nu}$ is calculated from the expectation value of Eq. (4.18) with respect to the unperturbed distribution function,

$$
\begin{aligned}
M_{\mu\nu} &= -\frac{\delta\left\langle J_{1\mu}^{\mathrm{Q}}\right\rangle}{\delta\partial_{\nu}\chi} \\
&= \frac{i}{8}\sum_{n,m=1}^{N}\sum_{\boldsymbol{k}}\Big[\rho(\varepsilon_{n\boldsymbol{k}})\left(T_{\boldsymbol{k}}^{\dagger}V_{\boldsymbol{k},\mu}T_{\boldsymbol{k}}\right)_{nm}\left(T_{\boldsymbol{k}}^{\dagger}V_{\boldsymbol{k},\nu}T_{\boldsymbol{k}}\right)_{mn} \\
&- \rho(\varepsilon_{n\boldsymbol{k}})\left(T_{\boldsymbol{k}}^{\dagger}V_{\boldsymbol{k},\mu}T_{\boldsymbol{k}}\right)_{n,m+N}\left(T_{\boldsymbol{k}}^{\dagger}V_{\boldsymbol{k},\nu}T_{\boldsymbol{k}}\right)_{m+N,n} \\
&- \rho(-\varepsilon_{n,-\boldsymbol{k}})\left(T_{\boldsymbol{k}}^{\dagger}V_{\boldsymbol{k},\mu}T_{\boldsymbol{k}}\right)_{n+N,m}\left(T_{\boldsymbol{k}}^{\dagger}V_{\boldsymbol{k},\nu}T_{\boldsymbol{k}}\right)_{m,n+N} \\
&+ \rho(-\varepsilon_{n,-\boldsymbol{k}})\left(T_{\boldsymbol{k}}^{\dagger}V_{\boldsymbol{k},\mu}T_{\boldsymbol{k}}\right)_{n+N,m+N}\left(T_{\boldsymbol{k}}^{\dagger}V_{\boldsymbol{k},\nu}T_{\boldsymbol{k}}\right)_{m+N,n+N}\Big] - (\mu\leftrightarrow\nu) \\
&- \frac{1}{2}\sum_{n=1}^{N}\sum_{\boldsymbol{k}}\Big[\left(T_{\boldsymbol{k}}^{\dagger}\left(x_{\nu}V_{\mu,\boldsymbol{k}}+V_{\mu,\boldsymbol{k}}x_{\nu}\right)T_{\boldsymbol{k}}\right)_{nn}\varepsilon_{n\boldsymbol{k}}\rho(\varepsilon_{n\boldsymbol{k}}) \\
&+ \left(T_{\boldsymbol{k}}^{\dagger}\left(x_{\nu}V_{\mu,\boldsymbol{k}}+V_{\mu,\boldsymbol{k}}x_{\nu}\right)T_{\boldsymbol{k}}\right)_{n+N,n+N}\varepsilon_{n,-\boldsymbol{k}}\rho(-\varepsilon_{n,-\boldsymbol{k}})\Big]. \qquad (4.27)
\end{aligned}
$$

$M_{\mu\nu}$ is related to $M_{\hat{Q}}^{z}$ in Ref [122] as $M_{xy}=2M_{\hat{Q}}^{z}$. Using Eq. (4.27) and

Eq. (C.11) derived in Appendix C, one can explicitly write $M_{\mu\nu}$ as

$$M_{xy} = 2M_Q^z = i\sum_{\boldsymbol{k}}\int_{-\infty}^{\infty} d\tilde{\eta}\mathrm{Tr}\left[\delta(\tilde{\eta}-\sigma_3\mathcal{E}_{\boldsymbol{k}})\sigma_3\frac{\partial T_{\boldsymbol{k}}^\dagger}{\partial k_x}\sigma_3\frac{\partial T_{\boldsymbol{k}}}{\partial k_y}\right]\cdot\int_0^{\tilde{\eta}}\eta\rho(\eta)d\eta$$
$$-\frac{i}{8}\sum_{\boldsymbol{k}}\int_{-\infty}^{\infty} d\tilde{\eta}\mathrm{Tr}\left[\delta(\tilde{\eta}-\sigma_3\mathcal{E}_{\boldsymbol{k}})\sigma_3\frac{\partial T_{\boldsymbol{k}}^\dagger}{\partial k_x}\left(3\sigma_3\tilde{\eta}^2-2\tilde{\eta}H_{\boldsymbol{k}}-H_{\boldsymbol{k}}\sigma_3 H_{\boldsymbol{k}}\right)\frac{\partial T_{\boldsymbol{k}}}{\partial k_y}\right]\rho(\tilde{\eta})$$
$$-(x\leftrightarrow y)\,. \tag{4.28}$$

Similarly, one obtains S_{xy} as

$$S_{xy} = -\frac{i}{8}\sum_{\boldsymbol{k}}\int_{-\infty}^{\infty} d\eta\rho(\eta)$$
$$\times\mathrm{Tr}\left[\delta\left(\eta-\sigma_3\mathcal{E}_{\boldsymbol{k}}\right)\sigma_3\frac{\partial T_{\boldsymbol{k}}^\dagger}{\partial k_x}\left(\eta+H_{\boldsymbol{k}}\sigma_3\right)^2\sigma_3\frac{\partial T_{\boldsymbol{k}}}{\partial k_y}-(x\leftrightarrow y)\right]. \tag{4.29}$$

Thus L_{xy} is written as

$$L_{xy} = -\frac{i}{2}\sum_{\boldsymbol{k}}\int_{-\infty}^{\infty} d\tilde{\eta}$$
$$\times\mathrm{Tr}\left[\delta\left(\tilde{\eta}-\sigma_3\mathcal{E}_{\boldsymbol{k}}\right)\sigma_3\frac{\partial T_{\boldsymbol{k}}^\dagger}{\partial k_x}\sigma_3\frac{\partial T_{\boldsymbol{k}}}{\partial k_y}-(x\leftrightarrow y)\right]\int_0^{\tilde{\eta}} d\eta\eta^2\frac{d\rho(\eta)}{d\eta}. \tag{4.30}$$

As a result, the thermal Hall conductivity in a clean limit is expressed as follows (see Appendix C for details):

$$\kappa_{xy} = -\frac{k_{\mathrm{B}}^2 T}{\hbar V}\sum_{\boldsymbol{k}}\sum_{n=1}^{N}\left(c_2\left(\rho\left(\varepsilon_{n\boldsymbol{k}}\right)\right)-\frac{\pi^2}{3}\right)\Omega_{n\boldsymbol{k}}. \tag{4.31}$$

Here $c_2(x)$ is defined as

$$c_2(x) \equiv \int_0^x dt\left(\log\frac{1+t}{t}\right)^2$$
$$= (1+x)\left(\log\frac{1+x}{x}\right)^2-(\log x)^2-2\mathrm{Li}_2(-x) \tag{4.32}$$

where $\mathrm{Li}_2(x)$ is a polylogarithm function $\mathrm{Li}_n(x)$ for $n=2$. $\Omega_{n\boldsymbol{k}}$ is the Berry curvature in momentum space for BdG Hamiltonian, which is defined as the following [114, 115]:

$$\Omega_{n\boldsymbol{k}} \equiv i\epsilon_{\mu\nu}\left[\sigma_3\frac{\partial T_{\boldsymbol{k}}^\dagger}{\partial k_\mu}\sigma_3\frac{\partial T_{\boldsymbol{k}}}{\partial k_\nu}\right]_{nn}\quad(n=1,2,\ldots,2N). \tag{4.33}$$

4.4 Berry curvature in momentum space for BdG Hamiltonian

In this section we discuss fundamental properties of $\Omega_{n\boldsymbol{k}}$ in Eq. (4.33). Equation (4.31) is written only with the Berry curvature in the particle space: $\Omega_{n\boldsymbol{k}}(1 \leq n \leq N)$. It is because we used a formula in deriving Eq. (4.31),

$$\Omega_{n\boldsymbol{k}} = -\Omega_{n+N,-\boldsymbol{k}} \tag{4.34}$$

which relates the Berry curvature in the hole space ($N+1 \leq n \leq 2N$) with that of the particle space. This formula is derived as follows. First we note that $H_{\boldsymbol{k}}$ has a particle-hole symmetry:

$$H_{\boldsymbol{k}} = \sigma_1 \left(H_{-\boldsymbol{k}}\right)^{\mathrm{t}} \sigma_1, \tag{4.35}$$

$$\sigma_1 = \begin{pmatrix} 0 & 1_{N\times N} \\ 1_{N\times N} & 0 \end{pmatrix}, \tag{4.36}$$

which follows from bosonic commutation relations. Due to the para-unitarity $T_{\boldsymbol{k}}^{\dagger}\sigma_3 T_{\boldsymbol{k}} = \sigma_3$, the eigenvalue problem is written as

$$H_{\boldsymbol{k}} T_{\boldsymbol{k}} = \sigma_3 T_{\boldsymbol{k}} \begin{pmatrix} E_{\boldsymbol{k}} & \\ & -E_{-\boldsymbol{k}} \end{pmatrix}. \tag{4.37}$$

By replacing of $\boldsymbol{k} \to -\boldsymbol{k}$ and utilizing Eq. (4.35), Eq. (4.37) becomes

$$H_{\boldsymbol{k}}\sigma_1 T_{-\boldsymbol{k}}^{*}\sigma_1 = \sigma_3\sigma_1 T_{-\boldsymbol{k}}^{*}\sigma_1 \begin{pmatrix} E_{\boldsymbol{k}} & \\ & -E_{-\boldsymbol{k}} \end{pmatrix}. \tag{4.38}$$

The above equation means that $\sigma_1 T_{-\boldsymbol{k}}^{*}\sigma_1$ also satisfies the same eigenvalue equation as $T_{\boldsymbol{k}}$. Thus $\sigma_1 T_{-\boldsymbol{k}}^{*}\sigma_1$ can be expressed as

$$T_{\boldsymbol{k}} = \sigma_1 T_{-\boldsymbol{k}}^{*}\sigma_1 M_{\boldsymbol{k}}, \tag{4.39}$$

Here $M_{\boldsymbol{k}}$ is a diagonal matrix. Imposing the para-unitarity onto the right hand side, one finds that $M_{\boldsymbol{k}}$ is an unitary matrix:

$$M_{\boldsymbol{k}}^{\dagger} M_{\boldsymbol{k}} = 1_{2N\times 2N}. \tag{4.40}$$

or equivalently $(M_{\boldsymbol{k}})_{ij} = \delta_{ij}\exp[i\theta_{j,\boldsymbol{k}}]$. Therefore the diagonal elements of $M_{\boldsymbol{k}}$ are phase factors. On the other hand, applying a replacement $\boldsymbol{k} \to -\boldsymbol{k}$ and taking complex conjugate of Eq. (4.39), one obtains $T_{-\boldsymbol{k}}^{*} = \sigma_1 T_{\boldsymbol{k}}\sigma_1 M_{-\boldsymbol{k}}^{*}$. Substituting this equation to the Eq. (4.39) again, one finds

$$\sigma_1 M_{-\boldsymbol{k}}^{*}\sigma_1 M_{\boldsymbol{k}} = 1_{2N\times 2N}, \tag{4.41}$$

which means $\theta_{j,\boldsymbol{k}} = \theta_{j+N,-\boldsymbol{k}}$ for $1 \leq j \leq N$.

Now we investigate the relation between the Berry curvature of the particle space and that of the hole space. It is convenient to introduce a gauge field $A_{n,\nu,\boldsymbol{k}}$ as

$$A_{n,\nu,\boldsymbol{k}} \equiv i\mathrm{Tr}\left(\Gamma_n \sigma_3 T_{\boldsymbol{k}}^{\dagger}\sigma_3 \partial_{k_\nu} T_{\boldsymbol{k}}\right), \tag{4.42}$$

where $(\Gamma_n)_{ij} \equiv \delta_{ij}\delta_{in}$. Then Eq. (4.39) leads

$$\begin{aligned} A_{n,\nu,\boldsymbol{k}} &= -i\mathrm{Tr}\left[\partial_{k_\nu}\left(M^t_{\boldsymbol{k}}\sigma_1 T^\dagger_{-\boldsymbol{k}}\right)\sigma_3 T_{-\boldsymbol{k}}\sigma_1 M^*_{\boldsymbol{k}}\sigma_3\Gamma_n\right] \\ &= i\mathrm{Tr}\left[\Gamma_n\left(\partial_{k_\nu}M^t_{\boldsymbol{k}}\right)M^*_{\boldsymbol{k}}\right] \\ &\quad - i\mathrm{Tr}\left[\Gamma_{n+N}T^\dagger_{-\boldsymbol{k}}\sigma_3\partial_{k_\nu}T_{-\boldsymbol{k}}\sigma_3\right] \\ &= -\partial_{k_\nu}\theta_{n,\boldsymbol{k}} + A_{n+N,\nu,-\boldsymbol{k}}, \end{aligned} \tag{4.43}$$

where we used a relation $\left(\partial_{k_\nu}T^\dagger_{\boldsymbol{k}}\right)\sigma_3 T_{\boldsymbol{k}} + T^\dagger_{\boldsymbol{k}}\sigma_3\left(\partial_{k_\nu}T_{\boldsymbol{k}}\right) = 0$. Because the gauge field generates the Berry curvature as $\Omega_{n\boldsymbol{k}} = \partial_{k_x}A_{n,y} - \partial_{k_y}A_{n,x}$, the Berry curvature of the hole space $\Omega_{n+N,\boldsymbol{k}}$ is related to that of the particle space as

$$\Omega_{n,\boldsymbol{k}} = -\Omega_{n+N,-\boldsymbol{k}}. \tag{4.44}$$

Thus one obtains Eq. (4.34). In the absence of the anomalous terms, namely the off-block-diagonal terms in Hamiltonian $H_{\boldsymbol{k}}$, one can retrieve the same results as in the previous works [78].

In a two-dimensional system with spatial periodicity, the wavevector is considered to be the Bloch wave vector, which is restricted within the first Brillouin zone. In such a periodic system, $C_n \equiv \frac{2\pi}{V}\sum_{\boldsymbol{k}}\Omega_{n\boldsymbol{k}}$ is quantized to be an integer. The integer C_n is called as the first Chern integer and specifies a number of chiral edge modes for spin-wave propagations. Specifically, the number of topological chiral spin-wave edge modes, which runs across a given spin-wave band gap, is equal to a sum of the Chern integers associated with those spin-wave bands which have positive energies below this band gap [114, 115]. In fact, one can prove that a sum of the Chern integer over particle band always reduces to zero. These clearly conclude an absence of topological edge modes which run across an energy gap at $\varepsilon = 0$.

In the rest of this section, we show that the sum of the Chern integers over all particle bands is always zero:

$$\sum_{n=1}^{N} C_n = 0. \tag{4.45}$$

To show this, we follow the argument given in Ref. [114] henceforth. First a $2N \times 2N$ bosonic Hamiltonian is separated as follows;

$$H_{\boldsymbol{k}} \equiv \begin{pmatrix} A_{\boldsymbol{k}} & B_{\boldsymbol{k}} \\ B^*_{-\boldsymbol{k}} & A^*_{-\boldsymbol{k}} \end{pmatrix} = t_{\boldsymbol{k}} 1_{2N\times 2N} + S_{\boldsymbol{k}}, \tag{4.46}$$

where $S_{\boldsymbol{k}}$ is a traceless part of $H_{\boldsymbol{k}}$. $H_{\boldsymbol{k}}$ is supposed to be paraunitarily positive definite for any $\boldsymbol{k}$. This leads to $t_{\boldsymbol{k}} > 0$. We introduce a parameter λ as

$$\begin{aligned} H_{\boldsymbol{k}}(\lambda) &= t_{\boldsymbol{k}} 1_{2N\times 2N} + \lambda S_{\boldsymbol{k}}, \\ &= (1-\lambda)t_{\boldsymbol{k}} 1_{2N\times 2N} + \lambda H_{\boldsymbol{k}} \end{aligned} \tag{4.47}$$

with $H_{\boldsymbol{k}}(1) = H_{\boldsymbol{k}}$ and $H_{\boldsymbol{k}}(0) = t_{\boldsymbol{k}} 1_{2N\times 2N}$. While changing λ from zero to one, $H_{\boldsymbol{k}}(\lambda)$ keeps unitarily positive definite for any $\boldsymbol{k}$; the eigenvalues of $H_{\boldsymbol{k}}(\lambda)$ are the sums of the eigenvalues of $\lambda H_{\boldsymbol{k}}$ and $(1-\lambda)t_{\boldsymbol{k}}$, both of which are positive.

Being unitarily positive definite, $H_{\boldsymbol{k}}(\lambda)$ is also paraunitarily positive definite [121]. Thus, there always exists a band gap between particle bands ($1 \leq n \leq N$) and hole bands ($N+1 \leq n \leq 2N$) during the change from $\lambda = 0$ to $\lambda = 1$. This guarantees that the sum of the Chern integer for all positive bands is invariant during the interpolation;

$$\sum_{n=1}^{N} C_n(\lambda) = \text{const.} \tag{4.48}$$

Here $C_n(\lambda)$ is a Chern number which is determined by $H_{\boldsymbol{k}}(\lambda)$. On the other hand, Eq. (4.48) vanishes at $\lambda = 0$, which leads to

$$\sum_{n=1}^{N} C_n(\lambda = 1) = 0. \tag{4.49}$$

Thus Eq. (4.45) is derived. Namely, provided that $H_{\boldsymbol{k}}$ is paraunitarily positive definite, the sum of the Berry curvature over the Brillouin zone (B.Z.) and over all particle bands is always zero.

4.5 Application to magnetostatic waves

4.5.1 Thermal Hall effect via MSFVW mode

In this section we apply the above theory to the magnetostatic spin wave. When a wavelength of the spin-wave excitation enters the micrometer length scale, the short-range exchange interaction becomes negligibly small. Instead, the spin wave propagation is driven by the long-range dipole-dipole interaction (dipolar regime), which gives rise to a spatially-dependent demagnetizing field. Having a role similar to the relativistic spin-orbit interaction in electron systems, the dipole-dipole interaction brings about a finite Berry curvature and thermal Hall effect in magnets.

In the following we consider a two-dimensional ferromagnetic film (e.g. YIG film) in the dipolar regime, where the exchange interaction is neglected. Take the 2-d plane to be xy plane. The saturation magnetization $\boldsymbol{M}_{\rm s}$ and internal static magnetic field $\boldsymbol{H}_0$ is parallel to the z direction; $\boldsymbol{H}_0 = \boldsymbol{H}_{\rm ex} - \boldsymbol{M}_{\rm s}$ where $\boldsymbol{H}_{\rm ex}$ is an external magnetic field. Spin wave mode with this geometry is called as the magnetostatic forward volume wave (MSFVW) [89]. We assume the spin-wave mode to be a plane wave and write the magnetization in the xy direction as $\begin{pmatrix} m_x(z) \\ m_y(z) \end{pmatrix} \exp[i(\boldsymbol{k}\cdot\boldsymbol{r}_\parallel - \omega t)]$, where $\boldsymbol{r}_\parallel = (x, y)$, $\boldsymbol{k}$ is a wave vector and ω is a frequency of the spin wave. The magnetization obeys the following equation of

motion [93] with the SI units,

$$\omega_H \boldsymbol{m}(z) - \omega_M \int_{-L/2}^{L/2} dz' \hat{G}(z,z') \boldsymbol{m}(z') = \omega \sigma_3 \boldsymbol{m}(z), \tag{4.50}$$

$$\sigma_3 \equiv \begin{pmatrix} 1 & 0 \\ 0 & -1 \end{pmatrix}, \quad \boldsymbol{m}(z) \equiv \frac{1}{\sqrt{2}} \begin{pmatrix} m_x(z) - i m_y(z) \\ m_x(z) + i m_y(z) \end{pmatrix}.$$

L is a thickness of the film. $\omega_H \equiv \gamma H_0$, $\omega_M \equiv \gamma M_\mathrm{s}$ and γ is the gyromagnetic ratio. $\hat{G}(z,z')$ is the 2×2 complex-valued matrix of the Green's function:

$$\hat{G}(z,z') = -\frac{1}{2} G_P(z,z') \begin{pmatrix} 1 & e^{-2i\varphi} \\ e^{2i\varphi} & 1 \end{pmatrix}, \tag{4.51}$$

$$G_P(z,z') = \frac{k}{2} \exp(-k|z-z'|), \tag{4.52}$$

where φ denotes a direction of the wave vector $\boldsymbol{k}$ as $\boldsymbol{k} = k(\cos\varphi, \sin\varphi)$. This integral equation is derived from the Landau-Lifshitz equation $d\boldsymbol{M}/dt = -\gamma(\boldsymbol{M} \times \boldsymbol{H})$ without the damping term, the Maxwell equation in the magnetostatic limit $\nabla \times \boldsymbol{H} = 0$, $\nabla \cdot \boldsymbol{B} = 0$, and the usual boundary conditions for $\boldsymbol{H}$ and $\boldsymbol{B}$. By assuming the form of the magnetic potential inside and outside the thin film in the conventional way [89, 90], Eq. (4.50) gives a band structure $\omega_{n\boldsymbol{k}}$ where n is the band index.

Equation (4.50) is a generalized eigenvalue problem;

$$\int dz' \boldsymbol{H}^{\boldsymbol{k}}_{z,z'} \boldsymbol{m}_{n\boldsymbol{k}} = \sigma_3 \omega_{n\boldsymbol{k}} \boldsymbol{m}_{n\boldsymbol{k}}, \tag{4.53}$$

$$\boldsymbol{H}^{\boldsymbol{k}}_{z,z'} \equiv \omega_H \delta(z-z') - \omega_M \hat{G}(z,z'), \tag{4.54}$$

where $m_{n\boldsymbol{k}}$ is the n-th eigen solution with its eigenfrequency being $\omega_{n\boldsymbol{k}}$. In the present case $\boldsymbol{H}^{\boldsymbol{k}}_{z,z'} = \sigma_1 \left(\boldsymbol{H}^{-\boldsymbol{k}}_{z,z'}\right)^{\mathrm{t}} \sigma_1$ holds, as is similar to Eq. (4.35). Therefore we have $\int dz' \boldsymbol{H}^{\boldsymbol{k}}_{z,z'} \left(\sigma_1 m^*_{n,-\boldsymbol{k}}\right) = -\sigma_3 \omega_{n,-\boldsymbol{k}} \left(\sigma_1 m^*_{n,-\boldsymbol{k}}\right)$. To summarize, we have

$$\int dz' \boldsymbol{H}^{\boldsymbol{k}}_{z,z'} \boldsymbol{T}_{z'} = \sigma_3 \boldsymbol{T}_z \tilde{\boldsymbol{E}}, \tag{4.55}$$

$$\boldsymbol{T}_z \equiv \begin{pmatrix} \boldsymbol{m}_{1,\boldsymbol{k}} & \cdots & \boldsymbol{m}_{N,\boldsymbol{k}} & \sigma_1 \boldsymbol{m}^*_{1,-\boldsymbol{k}} & \cdots & \sigma_1 \boldsymbol{m}^*_{N,-\boldsymbol{k}} \end{pmatrix}, \tag{4.56}$$

$$\tilde{\boldsymbol{E}} \equiv \begin{pmatrix} \boldsymbol{E}_{\boldsymbol{k}} & \\ & -\boldsymbol{E}_{-\boldsymbol{k}} \end{pmatrix}, \tag{4.57}$$

$$\boldsymbol{E}_{\boldsymbol{k}} \equiv \begin{pmatrix} \omega_{1,\boldsymbol{k}} & & \\ & \ddots & \\ & & \omega_{N,\boldsymbol{k}} \end{pmatrix}. \tag{4.58}$$

The number of modes N is infinity for Eq. (4.50). Nevertheless, physically speaking, the number of such eigen solutions is bounded, $N < \infty$, by ultraviolet cutoff, e.g. short-range exchange interaction length (see below). With a

normalization condition as $\int dz \boldsymbol{T}_z^\dagger \sigma_3 \boldsymbol{T}_z = \sigma_3$, the problem now reduces to diagonalizing BdG Hamiltonian $\boldsymbol{H}$ by a proper paraunitary matrix $\boldsymbol{T}$. The solution of Eq. (4.55) is written as follows [89]:

$$\boldsymbol{m}_{n\boldsymbol{k}}(z) = \sqrt{\mathcal{N}} \begin{pmatrix} i\kappa + i\nu & \kappa + \nu \\ i\kappa - i\nu & -\kappa + \nu \end{pmatrix} \begin{pmatrix} k_x \\ k_y \end{pmatrix} \cos\left(\sqrt{p}kz + \frac{n\pi}{2}\right). \tag{4.59}$$

Here $\kappa = \omega_M \omega_H / (\omega_H^2 - \omega_n^2)$, $\nu = \omega_M \omega_n / (\omega_H^2 - \omega_n^2)$, $p = -1 - \kappa > 0$, ω_n is the n-th band energy for $n = 0, 1, 2, \ldots$, which is determined by

$$\sqrt{p} \tan\left(\frac{\sqrt{p}kL + n\pi}{2}\right) = 1, \tag{4.60}$$

and $\mathcal{N}$ is a normalization factor which is determined by

$$\langle \boldsymbol{m}_{n,\boldsymbol{k}} | \, \sigma_z \, | \boldsymbol{m}_{n,\boldsymbol{k}} \rangle = 1. \tag{4.61}$$

The bra-ket product means a usual inner product of vectors and integral over z. To obtain Eq. (4.59), we have rewritten the solution in Ref. [89] in the polar coordinate into the form of the plane wave. The dispersion determined by (4.60) is shown in Fig. 4.1(a) for $H_0/M_\mathrm{s} = 1.0$. We use the normalization Eq. (4.61), because $\boldsymbol{m}_{n,\boldsymbol{k}}^\dagger \sigma_y \boldsymbol{m}_{n,\boldsymbol{k}}$ is proportional to the energy density for the magnon [126].

Before calculating the thermal Hall conductivity, we briefly discuss the Berry curvature $\Omega_{n\boldsymbol{k}}$. According to the Eq, (4.33), $\Omega_{n\boldsymbol{k}}$ for the MSFVW mode is calculated as

$$\Omega_{n\boldsymbol{k}} = \frac{1}{2\omega_H} \frac{1}{k} \frac{\partial \omega_{n\boldsymbol{k}}}{\partial k} \left(1 - \frac{\omega_H^2}{\omega_{n\boldsymbol{k}}^2}\right) \cdot (\sigma_3)_{nn}. \tag{4.62}$$

Figure 4.1(b)-(d) shows the numerical results of Eq. (4.62) for various magnitudes of the magnetic field. It is surprising that the Berry curvature for any MSFVW mode is always positive, because $\omega_H < \omega_n$ and the group velocity $\partial\omega/\partial k$ is positive. In the vicinity of $k = 0$, we can calculate asymptotic forms of the Berry curvature. When $k \sim 0$, ω_n is close to ω_H. If we set $\omega_n = \omega_H + \Delta\omega_n$, p can be written as $p \simeq \omega_M / 2\Delta\omega_n \gg 1$ since $\Delta\omega_n$ is small near $k = 0$. Using an approximation $\tan x \simeq x$ $(x \ll 1)$, we find

$$\Delta\omega_n = \begin{cases} \dfrac{1}{4}\omega_M kL & (n = 0), \\ \dfrac{\omega_M}{2}\left(\dfrac{kL}{n\pi}\right)^2 & (n > 0). \end{cases} \tag{4.63}$$

Therefore, the Berry curvature near $k = 0$ can be obtained from Eq. (4.62) and (4.63):

$$\Omega_{n,z}(\boldsymbol{k})/L^2 \simeq \begin{cases} \left(\dfrac{1}{4}\dfrac{M_\mathrm{s}}{H_0}\right)^2 \left(1 - \dfrac{\omega_M}{\omega_H}\dfrac{kL}{4}\right) & (n = 0), \\ \dfrac{1}{2}\left(\dfrac{1}{n\pi}\right)^4 \left(\dfrac{M_\mathrm{s}}{H_0}\right)^2 (kL)^2 & (n > 0). \end{cases} \tag{4.64}$$

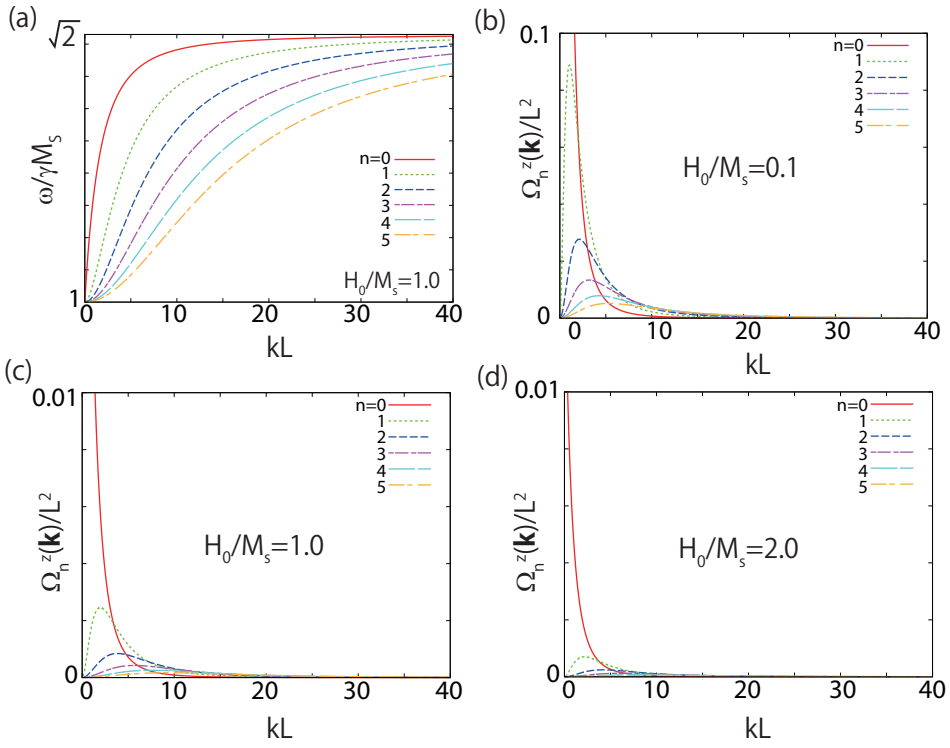

Figure 4.1: (a) Dispersion relation of the MSFVW mode for $H_0/M_s = 1.0$ and Berry curvature for the MSFVW mode for (b) $H_0/M_s = 0.1$, (c) $H_0/M_s = 1.0$, and (d) $H_0/M_s = 2.0$.

It is easy to see that $\Omega_{n,z}(\boldsymbol{k}=0)=0$ for $n>0$ mode, and that for $n=0$ mode $\Omega_{0,z}(\boldsymbol{k})$ enhances up to $\left(\frac{L}{4}\frac{M_\mathrm{s}}{H_0}\right)^2$ but does not diverge at $k=0$.

Now we calculate the thermal Hall conductivity for the MSFVW mode. With Eqs. (4.31) and (4.62), the thermal Hall conductivity κ_{xy} of the ferromagnetic film is derived as follows:

$$\kappa_{xy} = -\frac{\pi k_\mathrm{B}^2 T}{(2\pi)^2 \hbar\omega_H}\sum_{n=1}^{N}\int_{\omega_H}^{\sqrt{\omega_H(\omega_M+\omega_H)}} d\omega_{n\boldsymbol{k}} \times\left(c_2\left(\rho\left(\hbar\omega_{n\boldsymbol{k}}\right)\right)-\frac{\pi^2}{3}\right)\left(1-\frac{\omega_H^2}{\omega_{n\boldsymbol{k}}^2}\right). \tag{4.65}$$

Here we note that all energy bands of the MSFVW mode are equal to ω_H at $k=0$ and approach $\sqrt{\omega_H(\omega_M+\omega_H)}$ at $k\to\infty$ [89]. To show the results in a universal way, we introduce the following dimensionless parameters: $\tilde{\kappa}_{xy}\equiv\kappa_{xy}/\left(\frac{k_\mathrm{B}\omega_M N}{4\pi}\right)$, $r\equiv H_0/M_\mathrm{s}$ denoting a ratio between the internal magnetic field H_0 and saturation magnetization M_s, and $u\equiv k_\mathrm{B}T/\hbar\omega_M$ denoting a ratio between the temperature and the saturation magnetization. By using these parameters, Eq. (4.65) is rewritten as

$$\tilde{\kappa}_{xy} = -\frac{u}{r}\int_{r}^{\sqrt{r(1+r)}} dx\left(c_2\left(\frac{1}{e^{x/u}-1}\right)-\frac{\pi^2}{3}\right)\left(1-\frac{r^2}{x^2}\right). \tag{4.66}$$

$\tilde{\kappa}_{xy}$ converges zero in the zero temperature limit. However, in most of realistic cases $u\gg r$ holds true (e.g. $T=300$[K] and $H_0=1$[T] in YIG film, then $u/r=k_\mathrm{B}T/\hbar\omega_H=1.5\times10^5$). Therefore Eq. (4.66) is approximated to

$$\tilde{\kappa}_{xy}\simeq\frac{1}{2}-\frac{r}{2}\log\left(1+\frac{1}{r}\right). \tag{4.67}$$

This shows that the thermal Hall conductivity via the MSFVW seldom depends on the temperature, if the temperature is much higher than the energy scale of the external magnetic field. Figure. 4.2 shows a plot of the Eq. (4.67). It is easily shown that $\tilde{\kappa}_{xy}\to1/2$ when $r\to0$ and $\tilde{\kappa}_{xy}\to0$ when $r\to\infty$. A typical value is $\tilde{\kappa}_{xy}=2.9\times10^{-13}$[W/K], where parameters are set as follows: $\gamma=2.8$[MHz/Oe], $M_\mathrm{s}=1750$[G], $L=5$ [μm], $T=300$[K], $H_\mathrm{ex}=3000$[Oe].

The magnitude of the thermal Hall conductivity via the MSFVW is determined not only by the ratios among saturation magnetization, internal static field and temperature, but also by the ratio between the exchange length l_ex and thickness of the film L. Namely, when the wavelength in the direction normal to the film becomes shorter than the exchange length l_ex, spin-wave bands are mainly determined by the short-range exchange interaction, where no finite Berry curvature is expected. Since the n-th spin wave band obtained from Eq. (4.50) has n nodes along the z-direction, [93] the upper bound of n, should be roughly estimated as $N=L/l_\mathrm{ex}$, where $l_\mathrm{ex}=1.72\times10^{-8}$[m] for YIG film.

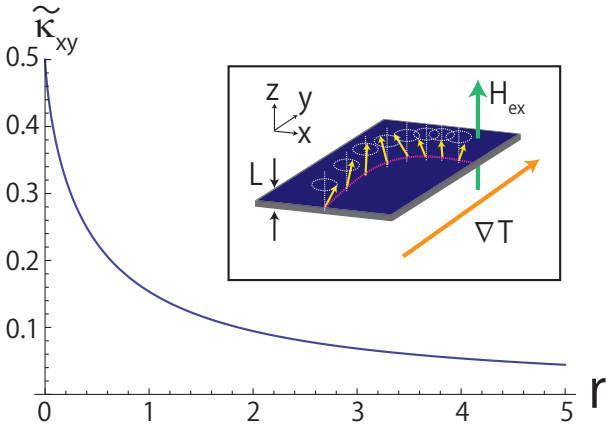

Figure 4.2: Dependence of the thermal Hall conductivity on a magnetic field. $r = 0$ ($H_0 = 0$) corresponds to the field at the saturation field; $H_{\rm ex} = M_s$. The inset shows a geometry of the thermal Hall effect via the MSFVW mode.

4.5.2 Extinction rule

In this subsection, we discuss supplemental extinction rules of the Berry curvature of magnetostatic spin waves. In the previous subsection, one may have a question why we have focused not on the MSBVW or MSSW mode but on the MSFVW mode, although they are all driven by the dipolar interaction. The answer is that the Berry curvature vanishes in the MSBVW and MSSW modes. To clarify this extinction rule, let us consider a magnetic film which is magnetized in an arbitrary direction. We introduce two coordinate systems xyz and $\xi\eta\zeta$, shown in Fig. 4.3. The film is taken to be infinite in the η- and ζ-direction, and perpendicular to the ξ direction. ζ axis is chosen to be along the magnon wave vector $\boldsymbol{k}$. The z direction is parallel to the saturation magnetization $\boldsymbol{M}_{\rm s}$ and the internal static magnetic field $\boldsymbol{H}_0 = \boldsymbol{H}_{\rm ex} - \boldsymbol{M}_{\rm s}$. As is similar to the previous subsection, it is assumed that the spin wave mode has a form of the plane wave: $\begin{pmatrix} m_x(\xi) \\ m_y(\xi) \end{pmatrix} \exp[i(\boldsymbol{k}\cdot\boldsymbol{r}_\parallel - \omega t)]$. The equation of motion of the magnetization is written as the following integral equation [93]:

$$\omega_H \boldsymbol{m}(\xi) - \omega_M \int_{-L/2}^{L/2} d\xi' \hat{G}(\xi,\xi')\boldsymbol{m}(\xi') = \omega\sigma_y \boldsymbol{m}(\xi) \tag{4.68}$$

$$\sigma_y \equiv \begin{pmatrix} 0 & -i \\ i & 0 \end{pmatrix}, \quad \boldsymbol{m}(\xi) \equiv \begin{pmatrix} m_x(\xi) \\ m_y(\xi) \end{pmatrix}.$$

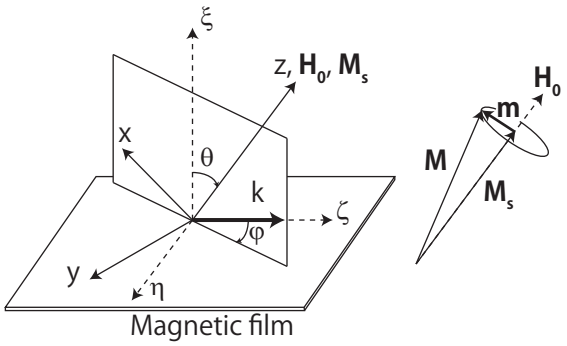

Figure 4.3: Geometry of the coordinate axes. The magnetization M precesses around $M_{\rm s}$.

$\hat{G}(\xi,\xi')$ is the 2×2 complex matrix of the Green's function:

$$\hat{G}(\xi,\xi') = \begin{pmatrix} G_{xx} & G_{xy} \\ G_{yx} & G_{yy} \end{pmatrix}, \tag{4.69}$$

$$\begin{aligned} G_{xx} &= (G_P - \delta(\xi-\xi'))\sin^2\theta - iG_Q \sin 2\theta\cos\varphi \\ &\quad - G_P\cos^2\theta\cos^2\varphi, \end{aligned} \tag{4.70}$$

$$\begin{aligned} G_{xy} &= G_{yx} \\ &= -iG_Q\sin\theta\sin\varphi - G_P\cos\theta\sin\varphi\cos\varphi, \end{aligned} \tag{4.71}$$

$$G_{yy} = -G_P\sin^2\varphi, \tag{4.72}$$

where

$$G_P = \frac{k}{2}\exp(-k|\xi-\xi'|), \tag{4.73}$$

$$G_Q = G_P \mathrm{sign}(\xi-\xi'), \tag{4.74}$$

and θ, φ are the spherical coordinates of $\boldsymbol{M}_{\rm s}$ in the $\xi\eta\zeta$-space (see Fig. 4.3). When the eigenvalue equation is written as Eq. (4.68), it is easily shown that the Berry curvature for the particle space in Eq. (4.33) is written as

$$\Omega_n(\boldsymbol{k}) = i\epsilon_{\alpha\beta}\left\langle \frac{\partial \boldsymbol{m}}{\partial k_\alpha}\right| \sigma_y \left|\frac{\partial \boldsymbol{m}}{\partial k_\beta}\right\rangle. \tag{4.75}$$

We note that the definitions of θ and φ is the same as those of Ref. [93], and they are different from the standard definition of the spherical coordinates. If $\theta = 0$, the mode reduces to the MSFVW mode, which have been discussed in the previous subsection. On the other hand, if $\theta = \pi/2$, the saturation magnetization lies in the film. This situation corresponds to the MSBVW or MSSW mode.

However, when $\theta = \pi/2$, we can show $\Omega_n(\boldsymbol{k}) = 0$ explicitly. By performing a gauge transformation $\boldsymbol{m}' \equiv U^{-1}\boldsymbol{m} = \begin{pmatrix} 1 & 0 \\ 0 & i \end{pmatrix} \boldsymbol{m}$, Eq. (4.69) becomes a generalized eigen value problem with real coefficients:

$$\omega_H \boldsymbol{m}'(\xi) - \omega_M \int_{-L/2}^{L/2} d\xi' \hat{G}'(\xi, \xi') \boldsymbol{m}'(\xi') = -\omega \sigma_x \boldsymbol{m}'(\xi), \tag{4.76}$$

where $\hat{G}'(\xi, \xi')$ is

$$\hat{G}'(\xi, \xi') = U^{-1}\hat{G}(\xi, \xi')U = \begin{pmatrix} G'_{xx} & G'_{xy} \\ G'_{yx} & G'_{yy} \end{pmatrix}, \tag{4.77}$$

$$G'_{xx} = G_P - \delta(\xi - \xi'), \quad G'_{xy} = -G_Q \sin\varphi, \tag{4.78}$$

$$G'_{yx} = G_Q \sin\varphi, \quad G'_{yy} = -G_P \sin^2\varphi. \tag{4.79}$$

Since all the terms in Eq. (4.76) are real, the eigen vector $\boldsymbol{m}'$ is also real. Correspondingly, the Berry curvature Eq. (4.75) becomes

$$\Omega_n(\boldsymbol{k}) = i\epsilon_{\alpha\beta} \left\langle \frac{\partial \boldsymbol{m}'_{n,\boldsymbol{k}}}{\partial k_\alpha} \middle| U^{-1}\sigma_y U \middle| \frac{\partial \boldsymbol{m}'_{n,\boldsymbol{k}}}{\partial k_\beta} \right\rangle, \tag{4.80}$$

$$= \epsilon_{\alpha\beta} \mathrm{Im} \left\langle \frac{\partial \boldsymbol{m}'_{n,\boldsymbol{k}}}{\partial k_\alpha} \middle| \sigma_x \middle| \frac{\partial \boldsymbol{m}'_{n,\boldsymbol{k}}}{\partial k_\beta} \right\rangle. \tag{4.81}$$

Because $\boldsymbol{m}'$ is real and there is no imaginary part, this Berry curvature vanishes. Thus when $\boldsymbol{M}_\mathrm{s}$ is in the film, we cannot expect either an orbital rotational motion of spin wave packet or the thermal Hall effect due to the Berry curvature effect. In other words, in the magnetostatic backward volume wave (MSBVW) and the magnetostatic surface wave (MSSW), the effects of the Berry curvature do not appear.

4.6 Conclusion

We derived the thermal current operator and thermal Hall conductivity for magnons described by the BdG Hamiltonian. κ_{xy} is expressed by the Berry curvature in momentum space. We applied our theory to the magnetostatic spin wave in YIG and clarified the dependence of the thermal Hall conductivity on temperature and magnetic field. The behaviors of the Berry curvature for the MSFVW mode are also identified, and extinction rules are found which forbid a finite $\Omega_{n\boldsymbol{k}}$ in the MSBVW and MSSW modes.

The present theory can also be widely applied to magnons expressed in the BdG Hamiltonian. Therefore it can be applied not only to ferromagnets with DM interactions or dipolar interactions, but also to magnons in other types of magnets such as antiferromagnets. It can also be applied to other bosonic systems such as phonons or photons, as long as they are expressed in the bosonic BdG Hamiltonian.

Chapter 5

Semi-Classical Theory for Magnon Transport

5.1 Introduction

The semiclassical theory in electron systems [127] is useful to understand transport properties of solids and to investigate influence of the Berry curvature on physical quantities, such as the density of states or the orbital magnetization [107, 108, 128]. The key point is that the electron is a wave and it has band structure, because the Berry curvature is based on the multi-band effect [102]. In this point, since the magnon also shares these properties, the theory is applicable to the magnon transport phenomena. Thereby, one can obtain an intuitive picture of the thermal Hall effect of magnons, and study generic properties in magnets.

In this section we construct a semiclassical theory for magnons. To clarify the properties of dynamics of magnons, we construct an equation of motion for magnon wave packets. It is shown that the thermal Hall effect of magnons arises from the chiral edge current of magnons, by breaking the balance of the thermal current in the transversal direction. The origin of the current is an anomalous velocity term in the equation of motion. In addition, we find that the magnon wave packet rotates around itself. This self-rotation motion produces an electric polarization in the radial direction from the relativistic theory. Orbital angular momentum of this motion is also calculated in analogy with electron systems. These unique motions are manifestations of the Berry curvature, which do not appear in other conventional magnetic properties.

We also propose experimental methods to observe the chiral edge motion of the magnon wave packet, by considering a reflection experiment. Our proposal will directly indicate an evidence of the Berry curvature effect in magnets.

5.2 Semiclassical Theory

Here we construct a semiclassical theory for magnon wavepacket [78]. We consider a magnon wavepacket which is well localized around the center $(\boldsymbol{r}_{\rm c}, \boldsymbol{k}_{\rm c})$ in the phase space:

$$|W_n\rangle = \int d\boldsymbol{k} a_n(\boldsymbol{k}, t) \, |\phi_{n\boldsymbol{k}}\rangle \, , \tag{5.1}$$

where $|\phi_{n\boldsymbol{k}}\rangle$ is the Bloch wave function in the nth magnon band, $a_n(\boldsymbol{k}, t)$ satisfies

$$\int d\boldsymbol{k} \, |a_n(\boldsymbol{k}, t)|^2 = 1, \tag{5.2}$$

$$\int d\boldsymbol{k} \, |a_n(\boldsymbol{k}, t)|^2 \, \boldsymbol{k} = \boldsymbol{k}_{\rm c}. \tag{5.3}$$

and $|W_n\rangle$ satisfies

$$\langle W_n | \, \hat{\boldsymbol{r}} \, | W_n \rangle = \boldsymbol{r}_{\rm c}. \tag{5.4}$$

Hereafter we omit the index c for brevity. The dynamics of the wavepacket is described by the semiclassical equation of motion, which includes the topological Berry phase term:

$$\dot{\boldsymbol{r}} = \frac{1}{\hbar} \frac{\partial \varepsilon_{n\boldsymbol{k}}}{\partial \boldsymbol{k}} - \dot{\boldsymbol{k}} \times \boldsymbol{\Omega}_n(\boldsymbol{k}), \tag{5.5}$$

$$\hbar \dot{\boldsymbol{k}} = -\nabla U(\boldsymbol{r}). \tag{5.6}$$

Here n is the band index, $\varepsilon_{n\boldsymbol{k}}$ is the energy of the magnon in the nth band, $\boldsymbol{\Omega}_n(\boldsymbol{k})$ is the Berry curvature in momentum space:

$$\boldsymbol{\Omega}_n(\boldsymbol{k}) = i \left\langle \frac{\partial u_n}{\partial \boldsymbol{k}} \right| \times \left| \frac{\partial u_n}{\partial \boldsymbol{k}} \right\rangle , \tag{5.7}$$

with $|u_n(\boldsymbol{k})\rangle$ being the periodic part of Bloch waves in the nth band defined as $\phi_{n\boldsymbol{k}}(\boldsymbol{r}) = u_n(\boldsymbol{k}, \boldsymbol{r}) e^{i\boldsymbol{k}\cdot\boldsymbol{r}}$. $U(\boldsymbol{r})$ is a confining potential which exists only near the boundary of the sample. This potential $U(\boldsymbol{r})$ forbids the magnon wavepacket going outside of the sample, and its gradient exerts a force on magnons. Such approach of the confining potential is successful in describing the edge picture of the quantum Hall effect in electron systems [129]. Thus we have similarly introduced the confining potential for magnons. Strictly speaking, for the validity of Eqs. (5.5) and (5.6), the spatial variation of $U(\boldsymbol{r})$ should be much slower, compared with the size of the wavepacket. Nevertheless, as we can see from the quantum Hall effect as an example, many of the results for the slowly varying $U(\boldsymbol{r})$ are expected to carry over to the case of rapidly changing $U(\boldsymbol{r})$ as well.

5.3 Thermal Hall effect of magnons in Semiclassical Theory

Near the edge of the sample, there exists an edge current of magnons due to the anomalous velocity term $-\dot{\boldsymbol{k}} \times \boldsymbol{\Omega}_n(\boldsymbol{k}) = \nabla U(\boldsymbol{r})/\hbar \times \boldsymbol{\Omega}_n(\boldsymbol{k})$ in Eq. (5.5). For

example, the magnon edge current for the edge along the y direction is expressed as

$$\begin{aligned} I_y &= \int_a^b dx \frac{1}{V} \sum_{n,\boldsymbol{k}} \rho(\varepsilon_{n\boldsymbol{k}} + U(\boldsymbol{r})) \left[\nabla U(\boldsymbol{r})/\hbar \times \boldsymbol{\Omega}_n(\boldsymbol{k})\right]_y , \\ &= -\frac{1}{\hbar V} \sum_{n,\boldsymbol{k}} \int_{\varepsilon_{n\boldsymbol{k}}}^{\infty} d\varepsilon \rho(\varepsilon) \Omega_{n,z}(\boldsymbol{k}), \end{aligned} \tag{5.8}$$

where $x = a$ and $x = b$ are chosen well inside and outside of the sample so that $U(a) = 0$ and $U(b) = \infty$, V is the area of the sample, $\rho(\varepsilon)$ is the Bose distribution function $\rho(\varepsilon) = (e^{\beta(\varepsilon-\mu)} - 1)^{-1}$, $\beta = 1/k_{\mathrm{B}}T$, k_{B} is the Boltzmann constant, μ is the chemical potential, and T is the temperature. Henceforth the magnon current means the current of the magnon number. We used in Eq. (5.8) the fact that $\boldsymbol{\Omega}_n(\boldsymbol{k})$ in the two-dimensional system is perpendicular to the plane.

The chemical potential μ can be nonzero, when the magnon number is conserved. Nevertheless, in real materials, there are inelastic scatterings which violate magnon conservation, and μ becomes zero. In experiments one can change the chemical potential by parametric pumping of magnons [130]. It is possible because only within a short timescale, the magnon number is almost conserved. Eventually the chemical potential is relaxed to zero anyway. In our theory, we introduced μ for theoretical convenience. Namely, we first consider nonzero chemical potential by assuming conservation of the number of magnons, and set μ=0 at last because the magnon number does not conserve due to inelastic scatterings.

Similarly to Eq. (5.8), we obtain the edge current for the edge along the x direction I_x, which turns out to be identical to I_y. Thus the edge current does not depend on the edge direction or the expression for the confining potential $U(\boldsymbol{r})$. Therefore, the magnon moves even along the curved edge. Here we should note that in addition to the velocity along the edge (i.e. the second term in the r.h.s. of Eq.(5.5)), there exists a group velocity (the first term in the r.h.s. of Eq.(5.5)). Because of this group velocity, a single wavepacket does not go purely along the edge. What we have shown is that there is an additional velocity along the edge due to Berry curvature, and the total magnon edge current is given by Eq. (5.8) when all the magnons in thermal equilibrium are summed over.

If the chemical potential μ or temperature T varies spatially, the thermal Hall effect will occur because the magnon edge current no longer cancels between one edge and the opposite edge, and a net current will appear. In the following we show the details and calculate thermal transport coefficients. First we separate the edge current of magnons into a collection of many small circulating currents shown in Fig. 5.1 (a). We focus on the edge current in the x direction with small temperature gradient in the y direction as an example, and set the coordinate system shown in Fig. 5.1 (b). Here w is chosen to be the coherence length of magnons, and is sufficiently short compared with the system size in order to define the local temperature. This is the same situation of the linear response theory in Ch. 3. The coordinates a, b_1, b_2 is defined as $U(a) = 0$, $U(b_1) =$

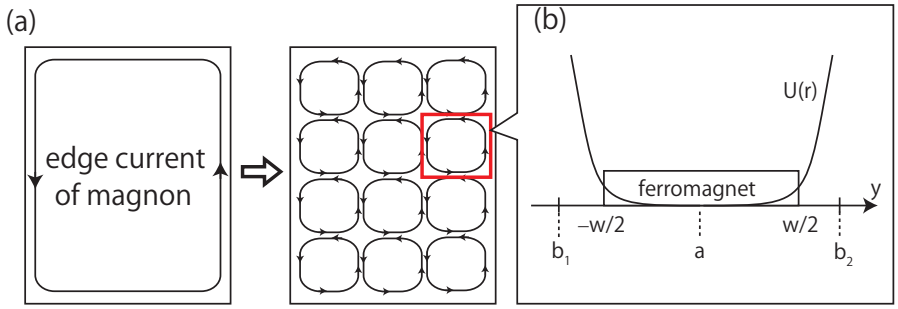

Figure 5.1: (a) Edge current of magnons is decomposed into circulating currents within the cells with size w. This size w corresponds to the coherence length of magnons. (b) Confining potential $U(r)$ within the cell.

$U(b_2) = \infty$ and $b_1 < -w/2 < a < w/2 < b_2$. The current density is obtained by summing up the local current density $j_x(y)$ and dividing it by the width:

$$j_x = \frac{1}{w}\int_{b_1}^{b_2} dy j_x(y) = \frac{1}{w}\int_{a}^{b_2} dy j_x(y) + \frac{1}{w}\int_{b_1}^{a} dy j_x(y). \tag{5.9}$$

From Eq. (5.8) $j_x(y)$ is given as the following:

$$j_x(y) = \frac{1}{\hbar V}\sum_{n,\boldsymbol{k}} \rho(\varepsilon_{n\boldsymbol{k}} + U(\boldsymbol{r}); T(y)) \frac{\partial U(\boldsymbol{r})}{\partial y} \Omega_{n,z}(\boldsymbol{k}). \tag{5.10}$$

This quantity is nonzero when $\partial U(\boldsymbol{r})/\partial y \neq 0$, i.e., $y \sim \pm w/2$. At these points,

$$\begin{aligned} &\rho(\varepsilon_{n\boldsymbol{k}} + U(\boldsymbol{r}); T(y)) \\ &\approx \begin{cases} \rho(\varepsilon_{n\boldsymbol{k}} + U(\boldsymbol{r}); T(\frac{w}{2})) & (y \sim \frac{w}{2}), \\ \rho(\varepsilon_{n\boldsymbol{k}} + U(\boldsymbol{r}); T(-\frac{w}{2})) & (y \sim -\frac{w}{2}). \end{cases} \end{aligned} \tag{5.11}$$

Thus the edge current density along the x direction (Eq. (5.9)) is written as

$$\begin{aligned} j_x &= \frac{1}{w}\frac{1}{\hbar V}\sum_{n,\boldsymbol{k}}\int_{\varepsilon_{n\boldsymbol{k}}}^{\infty} d\varepsilon \\ &\quad \times \left(\rho\left(\varepsilon; T\left(\frac{w}{2}\right)\right) - \rho\left(\varepsilon; T\left(-\frac{w}{2}\right)\right)\right)\Omega_{n,z}(\boldsymbol{k}) \\ &= \frac{\partial}{\partial y}\left(\frac{1}{\hbar V}\sum_{n,\boldsymbol{k}}\int_{\varepsilon_{n\boldsymbol{k}}}^{\infty} \rho(\varepsilon; T(y))\Omega_{n,z}(\boldsymbol{k}) d\varepsilon\right). \end{aligned} \tag{5.12}$$

The edge current along the y direction with temperature gradient in the x direction is similarly written as

$$j_y = -\frac{\partial}{\partial x}\left(\frac{1}{\hbar V}\sum_{n,\boldsymbol{k}}\int_{\varepsilon_{n\boldsymbol{k}}}^{\infty} \rho(\varepsilon; T(x))\Omega_{n,z}(\boldsymbol{k}) d\varepsilon\right). \tag{5.13}$$

In the presence of the chemical potential gradient the edge current can be written as the same form like Eqs. (5.12) and (5.13). Therefore, if the spatial variation is well gradual, the edge current density is written as:

$$\boldsymbol{j} = \nabla \times \frac{1}{\hbar V} \sum_{n,\boldsymbol{k}} \int_{\varepsilon_{n\boldsymbol{k}}}^{\infty} \rho(\varepsilon) \boldsymbol{\Omega}_n(\boldsymbol{k}) d\varepsilon. \tag{5.14}$$

In the same way, the energy current from the edge current density is written as

$$\boldsymbol{j}_{\mathrm{E}} = \nabla \times \frac{1}{\hbar V} \sum_{n,\boldsymbol{k}} \int_{\varepsilon_{n\boldsymbol{k}}}^{\infty} \varepsilon \rho(\varepsilon) \boldsymbol{\Omega}_n(\boldsymbol{k}) d\varepsilon. \tag{5.15}$$

It is worth noting that the Bose distribution function $\rho(\varepsilon)$ depends on T and μ, which vary spatially. From Eqs. (5.14) and (5.15), we can derive various transverse transport coefficients. For instance, in the presence of the temperature gradient in the y direction again, the edge current and energy current density in the x direction are written as

$$(j)_x^{\nabla T} = T \left(\partial_y \left(\frac{1}{T} \right) \right) \sum_{n,\boldsymbol{k}} \int_{\varepsilon_{n\boldsymbol{k}}}^{\infty} \frac{\varepsilon - \mu}{\hbar V} \left(\frac{d\rho}{d\varepsilon} \right) \Omega_{n,z}(\boldsymbol{k}) d\varepsilon, \tag{5.16}$$

$$(j_{\mathrm{E}})_x^{\nabla T} = T \left(\partial_y \left(\frac{1}{T} \right) \right) \sum_{n,\boldsymbol{k}} \int_{\varepsilon_{n\boldsymbol{k}}}^{\infty} \frac{\varepsilon(\varepsilon - \mu)}{\hbar V} \left(\frac{d\rho}{d\varepsilon} \right) \Omega_{n,z}(\boldsymbol{k}) d\varepsilon. \tag{5.17}$$

Here we note that the temperature gradient affects these currents through the Bose distribution function as $\partial_T \rho(\varepsilon) = (\varepsilon - \mu) (\partial \rho(\varepsilon) / \partial \varepsilon) T \partial_T (1/T)$. Similarly we obtain these currents in the presence of the gradient of the chemical potential in the y direction:

$$(j)_x^{\nabla \mu} = -(\partial_y \mu) \frac{1}{\hbar V} \sum_{n,\boldsymbol{k}} \int_{\varepsilon_{n\boldsymbol{k}}}^{\infty} \left(\frac{d\rho}{d\varepsilon} \right) \Omega_{n,z}(\boldsymbol{k}) d\varepsilon, \tag{5.18}$$

$$(j_{\mathrm{E}})_x^{\nabla \mu} = -(\partial_y \mu) \frac{1}{\hbar V} \sum_{n,\boldsymbol{k}} \int_{\varepsilon_{n\boldsymbol{k}}}^{\infty} \varepsilon \left(\frac{d\rho}{d\varepsilon} \right) \Omega_{n,z}(\boldsymbol{k}) d\varepsilon. \tag{5.19}$$

Now we define a heat current as $\boldsymbol{j}_{\mathrm{Q}} \equiv \boldsymbol{j}_{\mathrm{E}} - \mu \boldsymbol{j}$, and write down the linear response of the magnon current and heat current as

$$\boldsymbol{j} = L_{11} \left[-\nabla U - \nabla \mu \right] + L_{12} \left[T \nabla \left(\frac{1}{T} \right) \right], \tag{5.20}$$

$$\boldsymbol{j}_{\mathrm{Q}} = L_{12} \left[-\nabla U - \nabla \mu \right] + L_{22} \left[T \nabla \left(\frac{1}{T} \right) \right]. \tag{5.21}$$

From Eqs. (5.16)-(5.19), the transverse thermal transport coefficients L_{ij}^{xy} can be derived as

$$L_{ij}^{xy} = -\frac{1}{\hbar V \beta^q} \sum_{n,\boldsymbol{k}} \Omega_{n,z}(\boldsymbol{k}) c_q(\rho_n), \tag{5.22}$$

where $i,j=1,2$, $c_q(\rho_n)=\int_{\varepsilon_{n\boldsymbol{k}}}^{\infty}d\varepsilon(\beta(\varepsilon-\mu))^q\left(-\frac{d\rho}{d\varepsilon}\right)=\int_0^{\rho_n}\left(\log\frac{1+t}{t}\right)^q dt$, $q=i+j-2$, and $\rho_n\equiv\rho(\varepsilon_{n\boldsymbol{k}})$. For example, $c_0(\rho)=\rho$, $c_1(\rho)=(1+\rho)\log(1+\rho)-\rho\log\rho$, and $c_2(\rho)=(1+\rho)\left(\log\frac{1+\rho}{\rho}\right)^2-(\log\rho)^2-2\mathrm{Li}_2(-\rho)$, where $\mathrm{Li}_2(z)$ is the polylogarithm function. Finally we derive the thermal Hall conductivity in a clean limit by substituting Eq. (5.22) to $\kappa^{xy}=L_{22}^{xy}/T$,

$$\kappa^{xy}=\frac{2k_{\mathrm{B}}^2T}{\hbar V}\sum_{n,\boldsymbol{k}}c_2(\rho_n)\mathrm{Im}\left\langle\frac{\partial u_n}{\partial k_x}\middle|\frac{\partial u_n}{\partial k_y}\right\rangle. \tag{5.23}$$

Thus the thermal Hall conductivity is expressed as the Berry curvature in momentum space, which is sensitive to the magnon band structure. This result is identical with the result Eq. (3.37) in Ch. 3. Since the Berry curvature part is expressed as

$$\mathrm{Im}\left\langle\frac{\partial u_n}{\partial k_x}\middle|\frac{\partial u_n}{\partial k_y}\right\rangle=\sum_{m(\neq n)}\mathrm{Im}\frac{\left\langle u_n\left|\frac{\partial H}{\partial k_x}\right|u_m\right\rangle\left\langle u_m\left|\frac{\partial H}{\partial k_y}\right|u_n\right\rangle}{(\varepsilon_{n\boldsymbol{k}}-\varepsilon_{m\boldsymbol{k}})^2}. \tag{5.24}$$

Hence κ^{xy} in Eq. (5.23) is enhanced if there is an avoided band crossing.

So far we demonstrated two derivations for intrinsic thermal Hall conductivity. Eq. (3.37) is based on linear response theory, and the transverse current is carried by the bulk. On the other hand in Eq. (5.23), transverse thermal current is carried by the edge current. Coincidence between two results means that the two pictures are essentially identical. The edge current comes from bulk properties characterized by the Berry curvature. Indeed, as one can see from Eq. (5.23), κ^{xy} does not contain $U(\boldsymbol{r})$. This is because a thermal Hall conductivity is intrinsic for materials and is determined by bulk properties. Thus it is natural that both the bulk picture (Ch. 3) and the edge picture (Ch. 5) lead to the same result, as is similar to the quantum Hall system [131, 132].

5.4 Two Orbital Motions of Magnon Wavepacket

As we can see from Eqs. (3.26) and (3.27), these correction terms $(M^B)_{ij}^{\alpha\beta}$ are related to the orbital motion of the particle, namely, a reduced orbital angular momentum (which is defined as a usual orbital angular momentum without a mass of the particle: $\langle\boldsymbol{r}\times\boldsymbol{v}\rangle$). Equation (3.32) means that $(M^B)_{ij}^{\alpha\beta}$ are expressed in terms of the Berry curvature in momentum space, which is generally nonzero. Hence, in this case, the magnon has finite orbital angular momentum due to the Berry curvature. This orbital angular momentum consists of two parts: the edge current and the self-rotation motion of the wavepacket. The reduced angular momentum for the edge current per unit area is derived from Eq. (5.8),

$$l_z^{\mathrm{edge}}=-\frac{2}{\hbar V}\sum_{n,\boldsymbol{k}}\int_{\varepsilon_{n\boldsymbol{k}}}^{\infty}d\varepsilon\rho(\varepsilon)\Omega_{n,z}(\boldsymbol{k}), \tag{5.25}$$

and that for the self-rotation motion is calculated in analogy with the electron system [133] as

$$l_z^{\rm self} = -\frac{2}{\hbar V}{\rm Im}\sum_{n,\boldsymbol{k}}\rho_n \left\langle \frac{\partial u_n}{\partial k_x}\right| (H-\varepsilon_{n\boldsymbol{k}}) \left|\frac{\partial u_n}{\partial k_y}\right\rangle . \tag{5.26}$$

It is easy to show that $l_z^{\rm edge}+l_z^{\rm self}=2(M^B)_{12}^{xy}$. This result is expected from the Eq. (3.26), i.e., the correction terms comes from the orbital angular momentum of the magnon.

Thus the magnon in equilibrium has in general a nonvanishing orbital angular momentum due to the Berry curvature. This magnon orbital motion can be regarded as a generalized cyclotron motion, whereas the magnon feels no Lorentz force and cannot have a cyclotron motion in the same sense as that of electrons. In this respect, this motion is purely due to the magnon band structure. This effect is common in various wave phenomena like electrons [127], photons [134], and so forth.

As mentioned earlier, within the semiclassical theory, the result for the edge current is derived under the assumption that the spatial variation of the confining potential is slow. Nevertheless, as we have seen in this section, the linear response theory, which does not need assumptions for confining potential, gives the same transport coefficients as the semiclassical theory. This strongly suggests that the edge-current picture carries over to the abrupt spatial variation of the confining potential. In the quantum Hall systems, this idea is indeed true; at the abrupt edges of the quantum Hall system, the electrons undergo a skipping motion. Namely, near the edge, the electrons undergo a cyclotron motion and when the electrons hit the edge they are bounced. As a whole the electrons go along the edge with skipping orbitals, which are regarded as the chiral edge current in the quantum Hall system. Therefore, we can similarly expect that in the ferromagnets with edges, the magnon will undergo a superposition of a skipping motion along the edge and a motion along the group velocity of the magnon.

Well localized magnon modes at edges of the system are realized by using magnonic crystals [114, 115]. They are analogous to edge/surface states in the topological insulators [135,136] or topological superconductors [137,138], where unidirectional and localized modes appear at the interface between two materials with different topological numbers. Shindou *et al.* [114, 115] designed magnonic crystals by embedding Fe into YIG film periodically (Fig 5.2 (a)). They theoretically found the existence of chiral edge modes of magnons at the edge or interface of the magnonic crystals, where the Chern number changes. The edge modes run across the magnon band gap (Fig 5.2 (b)), and the number of the edge modes corresponds to the difference of the Chern integers between the magnonic crystal and vacuum or other magnonic crystal.

In the rest of this section, we estimate angular momentum of the above orbital motions in $Lu_2V_2O_7$ as an example. In this material, the lowest spin wave band dispersion is quadratic near $k=0$: $\varepsilon_{1\boldsymbol{k}}=2\beta k^2A^2+\beta g\mu_{\rm B}$. Thus one can introduce the effective mass of the magnon of the lowest band m_1^*, defined

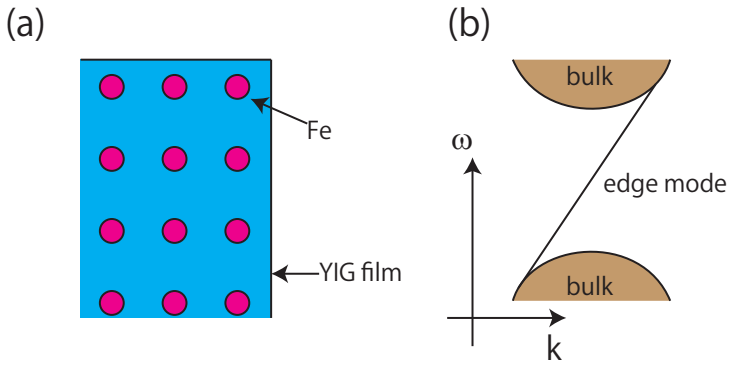

Figure 5.2: (a)Design of the magnonic crystal. Periodic holes are made in YIG film and then Fe filled into the each hole. (b) Chiral edge mode which run across a magnon band gap.

as $m_n^* \equiv \hbar^2(\partial^2\varepsilon_{n\boldsymbol{k}}/\partial k^2)^{-1}$. As is mentioned in Ref. [79], the Berry curvature is also expanded as $\Omega_{1,z} \simeq -\frac{A^4}{8\sqrt{2}}\frac{D}{J}\frac{H_z}{H}(k_x^2+k_y^2+2k_z^2)$. Using these relations, the orbital angular momentum of the self-rotation motion and edge current per unit volume are calculated from Eq. (5.26) and Eq (5.25) respectively:

$$\begin{aligned} L_z^{\rm self} &\simeq m_1^* l_z^{\rm self} = -\frac{16JSm_1^*}{\hbar V}{\rm Im}\sum_{\boldsymbol{k}}\rho_1\left\langle\frac{\partial u_1}{\partial k_\alpha}\middle|\frac{\partial u_1}{\partial k_\beta}\right\rangle \\ &= -\frac{JSm_1^*}{\hbar A}\frac{D}{J}\frac{1}{24\pi^2}\left(\frac{k_{\rm B}T}{JS}\right)^{5/2}\int_0^\infty\frac{x^{3/2}}{e^{(x+\beta g\mu_{\rm B}H)}-1}dx \\ &= -\frac{JSm_1^*}{\hbar A}\frac{D}{J}\frac{1}{32\pi^{3/2}}\left(\frac{k_{\rm B}T}{JS}\right)^{5/2}{\rm Li}_{\frac{5}{2}}\left(e^{-\frac{g\mu_{\rm B}H}{k_{\rm B}T}}\right), \end{aligned} \tag{5.27}$$

$$\begin{aligned} &L_z^{\rm edge} \simeq m_1^* l_z^{\rm edge} \\ &= -\frac{4m_1^*}{\hbar V}{\rm Im}\sum_{\boldsymbol{k}}\left[\rho_1\varepsilon_{1\boldsymbol{k}} - k_{\rm B}T\left((1+\rho_1)\log(1+\rho_1)-\rho_1\log\rho_1\right)\right]\left\langle\frac{\partial u_1}{\partial k_\alpha}\middle|\frac{\partial u_1}{\partial k_\beta}\right\rangle, \end{aligned} \tag{5.28}$$

where $\rho_1 \equiv \rho(\varepsilon_{1\boldsymbol{k}})$. Their typical values are $L_z^{\rm self} = -5.6\times10^{-4}\hbar$ and $L_z^{\rm edge} = 1.2\times10^{-4}\hbar$ per unit cell at $T = 20[{\rm K}], H = 1[{\rm T}]$.

5.5 Electric polarization in Magnon Wavepacket

Orbital rotational motions of electrons give rise to a magnetic moment due to the electron charge. On the other hand, magnons have no charge, but have a magnetic moment. Because the magnon carries magnetic dipole, the rotating

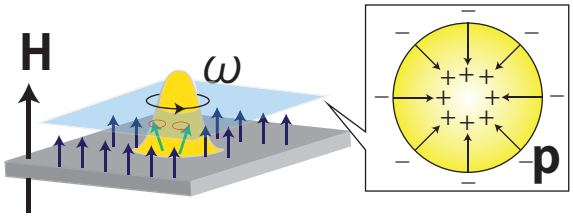

Figure 5.3: Electric polarization in magnon wavepacket.

magnon wavepacket can be regarded as a circulating spin current. Hence as is similar to the spin Hall effect, and its insulator counterpart, i.e. the magnetoelectric effect in noncollinear spin structure [139], the rotating magnon wavepacket should accompany a polarization charge. It requires the spin-orbit interaction, i.e., Dzyaloshinskii-Moriya (DM) interaction. This effect is dual to the rotation of electric charge, producing a magnetic dipole.

In the following, we estimate the electric polarization in a self-rotating magnon wavepacket. We consider a wavepacket of a magnon, which has gaussian shape: $f(\boldsymbol{r}) = \left(1/2\pi\sigma^2\right) e^{-r^2/2\sigma^2}$. Here σ is a radius of the wavepacket. It rotates around itself in xy plane, with the saturation magnetization and magnetic field being in the z direction. According to the relativistic theory, a moving magnetic moment $\boldsymbol{\mu}$ with a velocity $\boldsymbol{v}$ in the vacuum accompanies a electric dipole moment $\boldsymbol{p}$ [140]:

$$\boldsymbol{p} = \frac{\boldsymbol{v}}{c^2} \times \boldsymbol{\mu}. \tag{5.29}$$

Assuming that the magnon wavepacket possesses a magnetic moment $-g\mu_{\mathrm{B}}\hat{z}$, we estimate a local electric polarization density using the formula (5.29) for the vacuum:

$$\boldsymbol{p}(\boldsymbol{r}) = -\frac{g\mu_{\mathrm{B}}\omega\boldsymbol{r}}{2\pi\sigma^2c^2} e^{-r^2/2\sigma^2}. \tag{5.30}$$

The appearance of the electric polarization is related to the polarization charge. According to the Maxwell equation, the polarization charge density $\rho_{\mathrm{e}}(\boldsymbol{r})$ is written as

$$\rho_{\mathrm{e}}(\boldsymbol{r}) = -\nabla \cdot \boldsymbol{p}(\boldsymbol{r}). \tag{5.31}$$

From Eq. (5.31) one obtains

$$\rho_{\mathrm{e}}(\boldsymbol{r}) = \frac{g\mu_{\mathrm{B}}\omega}{2\pi\sigma^2c^2} \left(2 - \frac{r^2}{\sigma^2}\right) e^{-r^2/2\sigma^2}. \tag{5.32}$$

This result shows that positive charges inside the magnon wave packet ($r < \sqrt{2}\sigma$) is surrounded by negative charges, and the total charge is zero.

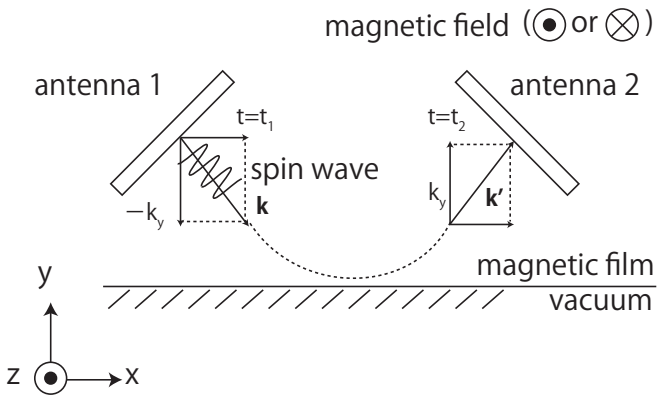

Figure 5.4: Schematic illustration of the reflection experiment of spin waves.

5.6 Experiment of Chiral Edge Motion of Magnon Wave Packet

In the previous section (Sec. 5.3 and 5.4), it is shown that a magnon wave packet moves along an edge of the system in a chiral way. In this section experimental methods to observe this chiral edge motion of magnons are proposed.

We consider a reflection experiment of spin waves at a boundary of YIG thin films, which is shown as Fig. 5.4. A magnetic film lies within the paper plane and an external magnetic field is applied in a direction perpendicular to the film so that the magnetization of the YIG is saturated in the z direction. In this condition the excited spin waves will be the MSFVW mode. Two antennas are attached on the film, both of which can excite and detect a spin wave. If there is an orbital motion of a spin wave wavepacket along the edge, spin waves from an antenna will be reflected with a shift along the edge due to the anomalous velocity term $-\dot{\boldsymbol{k}} \times \boldsymbol{\Omega}_n(\boldsymbol{k})$ in Eq. (5.5). Here we note that $\boldsymbol{\Omega}_n(\boldsymbol{k})$ is in the z direction. Such deviation increases or decreases the signal of spin waves, which is detected at the other antenna. For example, Fig. 5.5 shows two cases of the experiment. If a spin wave is excited at antenna 1, it will be deviated along the edge during the reflection due to the chiral edge motion. The direction of the deviation depends on the direction of the external magnetic field. If the magnetic field is applied in the $-z$ direction (Fig. 5.5 (a)) spin wave is deviated in the $+x$ direction, and the direction of the deviation reverses with inversion of the magnetic field (Fig. 5.5 (b)). Thus the total signal which is measured at the antenna 2 will be different between Fig. 5.5 (a) and (b).

The deviation, which we call as l_{Berry}, is calculated as follows. We assume the external magnetic field points in the $-z$ direction. When spin waves start at time $t = t_1$ from the antenna 1 and arrive at $t = t_2$ to the antenna 2 (Fig. 5.4),

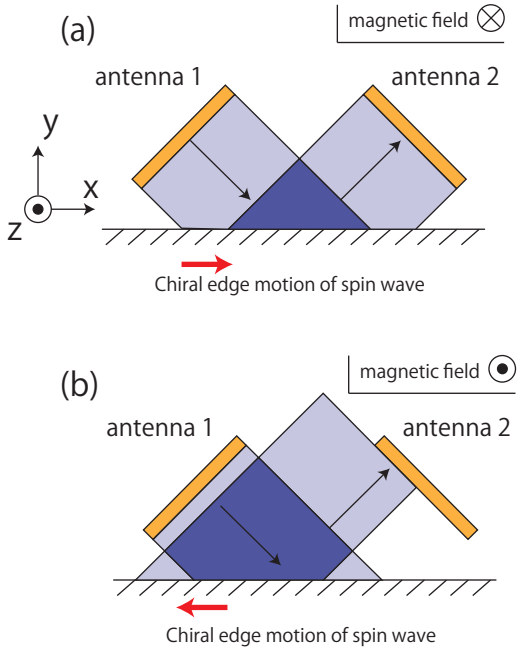

Figure 5.5: Two examples of the experiment. Due to a chiral edge motion of the spin wave, the measured signal increases (a) or decreases (b).

the deviation due to the anomalous velocity term in Eq. (5.5) is written as

$$\begin{aligned} l_{\mathrm{Berry}} &= \hat{\boldsymbol{e}}_x \cdot \int_{t_1}^{t_2} dt(-\dot{\boldsymbol{k}} \times \boldsymbol{\Omega}_n(\boldsymbol{k})) \\ &= \int_{-k_y}^{k_y} dk \Omega_n(k_x, k) = 2\int_0^{k_y} dk \Omega_n(k), \end{aligned} \tag{5.33}$$

where k_y is magnitude of the y-component of the wave vector at $t = t_1$ and $t = t_2$. In the process of the reflection, it is assumed that the energy of the spin wave is conserved and the x-component of the wave vector is also conserved. We adopt $n = 0$ mode for this calculation since $\Omega_{n=0}(\boldsymbol{k})$ is enhanced near a small k (Fig. 4.1 (b)-(d)). Here $\Omega_{n=0}(\boldsymbol{k})$ is written as follows:

$$\Omega_{n=0}(k) = \frac{1}{2\omega_H}\frac{1}{k}\frac{\partial \omega_n}{\partial k}\left(1 - \frac{\omega_H^2}{\omega_n^2}\right), \tag{5.34}$$

where $\omega_H \equiv \gamma\left(H_{\mathrm{ex}} - M_{\mathrm{s}}\right)$, $\omega_M \equiv \gamma M_{\mathrm{s}}$, ω_n is a frequency of the spin waves for n-th band, γ is a gyromagnetic ratio, H_{ex} is an external magnetic field and M_{s} is a saturation magnetization. If $kd \ll 1$, where d is a thickness of a film, one can write the frequency of the spin wave for $n = 0$ mode as

$$\begin{aligned} \omega_n &\sim \sqrt{\omega_H\left(\omega_H + \omega_M\left(1 - \frac{1 - e^{-kd}}{kd}\right)\right)} \\ &\sim \sqrt{\omega_H\left(\omega_H + \omega_M \cdot \frac{kd}{2}\right)}, \end{aligned} \tag{5.35}$$

where we used an approximation $e^{-x} \sim 1 - x + \dfrac{x^2}{2}$. Substituting this equation to Eq. (5.34), one obtains

$$l_{\mathrm{Berry}} = \int_0^{k_y} dk \frac{1}{4}\frac{d}{k}\frac{M_{\mathrm{s}}}{H_{\mathrm{ex}} - M_{\mathrm{s}}}\frac{1}{\sqrt{1 + \frac{M_{\mathrm{s}}}{H_{\mathrm{ex}} - M_{\mathrm{s}}}\frac{kd}{2}}}\left(1 - \frac{1}{1 + \frac{M_{\mathrm{s}}}{H_{\mathrm{ex}} - M_{\mathrm{s}}}\frac{kd}{2}}\right). \tag{5.36}$$

Equation (5.36) is roughly estimated as $l_{\mathrm{Berry}} \sim 4.4[\mu\mathrm{m}]$ by using the following parameters: $M_{\mathrm{s}} = 1750[\mathrm{G}]$, $H_{\mathrm{ex}} = 2000[\mathrm{Oe}]$, $d = 5[\mu\mathrm{m}]$, $\lambda = 100[\mu\mathrm{m}]$, where λ is the wave length.

Qualitative characters such that the signals S_{12} (from antenna 1 to 2) and S_{21} (from antenna 2 to 1) reverse with inversion of the external magnetic field H_{ex} are already observed, and more detailed and new experiments are in progress [141].

Chapter 6

Conclusion

This thesis addresses the Hall effect of magnons due to the Berry curvature in momentum space. The linear response theory and the semiclassical theory is used for this investigation.

In Chapter 3, the thermal Hall effect of exchange magnons in ferromagnets is theoretically studied by using the linear response theory. In the presence of a temperature gradient, the magnon current operator and the energy current operator acquire additional terms. Besides the thermal transport coefficients from the Kubo formula, we derived additional terms which are missing in the previous works. The thermal Hall conductivity of magnons is obtained which is expressed by the Berry curvature in momentum space. We applied our theory to $Lu_2V_2O_7$ and confirmed that our result roughly agrees with experiments.

An extensive theory for the thermal Hall effect of magnons, such as exchange magnons in antiferromagnets or magnetostatic spin waves, is constructed in Chapter 4. Those systems are described by the BdG Hamiltonian, which is diagonalized by para-unitary matrices instead of unitary matrices. From the continuity equations, the thermal current operator of magnons is derived. As is similar to Ch. 3, we derived thermal transport coefficients not only from the Kubo formula but also from the orbital magnetization term. We obtained the thermal Hall conductivity and the expression of the Berry curvature for the BdG Hamiltonian. The relation between the Berry curvature of the particle bands and that of the hole bands is discovered. Moreover, it is found that the sum of the Berry curvature over all particle bands is zero. Our theory is widely applicable not only to spin waves but also to other boson systems such as phonons and photons.

Application to the MSFVW mode is discussed as an example. MSFVW mode is described by a generalized eigenvalue equation. We point out that the equation can be regarded as a diagonalization of the BdG Hamiltonian. The Berry curvature for the MSFVW mode is calculated and its behavior is analyzed in detail. An extinction rule about the Berry curvature for the MSBVW and MSSW mode is discovered. Furthermore, the thermal Hall conductivity for the MSFVW mode is obtained analytically, and its dependence on the temperature

and external magnetic field is clarified.

In Chapter 5, a semiclassical theory for the Hall effect of magnons is developed. We construct the semiclassical equation of motion for the magnon wave packet, and find that there is an edge current of the magnon due to an anomalous velocity term. It is found that this edge current brings about the thermal Hall effect of magnons. The thermal Hall conductivity from the semiclassical theory coincides with that from the linear response theory. Besides the edge current, we discovered that the magnon wave packet rotates around itself. The rotating magnon wave packet generates an electric polarization and polarization charge. These two orbital motions, namely the self-rotation motion and edge current of magnons, are described by the Berry curvature in momentum space. In other words, they are intrinsic properties in magnets, and determined by the magnon band structure in bulk. To see the Berry curvature effect in magnets directly, we propose a reflection experiment. The deviation due to the edge current should be observed experimentally, which will be evidence of the Hall effect of spin waves.

Appendix A

Physical Origin of Potential for magnons

Magnons feel a potential due to a non-uniform magnetic field. Near an edge of a magnet, there is a confining potential for magnons, which is created by an external magnetic field and a demagnetization field. Let us consider a MS-FVW mode in a two-dimensional magnetic thin film for example. An external magnetic field $\boldsymbol{H}_{\mathrm{DC}}$ is applied in the direction perpendicular to the film. Since there is a demagnetization field $\boldsymbol{H}_{\mathrm{d}}$, magnons feel an internal magnetic field $\boldsymbol{H}_{\mathrm{i}} = \boldsymbol{H}_{\mathrm{DC}} - \boldsymbol{H}_{\mathrm{d}}$, which determines the dispersion relation. Here, $\boldsymbol{H}_{\mathrm{d}}$ is strong inside of the magnet ($\boldsymbol{H}_{\mathrm{d}} = \boldsymbol{M}_{\mathrm{s}}$, where $\boldsymbol{M}_{\mathrm{s}}$ is a saturation magnetization), reduces with approaching edges, and becomes to zero outside the magnet [89]. In other words, $\boldsymbol{H}_{\mathrm{i}}$ changes when magnons propagate toward an edge (Fig. A.1 (a)). Since the energy of magnons is conserved during the propagation, the wave number varies corresponding to the change of $\boldsymbol{H}_{\mathrm{i}}$ (Fig. A.1 (b)). However, if the change of $\boldsymbol{H}_{\mathrm{i}}$ is large, there is no wave number to satisfy the dispersion relation. This means that the spin wave is forbidden to go further, and is regarded as a confining potential for magnons. Generally speaking, such potential appears where the internal magnetic field changes abruptly. Thus a gradient of external magnetic fields, imperfection of crystals, and a mechanical gap of magnets [32] also behave as a potential for magnons.

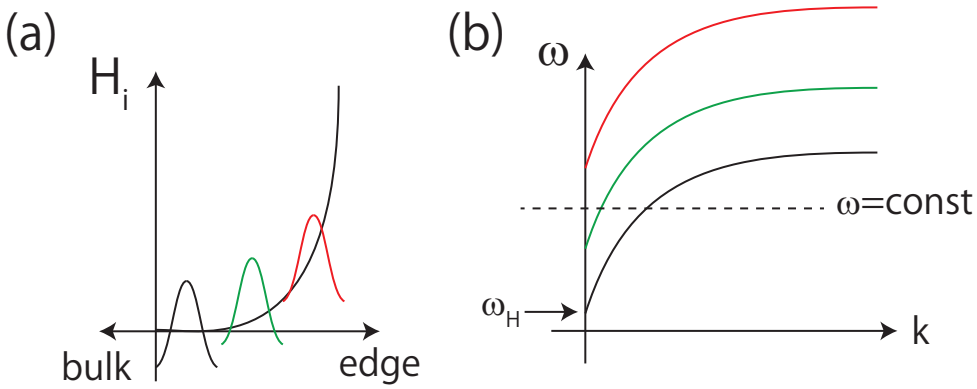

Figure A.1: (a) Effective magnetic field near an edge. (b) Dispersion relation for different effective magnetic fields. Each minimum ω_{H} is determined by H_{i}. When a spin wave comes from bulk near an edge, its wavenumber changes to satisfy the dispersion relation (green line). However, the change of the effective magnetic field is large, there is no allowed wavenumber (red line).

Appendix B

Derivation of thermal current operator

Here we derive the thermal current operator in Eqs. (4.16), (4.17) and (4.18) from the continuity equation

$$\dot{h}_{\mathrm{T}} + \nabla \cdot \boldsymbol{j}^{\mathrm{Q}}(\boldsymbol{r}) = 0. \tag{B.1}$$

We consider a lattice model for simplicity. The Hamiltonian is expressed as Eq. (4.1),

$$\mathcal{H} = \frac{1}{2} \sum_{\boldsymbol{r}} \Psi^{\dagger}(\boldsymbol{r}) \hat{H}_0 \Psi(\boldsymbol{r}), \tag{B.2}$$

where

$$\hat{H}_0 = \sum_{\boldsymbol{\delta}} H_{\boldsymbol{\delta}} e^{i\hat{\boldsymbol{p}}\cdot\boldsymbol{\delta}}, \tag{B.3}$$

$$H_{\boldsymbol{\delta}} = \begin{pmatrix} h_{\boldsymbol{\delta}} & \Delta_{\boldsymbol{\delta}} \\ \Delta^{*}_{\boldsymbol{\delta}} & h^{t}_{-\boldsymbol{\delta}} \end{pmatrix}, \tag{B.4}$$

$$\Psi_i(\boldsymbol{r}) = \begin{cases} \beta_i(\boldsymbol{r}) & (i = 1, \ldots, N) \\ \beta^{\dagger}_{i-N}(\boldsymbol{r}) & (i = N+1, \ldots, 2N) \end{cases}, \tag{B.5}$$

$$[\beta_i(\boldsymbol{r}), \beta^{\dagger}_j(\boldsymbol{r}')] = \delta_{ij}\delta_{\boldsymbol{r},\boldsymbol{r}'}, \tag{B.6}$$

and N is the number of degrees of freedom within the unit cell (e.g. sublattice and orbital degrees of freedom). Here $h_{\boldsymbol{\delta}}$ and $\Delta_{\boldsymbol{\delta}}$ represent hopping terms between sites belonging to unit cells apart by $\boldsymbol{\delta}$ with a translation operator:

$$e^{i\hat{\boldsymbol{p}}\cdot\boldsymbol{\delta}} \beta_i(\boldsymbol{r}) = \beta_i(\boldsymbol{r} + \boldsymbol{\delta}). \tag{B.7}$$

$\hat{H}_0$ is a hermitian operator so that $H_{\boldsymbol{\delta}}$ satisfies

$$H^{\dagger}_{\boldsymbol{\delta}} = H_{-\boldsymbol{\delta}}. \tag{B.8}$$

Thanks to the bosonic commutation relations, $H_{\boldsymbol{\delta}}$ satisfies

$$\sigma_1 H_{\boldsymbol{\delta}} \sigma_1 = H^t_{-\boldsymbol{\delta}}, \tag{B.9}$$

where σ_1 is defined as

$$\sigma_1 = \begin{pmatrix} 0 & 1_{N\times N} \\ 1_{N\times N} & 0 \end{pmatrix}. \tag{B.10}$$

Note Eq. (B.5) satisfies the following commutation relations,

$$[\Psi_i(\boldsymbol{r}), \Psi^\dagger_j(\boldsymbol{r}')] = (\sigma_3)_{ij}\, \delta_{\boldsymbol{r},\boldsymbol{r}'}, \tag{B.11}$$

$$[\Psi^\dagger_i(\boldsymbol{r}), \Psi^\dagger_j(\boldsymbol{r}')] = -i\,(\sigma_2)_{ij}\, \delta_{\boldsymbol{r},\boldsymbol{r}'}, \tag{B.12}$$

$$[\Psi_i(\boldsymbol{r}), \Psi_j(\boldsymbol{r}')] = i\,(\sigma_2)_{ij}\, \delta_{\boldsymbol{r},\boldsymbol{r}'}, \tag{B.13}$$

with

$$\sigma_2 = \begin{pmatrix} 0 & -i1_{N\times N} \\ i1_{N\times N} & 0 \end{pmatrix}, \tag{B.14}$$

$$\sigma_3 = \begin{pmatrix} 1_{N\times N} & 0 \\ 0 & -1_{N\times N} \end{pmatrix}. \tag{B.15}$$

Under a pseudo gravitational potential χ the total Hamiltonian is written as

$$H_{\mathrm{T}} = \sum_{\boldsymbol{r}} h_{\mathrm{T}}(\boldsymbol{r}), \tag{B.16}$$

where $h_{\mathrm{T}}(\boldsymbol{r})$ is a Hamiltonian density operator

$$h_{\mathrm{T}}(\boldsymbol{r}) \equiv \frac{1}{2}\tilde{\Psi}^\dagger(\boldsymbol{r})\hat{H}_0\tilde{\Psi}(\boldsymbol{r}) \tag{B.17}$$

with $\tilde{\Psi}(\boldsymbol{r}) \equiv \left(1+\frac{\chi}{2}\right)\Psi(\boldsymbol{r})$. Now the continuity equation leads

$$\begin{aligned}
\dot{h}_{\mathrm{T}}(\boldsymbol{r}) &= \frac{i}{\hbar}[H_{\mathrm{T}}, h_{\mathrm{T}}(\boldsymbol{r})] = \frac{i}{4\hbar}\left([H_{\mathrm{T}}, \tilde{\Psi}^\dagger(\boldsymbol{r})]\hat{H}_0\tilde{\Psi}(\boldsymbol{r}) + \tilde{\Psi}^\dagger(\boldsymbol{r})[H_{\mathrm{T}}, \hat{H}_0\tilde{\Psi}(\boldsymbol{r})] + \mathrm{h.c.}\right) \\
&= \frac{i}{8\hbar}\Bigg[\sum_{\boldsymbol{\delta},\boldsymbol{\delta}'} \tilde{\Psi}^\dagger(\boldsymbol{r}+\boldsymbol{\delta})\sigma_1 H^t_{\boldsymbol{\delta}}\,(-i\sigma_2)\left(1+\frac{\chi(\boldsymbol{r})}{2}\right)^2 H_{\boldsymbol{\delta}'}\tilde{\Psi}(\boldsymbol{r}+\boldsymbol{\delta}') \\
&\qquad + \tilde{\Psi}^\dagger(\boldsymbol{r}-\boldsymbol{\delta})H_{\boldsymbol{\delta}}\sigma_3\left(1+\frac{\chi(\boldsymbol{r})}{2}\right)^2 H_{\boldsymbol{\delta}'}\tilde{\Psi}(\boldsymbol{r}+\boldsymbol{\delta}') \\
&\qquad - \tilde{\Psi}^\dagger(\boldsymbol{r})H_{\boldsymbol{\delta}}\sigma_3\left(1+\frac{\chi(\boldsymbol{r}+\boldsymbol{\delta})}{2}\right)^2 H_{\boldsymbol{\delta}'}\tilde{\Psi}(\boldsymbol{r}+\boldsymbol{\delta}+\boldsymbol{\delta}') \\
&\qquad + \tilde{\Psi}^\dagger(\boldsymbol{r})H_{\boldsymbol{\delta}}\,(-i\sigma_2)\left(1+\frac{\chi(\boldsymbol{r}+\boldsymbol{\delta})}{2}\right)^2 \left(H^t_{\boldsymbol{\delta}'}\right)\sigma_1\tilde{\Psi}(\boldsymbol{r}+\boldsymbol{\delta}-\boldsymbol{\delta}') + \mathrm{h.c.}\Bigg] \\
&= \frac{i}{4\hbar}\sum_{\boldsymbol{\delta},\boldsymbol{\delta}'}\sum_{\mu=x,y}\left[\nabla_\mu\left(\delta_\mu H_{\boldsymbol{\delta}}\tilde{\Psi}(\boldsymbol{r}+\boldsymbol{\delta})\right)^\dagger \sigma_3\left(1+\frac{\chi(\boldsymbol{r})}{2}\right)^2 H_{\boldsymbol{\delta}'}\tilde{\Psi}(\boldsymbol{r}+\boldsymbol{\delta}') + \mathrm{h.c.}\right].
\end{aligned} \tag{B.18}$$

In Eq. (B.18) we have used $\tilde{\Psi}(\boldsymbol{r}) = \sigma_1 \tilde{\Psi}^\dagger(\boldsymbol{r})$ and $\tilde{\Psi}^\dagger(\boldsymbol{r}) = \sigma_1 \tilde{\Psi}(\boldsymbol{r})$. In terms of a velocity operator V_μ

$$V_\mu \equiv \frac{1}{i\hbar}[x_\mu, \hat{H}_0] = \frac{i}{\hbar} \sum_{\boldsymbol{\delta}} \delta_\mu H_{\boldsymbol{\delta}} e^{i\hat{\boldsymbol{p}}\cdot\boldsymbol{\delta}}, \tag{B.19}$$

one obtains the thermal current operator $j^{\mathrm{Q}}_\mu(\boldsymbol{r})$ from Eq. (B.18),

$$\begin{aligned} j^{\mathrm{Q}}_\mu(\boldsymbol{r}) = \frac{1}{4}\Psi^\dagger(\boldsymbol{r}) \left(1 + \frac{\chi(\boldsymbol{r})}{2}\right) \Bigg[V_\mu \sigma_3 \left(1 + \frac{\chi(\boldsymbol{r})}{2}\right)^2 \hat{H}_0 \\ + \hat{H}_0 \left(1 + \frac{\chi(\boldsymbol{r})}{2}\right)^2 \sigma_3 V_\mu \Bigg] \left(1 + \frac{\chi(\boldsymbol{r})}{2}\right) \Psi(\boldsymbol{r}). \end{aligned} \tag{B.20}$$

By expanding (B.20) in terms of $\nabla\chi$, one obtains Eq. (4.17) and Eq. (4.18).

The Hamiltonian is defined in Eqs. (B.2)-(B.6), and the Fourier transformation is introduced as Eq. (4.2) and Eq. (4.3). Substituting these equations to Eq. (B.2), one obtains the Fourier transformation of the Hamiltonian in Eq. (4.4) with $H_{\boldsymbol{k}} \equiv \sum_{\boldsymbol{\delta}} H_{\boldsymbol{\delta}} e^{i\boldsymbol{k}\cdot\boldsymbol{\delta}}$. Similarly one can obtain the Fourier transformation of the total thermal current operators from Eq. (4.17) and Eq. (4.18),

$$\begin{aligned} J^{\mathrm{Q}}_{0,\mu} &\equiv \int d\boldsymbol{r} j^{\mathrm{Q}}_{0,\mu}(\boldsymbol{r}) \\ &= \frac{1}{4} \sum_{\boldsymbol{k}} \Psi^\dagger_{\boldsymbol{k}} \left(V_{\boldsymbol{k},\mu} \sigma_3 H_{\boldsymbol{k}} + H_{\boldsymbol{k}} \sigma_3 V_{\boldsymbol{k},\mu} \right) \Psi_{\boldsymbol{k}}, \end{aligned} \tag{B.21}$$

$$\begin{aligned} J^{\mathrm{Q}}_{1,\mu} &\equiv \int d\boldsymbol{r} j^{\mathrm{Q}}_{1,\mu}(\boldsymbol{r}) \\ &= -\frac{i}{8} \nabla_\nu \chi \sum_{\boldsymbol{k}} \Psi^\dagger_{\boldsymbol{k}} (V_{\boldsymbol{k},\mu} \sigma_3 V_{\boldsymbol{k},\nu} - V_{\boldsymbol{k},\nu} \sigma_3 V_{\boldsymbol{k},\mu}) \Psi_{\boldsymbol{k}} \\ &+ \frac{1}{8} \nabla_\nu \chi \sum_{\boldsymbol{k}} \Big(\Psi^\dagger_{\boldsymbol{k}} (x_\nu V_{\boldsymbol{k},\mu} \sigma_3 + 3 V_{\boldsymbol{k},\mu} \sigma_3 x_\nu) H_{\boldsymbol{k}} \Psi_{\boldsymbol{k}} \\ &+ \Psi^\dagger_{\boldsymbol{k}} H_{\boldsymbol{k}} (3 x_\nu \sigma_3 V_{\boldsymbol{k},\mu} + \sigma_3 V_{\boldsymbol{k},\mu} x_\nu) \Psi_{\boldsymbol{k}} \Big), \end{aligned} \tag{B.22}$$

where $V_{\boldsymbol{k},\mu} \equiv \sum_{\boldsymbol{\delta}} \frac{i}{\hbar} \delta_\mu H_{\boldsymbol{\delta}} e^{i\boldsymbol{k}\cdot\boldsymbol{\delta}} = \frac{1}{\hbar} \frac{\partial H_{\boldsymbol{k}}}{\partial k_\mu}$ and

$$\Psi_{i,\boldsymbol{k}} = \begin{cases} \beta_{i,\boldsymbol{k}} & (i = 1, \ldots, N) \\ \beta^\dagger_{i-N,-\boldsymbol{k}} & (i = N+1, \ldots, 2N). \end{cases} \tag{B.23}$$

By using the new basis defined in Eq. (4.6), one can rewrite the bosonic field operator $\Psi_{\boldsymbol{k}}$ as

$$\Psi_{i,\boldsymbol{k}} = \sum_{n=1}^{N} (T_{\boldsymbol{k}})_{in} \gamma_{n\boldsymbol{k}} + \sum_{n=1}^{N} (T_{\boldsymbol{k}})_{i,n+N} \gamma^\dagger_{n,-\boldsymbol{k}}, \tag{B.24}$$

$$\Psi^\dagger_{i,\boldsymbol{k}} = \sum_{n=1}^{N} \left(T^\dagger_{\boldsymbol{k}}\right)_{ni} \gamma^\dagger_{n\boldsymbol{k}} + \sum_{n=1}^{N} \left(T^\dagger_{\boldsymbol{k}}\right)_{n+N,i} \gamma_{n,-\boldsymbol{k}}. \tag{B.25}$$

Appendix C

Derivation of thermal transport coefficient $L_{\mu\nu}$

The thermal transport coefficient consists of two parts:

$$\left\langle J_{\mu}^{\mathrm{Q}}\right\rangle =\left\langle J_{0,\mu}^{\mathrm{Q}}\right\rangle +\left\langle J_{1,\mu}^{\mathrm{Q}}\right\rangle \equiv-\left(S_{\mu\nu}+M_{\mu\nu}\right)\nabla_{\nu}\chi, \tag{C.1}$$

where $S_{\mu\nu}$ and $M_{\mu\nu}$ is written as Eqs. (4.26) and (4.27), respectively. Now the total thermal transport coefficient is obtained by $L_{\mu\nu}=S_{\mu\nu}+M_{\mu\nu}$. Using the relation $\left(\varepsilon_{n\boldsymbol{k}}\mp\varepsilon_{m\boldsymbol{k}}\right)^{2}=\left(\varepsilon_{n\boldsymbol{k}}\pm\varepsilon_{m\boldsymbol{k}}\right)^{2}\mp4\varepsilon_{n\boldsymbol{k}}\varepsilon_{m\boldsymbol{k}}$ in Eq. (4.26), we decompose $S_{\mu\nu}$ as $S_{\mu\nu}=S_{\mu\nu}^{(1)}+S_{\mu\nu}^{(2)}$, which corresponds to $\mp4\varepsilon_{n\boldsymbol{k}}\varepsilon_{m\boldsymbol{k}}$ and $\left(\varepsilon_{n\boldsymbol{k}}\pm\varepsilon_{m\boldsymbol{k}}\right)^{2}$, respectively. $M_{\mu\nu}$ is also decomposed as $M_{\mu\nu}=M_{\mu\nu}^{(1)}+M_{\mu\nu}^{(2)}$ where $M_{\mu\nu}^{(1)}$ denotes the term containing $T_{\boldsymbol{k}}^{\dagger}\left(x_{\nu}V_{\mu}+V_{\mu}x_{\nu}\right)T_{\boldsymbol{k}}$. Then one finds that $S_{\mu\nu}$ and $M_{\mu\nu}$ cancel out partially, $S_{\mu\nu}^{(2)}+M_{\mu\nu}^{(2)}=0$. The remainders $S_{\mu\nu}^{(1)}$ and $M_{\mu\nu}^{(1)}$ are written as the followings respectively,

$$\begin{aligned}
S_{\mu\nu}^{(1)} &= -\frac{i}{2}\sum_{n,m=1}^{2N}\sum_{\boldsymbol{k}}\left[\left(T_{\boldsymbol{k}}^{\dagger}V_{\boldsymbol{k},\mu}T_{\boldsymbol{k}}\right)_{nm}\left(\frac{\left(\mathcal{E}_{\boldsymbol{k}}\right)_{nn}\mathcal{E}_{\boldsymbol{k}}}{\left(\left(\sigma_{3}\mathcal{E}_{\boldsymbol{k}}\right)_{nn}-\mathcal{E}_{\boldsymbol{k}}\sigma_{3}\right)^{2}}\right)_{mm}\right.\\
&\qquad\left.\times\left(T_{\boldsymbol{k}}^{\dagger}V_{\boldsymbol{k},\nu}T_{\boldsymbol{k}}\right)_{mn}\left(\rho(\sigma_{3}\mathcal{E}_{\boldsymbol{k}})\right)_{nn}\right]-(\mu\leftrightarrow\nu)\\
&= -\frac{i}{2}\sum_{\boldsymbol{k}}\int_{-\infty}^{\infty}\eta\rho(\eta)\\
&\times\mathrm{Tr}\left[\delta(\eta-\sigma_{3}\mathcal{E}_{\boldsymbol{k}})\sigma_{3}\left(T_{\boldsymbol{k}}^{\dagger}V_{\boldsymbol{k},\mu}T_{\boldsymbol{k}}\frac{\mathcal{E}_{\boldsymbol{k}}}{\left(\eta-\sigma_{3}\mathcal{E}_{\boldsymbol{k}}\right)^{2}}T_{\boldsymbol{k}}^{\dagger}V_{\boldsymbol{k},\nu}T_{\boldsymbol{k}}\right)\right]d\eta-(\mu\leftrightarrow\nu)\\
&= -\frac{i}{2}\sum_{\boldsymbol{k}}\int_{-\infty}^{\infty}\eta\rho(\eta)\mathrm{Tr}\left[\delta(\eta-\sigma_{3}\mathcal{E}_{\boldsymbol{k}})\sigma_{3}\frac{\partial T_{\boldsymbol{k}}^{\dagger}}{\partial k_{\mu}}H_{\boldsymbol{k}}\frac{\partial T_{\boldsymbol{k}}}{\partial k_{\nu}}\right]d\eta-(\mu\leftrightarrow\nu),
\end{aligned} \tag{C.2}$$

$$M^{(1)}_{\mu\nu} = -\frac{1}{2}\sum_{n=1}^{2N}\sum_{\boldsymbol{k}}\left[T^{\dagger}_{\boldsymbol{k}}\left(x_\nu V_{\boldsymbol{k},\mu} + V_{\boldsymbol{k},\mu}x_\nu\right)T_{\boldsymbol{k}}\mathcal{E}_{\boldsymbol{k}}\rho(\sigma_3\mathcal{E}_{\boldsymbol{k}})\right]_{nn}$$
$$= -\frac{1}{2}\sum_{\boldsymbol{k}}\int_{-\infty}^{\infty}\eta\rho(\eta)\mathrm{Tr}\left[\sigma_3\left(x_\nu V_{\boldsymbol{k},\mu} - x_\mu V_{\boldsymbol{k},\nu}\right)\delta(\eta-\sigma_3 H_{\boldsymbol{k}})\right]d\eta. \quad \text{(C.3)}$$

In the Eq. (C.2) we have used the relation $T^{\dagger}_{\boldsymbol{k}}\sigma_3 T_{\boldsymbol{k}} = \sigma_3$ and $T^{-1}_{\boldsymbol{k}} f\left(\sigma_3 H_{\boldsymbol{k}}\right) T_{\boldsymbol{k}} = f\left(\sigma_3\mathcal{E}_{\boldsymbol{k}}\right)$, where $f(x)$ is an arbitrary function.

In order to calculate $S^{(1)}_{\mu\nu} + M^{(1)}_{\mu\nu}$ we follow Smrčka and Středa [104], to introduce the following two functions $A(\eta)$ and $B(\eta)$ as,

$$A(\eta) \equiv i\mathrm{Tr}\left[\sigma_3 V_{\boldsymbol{k},\mu}\frac{dG^+}{d\eta}\sigma_3 V_{\boldsymbol{k},\nu}\delta(\eta-\sigma_3 H_{\boldsymbol{k}})\right.$$
$$\left. -\sigma_3 V_{\boldsymbol{k},\mu}\delta(\eta-\sigma_3 H_{\boldsymbol{k}})\sigma_3 V_{\boldsymbol{k},\nu}\frac{dG^-}{d\eta}\right], \quad \text{(C.4)}$$
$$B(\eta) \equiv i\mathrm{Tr}\left[\sigma_3 V_{\boldsymbol{k},\mu}G^+\sigma_3 V_{\boldsymbol{k},\nu}\delta(\eta-\sigma_3 H_{\boldsymbol{k}})\right.$$
$$\left. -\sigma_3 V_{\boldsymbol{k},\mu}\delta(\eta-\sigma_3 H_{\boldsymbol{k}})\sigma_3 V_{\boldsymbol{k},\nu}G^-\right], \quad \text{(C.5)}$$

where $G^{\pm}$ is defined as $G^{\pm} \equiv \frac{1}{\eta\pm i0-\sigma_3 H_{\boldsymbol{k}}}$. They obey the following identity:

$$A(\eta) - \frac{1}{2}\frac{dB(\eta)}{d\eta}$$
$$= \frac{1}{4\pi}\mathrm{Tr}\left[\sigma_3 V_{\boldsymbol{k},\mu}\left(G^+\right)^2\sigma_3 V_{\boldsymbol{k},\nu}G^+ - \sigma_3 V_{\boldsymbol{k},\mu}\left(G^-\right)^2\sigma_3 V_{\boldsymbol{k},\nu}G^-\right] - (\mu\leftrightarrow\nu)$$
$$= \frac{i}{4\pi}\mathrm{Tr}\left[x_\mu G^+\sigma_3 V_{\boldsymbol{k},\nu}G^+ - x_\mu\left(G^+\right)^2\sigma_3 V_{\boldsymbol{k},\nu}\right.$$
$$\left. -x_\mu G^-\sigma_3 V_{\boldsymbol{k},\nu}G^- + x_\mu\left(G^-\right)^2\sigma_3 V_{\boldsymbol{k},\nu}\right] - (\mu\leftrightarrow\nu)$$
$$= \frac{1}{4\pi i}\mathrm{Tr}\left[x_\mu\left(\left(G^+\right)^2 - \left(G^-\right)^2\right)\sigma_3 V_{\boldsymbol{k},\nu}\right] - (\mu\leftrightarrow\nu)$$
$$= -\frac{1}{2}\mathrm{Tr}\left[\sigma_3\left(x_\nu V_{\boldsymbol{k},\mu} - x_\mu V_{\boldsymbol{k},\nu}\right)\frac{d}{d\eta}\delta(\eta-\sigma_3 H_{\boldsymbol{k}})\right]. \quad \text{(C.6)}$$

To see this, we have used the relations: $G^+ - G^- = -2\pi i\delta\left(\eta-\sigma_3 H_{\boldsymbol{k}}\right)$ and $V_{\boldsymbol{k},\mu} = i[x_\mu, \sigma_3\left(G^{\pm}\right)^{-1}]$. We now integrate Eq. (C.6) to obtain

$$\mathrm{Tr}\left[\sigma_3\left(x_\nu V_{\boldsymbol{k},\mu} - x_\mu V_{\boldsymbol{k},\nu}\right)\delta(\eta-\sigma_3 H_{\boldsymbol{k}})\right]$$
$$= 2\int_{\eta}^{\infty}d\tilde{\eta}\left(A(\tilde{\eta}) - \frac{1}{2}\frac{dB(\tilde{\eta})}{d\tilde{\eta}}\right) = -2\int_{-\infty}^{\eta}d\tilde{\eta}\left(A(\tilde{\eta}) - \frac{1}{2}\frac{dB(\tilde{\eta})}{d\tilde{\eta}}\right), \quad \text{(C.7)}$$

where the magnon spectrum is supposed to be bounded. The last equality in

Eq. (C.7) was based on the following identity,

$$
\begin{aligned}
&\int_{-\infty}^{\infty} d\tilde{\eta} \left(A(\tilde{\eta}) - \frac{1}{2} \frac{dB(\tilde{\eta})}{d\tilde{\eta}} \right) \\
&= i \int_{-\infty}^{\infty} \mathrm{Tr} \left[\sigma_3 V_{\boldsymbol{k},\mu} \frac{dG^+}{d\tilde{\eta}} \sigma_3 V_{\boldsymbol{k},\nu} \delta(\tilde{\eta} - \sigma_3 H_{\boldsymbol{k}}) - \sigma_3 V_{\boldsymbol{k},\mu} \delta(\tilde{\eta} - \sigma_3 H_{\boldsymbol{k}}) \sigma_3 V_{\boldsymbol{k},\nu} \frac{dG^-}{d\tilde{\eta}} \right] d\tilde{\eta} \\
&= -i \int_{-\infty}^{\infty} d\tilde{\eta} \sum_{n=1}^{2N} (\sigma_3)_{nn} \, \delta(\tilde{\eta} - (\sigma_3 \mathcal{E}_{\boldsymbol{k}})_{nn}) \\
&\qquad \times \left[T_{\boldsymbol{k}}^\dagger V_{\boldsymbol{k},\mu} T_{\boldsymbol{k}} \frac{1}{\left((\sigma_3 \mathcal{E}_{\boldsymbol{k}})_{nn} - \sigma_3 \mathcal{E}_{\boldsymbol{k}} \right)^2} \sigma_3 T_{\boldsymbol{k}}^\dagger V_{\boldsymbol{k},\nu} T_{\boldsymbol{k}} \right]_{nn} - (\mu \leftrightarrow \nu) \\
&= -i \int_{-\infty}^{\infty} \mathrm{Tr} \left[\delta(\tilde{\eta} - \sigma_3 \mathcal{E}_{\boldsymbol{k}}) \sigma_3 \frac{\partial T_{\boldsymbol{k}}^\dagger}{\partial k_\mu} \sigma_3 \frac{\partial T_{\boldsymbol{k}}}{\partial k_\nu} \right] d\tilde{\eta} - (\mu \leftrightarrow \nu) \\
&= -\sum_{n=1}^{2N} \Omega_{n\boldsymbol{k}} = 0.
\end{aligned}
\tag{C.8}
$$

Here $\Omega_{n\boldsymbol{k}}$ is a Berry curvature in momentum space

$$
\Omega_{n\boldsymbol{k}} \equiv i \epsilon_{\mu\nu} \left[\sigma_3 \frac{\partial T_{\boldsymbol{k}}^\dagger}{\partial k_\mu} \sigma_3 \frac{\partial T_{\boldsymbol{k}}}{\partial k_\nu} \right]_{nn}, \tag{C.9}
$$

which can be naturally defined in terms of a projection operator [114, 142]. In fact, the Berry curvature thus introduced satisfies the following sum rule, which was used in Eq. (C.8):

$$
\begin{aligned}
\sum_{n=1}^{2N} \Omega_{n\boldsymbol{k}} &= i \mathrm{Tr} \left[\sigma_3 \frac{\partial T_{\boldsymbol{k}}^\dagger}{\partial k_\mu} \sigma_3 \frac{\partial T_{\boldsymbol{k}}}{\partial k_\nu} - (\mu \leftrightarrow \nu) \right] \\
&= i \mathrm{Tr} \left[\sigma_3 \frac{\partial T_{\boldsymbol{k}}^\dagger}{\partial k_\mu} \sigma_3 T_{\boldsymbol{k}} \sigma_3 T_{\boldsymbol{k}}^\dagger \sigma_3 \frac{\partial T_{\boldsymbol{k}}}{\partial k_\nu} - (\mu \leftrightarrow \nu) \right] \\
&= -i \mathrm{Tr} \left[\sigma_3 T_{\boldsymbol{k}}^\dagger \sigma_3 \frac{\partial T_{\boldsymbol{k}}}{\partial k_\mu} \sigma_3 \frac{\partial T_{\boldsymbol{k}}^\dagger}{\partial k_\nu} \sigma_3 T_{\boldsymbol{k}} - (\mu \leftrightarrow \nu) \right] \\
&= -\sum_{n=1}^{2N} \Omega_{n\boldsymbol{k}} = 0.
\end{aligned}
\tag{C.10}
$$

Now we calculate $M^{(1)}_{\mu\nu}$ in Eq. (C.3). By using Eq. (C.7),

$$
\begin{aligned}
M^{(1)}_{\mu\nu} &= -\sum_{\boldsymbol{k}} \left(\int_0^\infty d\eta \int_\eta^\infty d\tilde{\eta} + \int_{-\infty}^0 d\eta \int_\eta^{-\infty} d\tilde{\eta} \right) \eta\rho(\eta) \left(A(\tilde{\eta}) - \frac{1}{2}\frac{dB(\tilde{\eta})}{d\tilde{\eta}} \right) \\
&= -\sum_{\boldsymbol{k}} \int_{-\infty}^\infty d\tilde{\eta} \left(A(\tilde{\eta}) - \frac{1}{2}\frac{dB(\tilde{\eta})}{d\tilde{\eta}} \right) \cdot \int_0^{\tilde{\eta}} \eta\rho(\eta) d\eta \\
&= i\sum_{\boldsymbol{k}} \int_{-\infty}^\infty d\tilde{\eta} \mathrm{Tr} \left[\delta(\tilde{\eta} - \sigma_3 \mathcal{E}_{\boldsymbol{k}}) \sigma_3 \frac{\partial T^\dagger_{\boldsymbol{k}}}{\partial k_\mu} \sigma_3 \frac{\partial T_{\boldsymbol{k}}}{\partial k_\nu} \right] \cdot \int_0^{\tilde{\eta}} \eta\rho(\eta) d\eta \\
&- \frac{i}{2}\sum_{\boldsymbol{k}} \int_{-\infty}^\infty d\tilde{\eta} \mathrm{Tr} \left[\delta(\tilde{\eta} - \sigma_3 \mathcal{E}_{\boldsymbol{k}}) \sigma_3 \frac{\partial T^\dagger_{\boldsymbol{k}}}{\partial k_\mu} \sigma_3 \left(\tilde{\eta} - \sigma_3 H_{\boldsymbol{k}} \right) \frac{\partial T_{\boldsymbol{k}}}{\partial k_\nu} \right] \tilde{\eta}\rho(\tilde{\eta}) - (\mu \leftrightarrow \nu) \,.
\end{aligned}
\tag{C.11}
$$

From Eqs. (C.2) and (C.11), the total thermal transport coefficient $L_{\mu\nu}$ is calculated as follows,

$$
\begin{aligned}
L_{\mu\nu} &= S^{(1)}_{\mu\nu} + M^{(1)}_{\mu\nu} \\
&= \frac{i}{2}\sum_{\boldsymbol{k}} \int_{-\infty}^\infty d\tilde{\eta} \mathrm{Tr} \left[\delta(\tilde{\eta} - \sigma_3 \mathcal{E}_{\boldsymbol{k}}) \sigma_3 \frac{\partial T^\dagger_{\boldsymbol{k}}}{\partial k_\mu} \sigma_3 \frac{\partial T_{\boldsymbol{k}}}{\partial k_\nu} \right] \\
&\times \left(2\int_0^{\tilde{\eta}} \eta\rho(\eta) d\eta - \tilde{\eta}^2 \rho(\tilde{\eta}) \right) - (\mu \leftrightarrow \nu) \\
&= -\frac{1}{2}\sum_{\boldsymbol{k}} \sum_{n=1}^{2N} \int_0^{(\sigma_3 \mathcal{E}_{\boldsymbol{k}})_{nn}} \eta^2 \frac{d\rho(\eta)}{d\eta} \Omega_{n\boldsymbol{k}} d\eta \\
&= \sum_{\boldsymbol{k}} \sum_{n=1}^{N} \left(k_{\mathrm{B}} T \right)^2 \left(c_2 \left(\rho \left(\varepsilon_{n\boldsymbol{k}} \right) \right) - \frac{\pi^2}{3} \right) \Omega_{n\boldsymbol{k}}.
\end{aligned}
\tag{C.12}
$$

Here $c_2(x)$ is defined in Eq. (4.32), and we have used $c_2(\infty) = \pi^2/3$ in Eq. (C.12). These results are identical with Eq. (4.31).

References

[1] F. Bloch, *Z. f. Phys.* **61,** 206 (1930).

[2] T. Holstein and H. Primakoff, *Phys. Rev.* **58,** 1094 (1940).

[3] F. J. Dyson, *Phys. Rev.* **102,** 1217 (1956).

[4] J. H. E. Griffiths, *Nature* **158,** 670 (1946).

[5] P. A. Fleury, S. P. S. Porto, L. E. Cheesman and H. J. Guggenheim, *Phys. Rev. Lett.* **17,** 84 (1966).

[6] S. O. Demokritov, B. Hillebrands, and A. N. Slavin, *Phys. Rep.* **348,** 441 (2001).

[7] A. A. Serga, S. O. Demokritov, B. Hillebrands, and A. N. Slavin, *Phys. Rev. Lett.* **92,** 117203 (2004).

[8] A. Schreyer, T. Schmitte, R. Siebrecht, P. Bödeker, H. Zabel, S. H. Lee, R. W. Erwin, C. F. Majkrzak, J. Kwo and M. Hong, *J. Appl. Phys.* **87,** 5443 (2000).

[9] M. Bauer, R. Lopusnik, H. DöKtsch, B. A. Kalinikos, C. E. Patton, J. Fassbender, and B. Hillebrands, *J. Magn. Magn. Mater.* **226-230,** 507 (2001).

[10] S. Tamaru, J. A. Bain, R. J. M. van de Veerdonk, T. M. Crawford, M. Covington, and M. H. Kryder, *Phys. Rev. B* **70,** 104416 (2004).

[11] M. Bauer, R. Lopusnik, J. Fassbender, and B. Hillebrands, *J. Appl. Phys.* **76,** 2758 (2000).

[12] J. R. Eshbach, *Phys. Rev. Lett.* **8,** 357 (1962).

[13] M. Bailleul, D. Olligs, C. Fermon and S. O. Demokritov, *Eur. Phys. Lett.* **56,** 741 (2001).

[14] M. Covington, T. M. Crawford, and G. J. Parker, *Phys. Rev. Lett.* **89,** 237202 (2002).

[15] V. E. Demidov, J. Jersch, and S. O. Demokritov, *Phys. Rev. B* **79,** 054417 (2009).

[16] J. Gouzerh, A. A. Stashkevich, N. G. Kovshikov, V. V. Matyushev, and J. M. Desvignes, *J. Magn. Magn. Mater.* **101,** 189 (1991).

[17] Y. I. Gorobets and S. A. Reshetnyak, *Tech. Phys.* **43,** 188 (1998).

[18] A. V. Vashkovskii and E. G. Lokk, *Phys. -Usp.* **47,** 601 (2004).

[19] A. V. Vashkovskii and E. H. Lock, *Phys. -Usp.* **49,** 389 (2006).

[20] S. -K. Kim, S. Choi, K.-S. Lee, D. -S. Han, D. -E. Jung, and Y. -S. Choi, *Appl. Phys. Lett.* **92,** 212501 (2008).

[21] V. E. Demidov, S. O. Demokritov, D. Birt, B. O 'Gorman, M. Tsoi, and X. Li, *Phys. Rev. B* **80,** 014429 (2009).

[22] V. K. Dugaev, P. Bruno, B. Canals, and C. Lacroix, *Phys. Rev. B* **72,** 024456 (2005).

[23] S. Yang, Z. Song, and C. P. Sun, *Eur. Phys. J. B* **52,** 377 (2006).

[24] S. Choi, K.-S. Lee, and S. -K. Kim, *Appl. Phys. Lett.* **89,** 062501 (2006).

[25] K. Perzlmaier, G. Woltersdorf, and C. H. Back, *Phys. Rev. Lett.* **77,** 054425 (2008).

[26] R. L. Stamps, R. E. Camley, B. Hillebrands, and G. Guntherodt, *Phys. Rev. B* **47,** 5072 (1993).

[27] V. E. Demidov, U. -H. Hansen, and S. O. Demokritov, *Phys. Rev. B* **78,** 054410 (2008).

[28] D. R. Birt, B. O 'Gorman, M. Tsoi, X. Li, V. E. Demidov, and S. O. Demokritov, *Appl. Phys. Lett.* **95,** 122510 (2009).

[29] S. O. Demokritov, A. A. Serga, A. Andre, V. E. Demidov, M. P. Kostylev, B. Hillebrands, and A. N. Slavin, *Phys. Rev. Lett.* **93,** 047201 (2004).

[30] A. Kozhanov, D. Ouellette, M. Rodwell, S. J. Allen, A. P. Jacob, D. W. Lee, and S. X. Wang, *J. Appl. Phys.* **105,** 07D311 (2009).

[31] U. -H. Hansen, M. Gatzen, V. E. Demidov, and S. O. Demokritov, *Phys. Rev. Lett.* **99,** 127204 (2007).

[32] T. Schneider, A. A. Serga, A. V. Chumak, B. Hillebrands, R. L. Stamps and M. P. Kostylev, *Eur. Phys. Lett.* **90,** 27003 (2010).

[33] E. A. Vilkov, *Phys. Solid State* **48,** 1754 (2006).

[34] D. D. Stancil, B. E. Henty, A. G. Cepni, and J. P. Van't Hof, *Phys. Rev. B* **74,** 060404(R) (2006).

[35] V. Vlaminck and M. Baileul *Science* **322,** 410 (2008).

[36] C. Rüegg, A. Furrer, D. Sheptyakov, T. Strässle, K. W. Krämer, H.-U. Güdel, and L. Mélési, *Phys. Rev. Lett.* **93,** 257201 (2004).

[37] Y. M. Bunkov and G. E. Volovik, *J. Low. Temp. Phys.* **150,** 135 (2008).

[38] T. Nikuni, M. Oshikawa, A. Oosawa, and H. Tanaka, *Phys. Rev. Lett.* **84,** 5868 (2000).

[39] S. O. Demokritov, V. E. Demidov, O. Dzyapko, G. A. Mellkov, A. A. Serga, B. Hillbrands and A. N. Slavin, *Nature* **443,** 440 (2006).

[40] S. M. Rezende, *Phys. Rev. Lett.* **80,** 092409 (2009).

[41] S. M. Rezende, *Phys. Rev. B* **79,** 174411 (2009).

[42] Y. Kajiwara, K. Harii, S. Takahashi, J. Ohe, K. Uchida, M. Mizuguchi, H. Umezawa, H. Kawai, K. Ando, K. Takahashi, S. Maekawa and E. Saitoh, *Nature* **464,** 262 (2010).

[43] S. A. Nikitov, Ph. Tailhades, and C. S. Tsai, *J. Magn. Magn. Mater.* **236,** 320 (2001).

[44] R. E. Camley, T. S. Rahman and D. L. Mills, *Phys. Rev. B* **27,** 261 (1983).

[45] P. Grünberg and K. Mika, *Phys. Rev. B* **27,** 2955 (1983).

[46] A. Kueny, M. R. Khan, I. K. Schuller, and M. Grimsditch, *Phys. Rev. B* **29,** 2879 (1984).

[47] R. P. van Stapele, F. J. A. M. Greidanus, and J. W. Smits, *J. Appl. Phys.* **57,** 1282 (1985).

[48] L. Dobrzynski, B. Djafari-Rouhani, and H. Puszkarski, *Phys. Rev. B* **33,** 3251 (1986).

[49] E. L. Albuquerque, P. Fulco, E. F. Sarmento, D. R. Tilley *Solid. State. Commun.* **58,** 41 (1986).

[50] S. W. McKnight and C. Vittoria, *Phys. Rev. B* **36,** 8574 (1987).

[51] R. E. Camley and M. G. Cottam, *Phys. Rev. B* **35,** 189 (1987).

[52] J. G. LePage and R. E. Camley, *Phys. Rev. B* **40,** 9113 (1989).

[53] J. Barnaś, *J. Phys. C: Solid State Phys.* **21,** 1021 (1988); *J. Phys. C: Solid State Phys.* **21,** 4097 (1988).

[54] K. Vayhinger and H. Kronmüller, *J. Magn. Magn. Mater.* **62,** 159 (1986); *J. Magn. Magn. Mater.* **72,** 307 (1988).

[55] B. Hillebrands, *Phys. Rev. B* **41,** 530 (1990).

[56] N. -N. Chen and M.G. Cottam, *Solid State Commun.* **76,** 437 (1990).

[57] R. L. Stamps and B. Hillebrands, *Phys. Rev. B* **44,** 5095 (1991).

[58] J. Barnaś, *Phys. Rev. B* **45,** 10427 (1992).

[59] B. Li, J. Yang, J.-L. Shen, and G.-Z. Yang, *Phys. Rev. B* **50,** 9906 (1994).

[60] S. -C. Lü, X. -z. Wang, and D. R. Tilley, *Phys. Rev. B* **55,** 12402 (1997).

[61] J. O. Vasseur, L. Dobrzynski, B. Djafari-Rouhani, and H. Puszkarski, *Phys. Rev. B* **54,** 1043 (1996).

[62] M. Krawczyk, Jean-Claude Lévy, Daniel Mercier, and H. Puszkarski, *Phys. Lett. A* **282,** 186 (2001).

[63] D. S. Deng, X. F. Jin, and R. Tao, *Phys. Rev. B* **66,** 104435 (2002).

[64] V. V. Kruglyak, R. J. Hicken, A. N. Kuchko, and V. Yu. Gorobets, *J. Appl. Phys.* **98,** 014304 (2005).

[65] V. V. Kruglyak, M. L. Sokolovskii, V. S. Tkachenko, and A. N. Kuchko, *J. Appl. Phys.* **99,** 08C906 (2006).

[66] V. S. Tkachenko, V. V. Kruglyak, and A. N. Kuchko, *J. Magn. Magn. Mater.* **307,** 48 (2006).

[67] M. Krawczyk and H. Puszkarski, *Acta Phys. Pol. A* **93,** 805 (1998).

[68] Yu. V. Gulyaev, S. A. Nikitov, L. V. Zhivotovskii, A. A. Klimov, Ph. Tailhades, L. Presmanes, C. Bonningue, C. S. Tsai, S. L. Vysotskii, and Yu. A. Filimonov, *JETP Lett.* **77,** 567 (2003).

[69] M. Krawczyk and H. Puszkarski, *J. Appl. Phys.* **100,** 073905 (2006).

[70] M. Krawczyk and H. Puszkarski, *Phys. Rev. B* **77,** 054437 (2008).

[71] V. V. Kruglyak and R. J. Hicken, *J. Magn. Magn. Mater.* **306,** 191 (2006).

[72] S. Neusser and D. Grundler, *Adv. Mater.* **21,** 2927 (2009).

[73] V. V. Kruglyak, S. O. Demokritov, and D. Grundler, *J. Phys. D: Appl. Phys.* **43,** 264001 (2010).

[74] A. A. Serga, A. V. Chumak, and B. Hillebrands, *J. Phys. D: Appl. Phys.* **43,** 264002 (2010).

[75] A. Khitun, M. Bao, and K. L. Wang, *J. Phys. D: Appl. Phys.* **43,** 264005 (2010).

[76] S. Fujimoto, *Phys. Rev. Lett.* **103,** 047203 (2009).

[77] H. Katsura, N. Nagaosa, and P. A. Lee, *Phys. Rev. Lett.* **104,** 066403 (2010).

[78] R. Matsumoto and S. Murakami, *Phys. Rev. Lett.* **106,** 197202 (2011) ; *Phys. Rev. B* **84,** 184406 (2011).

[79] Y. Onose, T. Ideue, H. Katsura, Y. Shiomi, N. Nagaosa, and Y. Tokura, *Science* **329,** 297 (2010).

[80] T. Ideue *et al.*, *Phys. Rev. B* **85,** 134411 (2012).

[81] C. Kittel, *Phys. Rev.* **73,** 155 (1948).

[82] C. Herring and C. Kittel, *Phys. Rev.* **81,** 869 (1951).

[83] see, for example, D. J. Kim, *New Perspectives in Magnetism of Megals* (Springer, Berlin, 1999) p. 43

[84] C. Herring and C. Kittel, *Phys. Rev.* **81,** 869 (1951).

[85] L. R. Walker, *Phys. Rev.* **105,** 390 (1957).

[86] R. L. White and I. H. Solt, Jr., *Phys. Rev.* **104,** 56 (1956).

[87] P. Röschmann and H. Dötsch, *Phys. Stat. Sol. (b)* **82,** 11 (1977).

[88] R. W. Damon and J. R. Eshbach, *J. Phys. Chem. Solids* **19,** 308 (1961).

[89] R. W. Damon and H. van de Vaart, *J. Appl. Phys.* **36,** 3453 (1965).

[90] M. J. Hurben and C. E. Patton, *J. Magn. Magn. Mater.* **139,** 263 (1995).

[91] M. J. Hurben and C. E. Patton, *J. Magn. Magn. Mater.* **163,** 39 (1996).

[92] M. Sparks, *Phys. Rev. B* **1,** 3831 (1970).

[93] B. A. Kalinikos, and A. N. Slavin, *J. Phys. C: Solid State Phys.* **19,** 7013-7033 (1986).

[94] B. Heinrich and Z. Frait, *Phys. Status Solidi B* **16** K11 (1966).

[95] C. E. Patton, *J. Appl. Phys.* **39,** 3060 (1968).

[96] V. E. Demidov, S. O. Demokritov, K. Rott, P. Krzysteczko and G. Reiss, *J. Phys. D: Appl. Phys.* **41,** 164012 (2008).

[97] A. V. Chumak, P. Pirro, A. A. Serga, M. P. Kostylev, R. L. Stamps, H. Schultheiss, K. Vogt, S. J. Hermsdoerfer, B. Laegel, P. A. Beck, and B. Hillebrands, *Appl. Phys. Lett.* **95,** 262508 (2009).

[98] H. J. Levinstein, S. Licht, R. W. Landorf, and S. L. Blank, *Appl. Phys. Lett.* **19,** 486 (1971).

[99] S. L. Blank and J. W. Nielsen, *J. Cryst. Growth.* **17** 302 (1972).

[100] H. L. Glass, *Proc. IEEE* **76,** 151 (1988).

[101] S. Pancharatnam, *Proc. Indian Acad. Sci. A* **44,** 247 (1956).

[102] M. V. Berry, *Proc. R. Soc. Lond.* **A392,** 45 (1984).

[103] Y. Aharonov and D. Bohm, *Phys. Rev.* **115,** 485 (1959).

[104] L. Smrčka, and P. Středa, *J. Phys. C* **10,** 2153 (1977).

[105] H. Oji, and P. Středa, *Phys. Rev. B* **31,** 7291 (1985).

[106] T. Thonhauser, D. Ceresoli, D. Vanderbilt, and R. Resta, *Phys. Rev. Lett.* **95,** 137205 (2005).

[107] D. Xiao, J. Shi, and Q. Niu, *Phys. Rev. Lett.* **95,** 137204 (2005).

[108] D. Xiao, Y. Yao, Z. Fang, and Q. Niu, *Phys. Rev. Lett.* **97,** 026603 (2006).

[109] R. Resta *J. Phys.* C **117,** 012024 (2008).

[110] D. L. Bergman, and V. Oganesyan, *Phys. Rev. Lett.* **104,** 066601 (2010).

[111] L. M. Luttinger, *Phys. Rev.* **135,** A1505 (1964).

[112] I. Dzyaloshinskii, *J. Phys. Chem. Solids* **4,** 241 (1958).

[113] T. Moriya, *Phys. Rev.* **120,** 91 (1960).

[114] R. Shindou, J. Ohe, R. Matsumoto, S. Murakami and E. Saitoh, *Phys. Rev. B* **87,** 174402 (2013).

[115] R. Shindou, R. Matsumoto, S. Murakami, and J. Ohe, *Phys. Rev. B* **87,** 174427 (2013).

[116] O. Vafek, A. Melikyan, and Z. Tešanović, *Phys. Rev. B* **64,** 224508 (2001).

[117] K. Nomura, S. Ryu, A. Furusaki, and N. Nagaosa, *Phys. Rev. Lett.* **108,** 026802 (2012).

[118] H. Sumiyoshi and S. Fujimoto, *J. Phys. Soc. J* **82,** 023602 (2013).

[119] S. Neusser, B. Botters, and D. Grundler, *Phys. Rev. B* **78,** 054406 (2008).

[120] B. Lenk, H. Ulrichs, F. Garbs, and M. Münzenberg, *Phys. Rep.* **507,** 107 (2011).

[121] J. H. P. Colpa, *Physica* **93A,** 327 (1978).

[122] T. Qin, Q. Niu and J. Shi, *Phys. Rev. Lett.* **107,** 236601 (2011).

[123] T. Qin, J. Zhou and J. Shi, *Phys. Rev. B* **86,** 104305 (2012).

[124] R. Kubo, M. Yokota and S. Nakajima, *J. Phys. Soc. Jpn.* **12,** 1203 (1957).

[125] G. D. Mahan, *Many-Particle Physics* 3rd ed. (Plenum, NewYork, 2000).

[126] D. A. Fishman and F. R. Morgenthaler, *J. Appl. Phys.* **54,** 3387 (1983).

[127] D. Xiao, M. C. Chang, and Q. Niu, *Rev. Mod. Phys.* **82,** 1959 (2010).

[128] G. Sundaram and Q. Niu, *Phys. Rev. B* **59,** 14915 (1999).

[129] M. Büttiker, *Phys. Rev. B* **38**, 9375 (1988).

[130] O. Dzyapko *et al.*, *J. Appl. Phys.* **101**, 09C103 (2007).

[131] D. J. Thouless, M. Kohmoto, M. P. Nightingale, and M. den Nijs, *Phys. Rev. Lett.* **49,** 405 (1982).

[132] B. I. Halperin, *Phys. Rev. Lett.* **25,** 2185 (1982).

[133] M. C. Chang, and Q. Niu, *Phys. Rev. B.* **53**, 7010 (1996).

[134] M. Onoda, and T. Ochiai, *Phys. Rev. Lett.* **103,** 033903 (2009).

[135] L. Fu, C. L. Kane, and E. J. Mele, *Phys. Rev. Lett.* **98,** 106803 (2007).

[136] X. L. Qi, T. L. Hughes, and S. C. Zhang, *Phys. Rev. B* **78,** 195424 (2008).

[137] N. Read and D. Green, *Phys. Rev. B* **61,** 10267 (2000).

[138] D. A. Ivanov, *Phys. Rev. Lett.* **86,** 268 (2001).

[139] H. Katsura, N. Nagaosa, and A. V. Balatsky, *Phys. Rev. Lett.* **95,** 057205 (2005).

[140] G. P. Fisher, *American Journal of Physics,* **39,** 1528 (1971).

[141] K. Tanabe *et al.,* private communication.

[142] J. E. Avron, R. Seiler, and B. Simon, *Phys. Rev. Letters*, **51,** 51 (1983).

Acknowledgement

First I would like to sincerely thank Prof. Shuichi Murakami, for his kind support, appropriate advice, fruitful discussion, and thoughtful guidance over the last six years. He always make time for discussions even if he has few time for his tight schedule. I have learned from him the way of presentations, methods to write scientific papers, and everything which is necessary to develop study.

I also thank Prof. Murakami's group: assistant Prof. Takehito Yokoyama, research and educational assistant Rie Tsukui, students Drs. Masaki Noro, Yuji Kitamura, Kazuhiro Tsutsui, Zheng-Yuan Wang, Junya Tanaka, Koukin Nakajin, Akihiro Okamoto, Ryo Okugawa, Masato Hamada, Taiki Yoda, former students Drs. Ryuji Takahashi, Masaki Wada, Tetsuro Misawa, Kenji Sasaki, Daichi Asahi, Yoichi Omae, and former assistant Prof. Ryuichi Shindou. Without their persistent help this thesis would not have been possible. Surrounded by the above nice members, I have had a wonderful life every day.

Special thanks to Prof. Eiji Saitou, Prof. Gen Tatara, Prof. Teruo Ono, Prof. Jun-ichiro Ohe and their groups for helpful discussions. I have greatly benefited from their valuable advice and comments.

Finally, I would like to express the deepest appreciation to my parents and brother for always encouraging me. Thank you for giving opportunities to reach this point.

Publication list

Chapter 3 and 5 partially include contents in the following publications:

1. R. Matsumoto and S. Murakami, *Phys. Rev. Lett.* **106,** 197202 (2011). Copyright ©2011 American Physical Society.

2. R. Matsumoto and S. Murakami, *Phys. Rev. B* **84,** 184406 (2011). Copyright ©2011 American Physical Society.

3. R. Matsumoto and S. Murakami, *J. Phys: Conference Series* **302,** 012025 (2011). Published under licence in Journal of Physics: Conference Series by IOP Publishing Ltd.

4. R. Matsumoto, *Bussei Kenkyu* **96,** 580 (2011) (in Japanese). Copyright ©2011 Bussei Kenkyu.

Publication added for reference

1. R. Shindou, J. Ohe, R. Matsumoto, S. Murakami and E. Saitoh, *Phys. Rev. B* **87,** 174402 (2013).

2. R. Shindou, R. Matsumoto, and S. Murakami and J. Ohe, *Phys. Rev. B* **87,** 174427 (2013).